EQUALIZATION FOR DS-UWB SYSTEMS

by

Ambuj Parihar

B.Eng., Malaviya National Institute of Technology, India, 1999

A THESIS SUBMITTED IN PARTIAL FULFILLMENT OF

THE REQUIREMENTS FOR THE DEGREE OF

MASTER OF APPLIED SCIENCE

in

THE FACULTY OF GRADUATE STUDIES

(Electrical and Computer Engineering)

THE UNIVERSITY OF BRITISH COLUMBIA

November 2005

Abstract

Ultra-wideband wireless transmission has attracted considerable attention both in academia and industry. For high-rate transmission, direct sequence based ultra-wideband (DS-UWB) systems are a strong contender for standardization by the IEEE 802.15.3a Wireless Personal Area Networks (WPAN) committee. The DS-UWB proposal envisages two modulation formats: binary phase shift keying (BPSK) and 4-ary bi-orthogonal shift keying (4BOK). Due to the large transmission bandwidth, the UWB channel is characterized by a long root-mean-square delay spread and the RAKE receiver cannot always overcome the resulting intersymbol interference. We therefore study equalization for DS-UWB systems employing BPSK and 4BOK modulation.

In the first part of this work, we consider equalization for DS-UWB with BPSK modulation, which is mandatory for standard-proposal compliant DS-UWB devices. Assuming RAKE preprocessing at the receiver, we analyze the performance limits applicable to any equalizer, taking into account practical constraints such as receiver filtering, sampling, and the number of RAKE fingers. Our results show that chip-rate sampling is sufficient for close-to-optimum performance. For analysis of suboptimum equalization strategies, we further study the distribution of the zeros of the channel transfer function including RAKE combining. Our findings suggest that linear equalization is well suited for the lower data rate modes of DS-UWB systems, whereas nonlinear equalization is required for high-data rate modes. Moreover, we devise equalization schemes with widely linear processing, which

improves performance without increasing equalizer complexity. Simulation and numerical results confirm the significance of our analysis and equalizer designs and show that low-complexity (widely) linear and nonlinear equalizers perform close to the pertinent theoretical limit.

In the second part, we investigate equalization for DS-UWB with 4BOK. To this end, we first derive expressions for the bit-error rate according to the matched-filter bound for 4BOK DS-UWB, which serve as theoretical performance limits for equalization. We then devise structures and methods for filter optimization for low-complexity linear and nonlinear equalization schemes. In this context, we develop a new equivalent multiple-input multiple-output (MIMO) description of 4BOK DS-UWB, which facilitates the design of efficient equalizers using MIMO filter optimization techniques. Furthermore, we propose the application of widely linear processing to these equalizers. Simulation and semi-analytical results show that (a) MIMO equalization is greatly advantageous over more obvious non-MIMO schemes, and (b) the proposed MIMO equalizers allow for power-efficient 4BOK DS-UWB transmission close to the theoretical limits with moderate computational complexity.

Contents

Abstract ii

Contents iv

List of Tables viii

List of Figures ix

List of Abbreviations and Symbols xiii

Acknowledgments xvi

1 Introduction 1

1.1 Ultra-wideband Technology 2

1.2 DS-UWB Proposal for IEEE 802.15.3 WPAN Physical Layer Standard . . . 5

1.3 Challenges and Motivation 6

1.4 Contributions 8

1.4.1 Contributions for BPSK DS-UWB Systems 8

1.4.2 Contributions for 4BOK DS-UWB Systems 9

1.5 Thesis Organization 11

2 Transmission System **13**

2.1 Introduction 13

2.2 Transmission Model 13

2.2.1 BPSK Modulation 14

2.2.2 4BOK Modulation 15

2.3 Channel Model 16

2.4 Receiver 20

2.4.1 Receiver for BPSK 21

2.4.2 Receiver for 4BOK 22

3 Equalization for BPSK **25**

3.1 Performance Measures for Equalization 26

3.1.1 Matched Filter Bound (MFB) 26

3.1.1.1 MFB I 27

3.1.1.2 MFB II 27

3.1.1.3 MFB III 28

3.1.2 Densities of Zeros of the Overall Transfer Function 29

3.1.2.1 Overall Transfer Function 29

3.1.2.2 Density of Zeros 30

3.1.2.3 Marginal Density and Cumulative Distribution 31

3.1.2.4 Application to Equalizer Design for DS-UWB 31

3.2 Equalization Strategies 32

3.2.1 Classical Equalization Schemes 32

3.2.1.1 Linear Equalization 32

3.2.1.2 Decision Feedback Equalization (DFE) 33

3.2.1.3 Delayed Decision-Feedback Sequence Estimation (DDFSE) . 34

3.2.2 Equalization Schemes with WL Processing 36

3.2.2.1 Widely Linear Equalization (WLE) 37

3.2.2.2 Widely Linear Decision Feedback Equalization (WDFE) . . 38

3.2.2.3 Widely Linear DDFSE (WDDFSE) 39

4 Equalization for 4BOK **40**

4.1 Performance Bound for 4BOK Equalization 41

4.1.1 MFB I 41

4.1.2 MFB II 43

4.2 Equalization Strategies 45

4.2.1 4BOK Equalization with SIMO Filter Optimization 45

4.2.1.1 Filter Design I 48

4.2.1.2 Filter Design II 49

4.2.1.3 LE based on Filter I and Filter II 51

4.2.1.4 DDFSE based on Filter I and Filter II 52

4.2.2 4BOK Equalization with MIMO Filter Optimization 53

4.2.2.1 MIMO Optimization based LE and DDFSE 57

4.2.3 4BOK Equalization with WL-MIMO Filter Optimization 58

4.2.3.1 WL-MIMO-LE and WL-MIMO-DDFSE 60

5 Results and Discussion **61**

5.1 Performance Results and Discussion for BPSK DS-UWB Systems 62

5.1.1 Simulation Parameters 62

5.1.2 Application of Distribution of Zeros to Equalizer Design for DS-UWB 63

5.1.3 Simulation Results for BPSK DS-UWB Systems 65

5.1.3.1 Equalization Strategies and MFBs 66

5.1.3.2 Linear vs. WL Processing 70

5.1.3.3 Number of RAKE Fingers 71

5.2 Performance Results and Discussion for 4BOK DS-UWB Systems 73

5.2.1 Simulation Parameters 74

5.2.2 Simulation Results 75

5.2.2.1 Filter Optimization 75

5.2.2.2 Equalization for 4BOK and MFBs 80

6 Conclusions **84**

Bibliography **87**

List of Tables

2.1 UWB channel parameters for different scenario models 18

5.1 Parameters for the considered BPSK DS-UWB systems. 63

5.2 Parameters for the considered 4BOK DS-UWB systems. 75

List of Figures

1.1 UWB spectral mask for indoor and outdoor communications systems. 3

2.1 Block diagram of BPSK DS-UWB transmission system. 14

2.2 Block diagram of 4BOK DS-UWB transmission system. 16

2.3 Impulse response of a sample realization for channel scenarios, a) CM1 b)CM4. 19

4.1 Block diagram of DFE with SIMO filter optimization for 4BOK DS-UWB. . 46

4.2 SIMO Filter Design I: Magnitudes of the impulse responses $i_\nu[k] = f_{F,\nu}[k] * h_{\nu 1}[k]$ at the FFF outputs (circles) and of the FBF coefficients $f_{B,\nu 1}[k]$ (stars) (see also Figs. 4.1 and 4.4) for an exemplary CM4 channel realization and spreading with code length $N = 6$. 50

4.3 SIMO Filter Design II: Magnitudes of the impulse responses $i_\nu[k] = f_{F,\nu}[k] * h_{\nu 1}[k]$ at the FFF outputs (circles) and of the FBF coefficients $f_{B,\nu 1}[k]$ (stars) (see also Figs. 4.1 and 4.4) for an exemplary CM4 channel realization and spreading with code length $N = 6$. 51

4.4 Block diagram of DFE with MIMO filter optimization for 4BOK DS-UWB. 54

4.5 MIMO Filter Design: Magnitudes of the impulse responses $i_\nu[k] = f_{F,\nu}[k] * h_{\nu 1}[k]$ at the FFF outputs (circles) and of the FBF coefficients $f_{B,\nu 1}[k]$ (stars) (see also Figs. 4.1 and 4.4) for an exemplary CM4 channel realization and spreading with code length $N = 6$. 57

5.1 UWB CM1 and $N = 24$. $z = x + \mathrm{j}y$. (a) Normalized density $f_z(z)/(L-1)$ of zeros of effective transfer function $H(z)$. (b) Normalized marginal density $f_r(r)/(L-1)$ of zeros of $H(z)$. (c) Normalized average number $n(R)/(L-1)$ of zeros of $H(z)$ inside the disc $|z| \leq R$. 64

5.2 UWB CM4 and $N = 24$. $z = x + \mathrm{j}y$. (a) Normalized density $f_z(z)/(L-1)$ of zeros of effective transfer function $H(z)$. (b) Normalized marginal density $f_r(r)/(L-1)$ of zeros of $H(z)$. (c) Normalized average number $n(R)/(L-1)$ of zeros of $H(z)$ inside the disc $|z| \leq R$. 65

5.3 UWB CM4 and $N = 6$. $z = x + \mathrm{j}y$. (a) Normalized density $f_z(z)/(L-1)$ of zeros of effective transfer function $H(z)$. (b) Normalized marginal density $f_r(r)/(L-1)$ of zeros of $H(z)$. (c) Normalized average number $n(R)/(L-1)$ of zeros of $H(z)$ inside the disc $|z| \leq R$. 66

5.4 BER versus $10\log_{10}(E_b/N_0)$ for MMSE-LE and MMSE-DFE for CM1 and $N = 24$. Also shown: RAKE combining without equalization and MFBs I-III (cf. Section 3.1.1). 67

5.5 BER versus $10\log_{10}(E_b/N_0)$ for MMSE-LE, MMSE-DFE, and MMSE-DDFSE for CM4 and $N = 24$. Also shown: RAKE combining without equalization and MFBs I-III (cf. Section 3.1.1). 68

5.6 BER versus $10\log_{10}(E_b/N_0)$ for MMSE-LE, MMSE-DFE, and MMSE-DDFSE with different filter lengths for CM4 and $N = 6$. Also shown: RAKE combining without equalization and MFBs I-III (cf. Section 3.1.1). 69

5.7 BER versus $10\log_{10}(E_b/N_0)$ for MMSE-(W)LE and MMSE-(W)DFE for CM4 and $N = 24$. Also shown: MMSE-WDDFSE, RAKE combining without equalization, and MFBs I-III (cf. Section 3.1.1). 71

5.8 BER versus $10\log_{10}(E_b/N_0)$ for MMSE-LE and MMSE-WLE with different filter lengths for CM4 and $N = 6$. Also shown: MMSE-DFE with $q_F = 50$ and $q_B = 23$, RAKE combining without equalization, and MFBs I-III (cf. Section 3.1.1). 72

5.9 BER versus $10\log_{10}(E_b/N_0)$ for MMSE-DFE and MMSE-WDFE with different filter lengths for CM4 and $N = 6$. Also shown: RAKE combining without equalization, and MFBs I-III (cf. Section 3.1.1). 73

5.10 Average SNR loss $\Delta\text{SNR}(F)$ as function of the number of RAKE fingers F for the three scenarios (CM1, $N = 24$), (CM4, $N = 24$), and (CM4, $N = 6$). 74

5.11 Performance comparison for equalization with SIMO and MIMO filter optimization. CM4 and $N = 6$. 76

5.12 Performance comparison for equalization for CM4 and $N = 24$. (a) Between SIMO and MIMO filter optimization. (b)Between MIMO and WL-MIMO filter optimization. 78

5.13 Performance comparison for equalization with MIMO and WL-MIMO filter optimization. CM4 and $N = 6$. 79

5.14 BER versus $10\log_{10}(E_b/N_0)$ for CM1 and $N = 24$. RAKE combining without equalization, WLE, and WDFE (MIMO equalization). Also shown: $\mathsf{BER}^{\mathsf{u}}_{\mathsf{MFB-I}}$, $\mathsf{BER}^{\mathsf{l}}_{\mathsf{MFB-I}}$ according to MFB I and $\mathsf{BER}^{\mathsf{u}}_{\mathsf{MFB-II}}$, $\mathsf{BER}^{\mathsf{l}}_{\mathsf{MFB-II}}$ according to MFB II from Section 4.1. 80

5.15 BER versus $10\log_{10}(E_b/N_0)$ for CM4 and $N = 24$. RAKE combining without equalization, WLE, WDFE, and WDDFSE (MIMO equalization). Also shown: $\mathsf{BER}^{\mathsf{u}}_{\mathsf{MFB-I}}$, $\mathsf{BER}^{\mathsf{l}}_{\mathsf{MFB-I}}$ according to MFB I and $\mathsf{BER}^{\mathsf{u}}_{\mathsf{MFB-II}}$, $\mathsf{BER}^{\mathsf{l}}_{\mathsf{MFB-II}}$ according to MFB II from Section 4.1. 81

5.16 BER versus $10\log_{10}(E_b/N_0)$ for CM4 and $N = 6$. RAKE combining without equalization, WLE and WDFE with different filter lengths, and WDDFSE and DFE for $q_F = 50$, $q_B = 35$ (MIMO equalization). Also shown: $\mathsf{BER}^{\mathsf{u}}_{\mathsf{MFB-I}}$, $\mathsf{BER}^{\mathsf{l}}_{\mathsf{MFB-I}}$ according to MFB I and $\mathsf{BER}^{\mathsf{u}}_{\mathsf{MFB-II}}$, $\mathsf{BER}^{\mathsf{l}}_{\mathsf{MFB-II}}$ according to MFB II from Section 4.1. 83

List of Abbreviations and Symbols

Acronyms

AWGN	Additive White Gaussian Noise
BER	Bit Error Rate
BPSK	Binary Phase Shift Keying
cdf	Cumulative Distribution Function
CDMA	Code Division Multiple Access
DDFSE	Delayed Decision Feedback Sequence Estimation
DFE	Decision-Feedback Equalization
DS-UWB	Direct Sequence Ultra Wideband
FBF	Feedback Filter
FFF	Feed-Forward Filter
GPS	Global Positioning System
ISI	Intersymbol Interference
LE	Linear Equalization
LOS	Line-of-Sight
NLOS	Non-Line-of-Sight
BOK	Bi-Orthogonal Keying
MFB	Matched Filter Bound
MIMO	Multiple-Input Multiple-Output

MLSE	Maximum-likelihood sequence estimation
MMSE	Minimum Mean-Square Error
MSE	Mean-Square Error
OFDM	Orthogonal Frequency Division Multiplexing
pdf	Probability Density Function
PEP	Pairwise Error Probability
SIMO	Single-Input Multiple-Output
SISO	Single-Input Single-Output
SNR	Signal-to-Noise Ratio
SRRC	Square-Root Raised Cosine
UWB	Ultra-Wideband
UMTS	Universal Mobile Telecommunication System
VA	Viterbi Algorithm
WDFE	Widely-Linear Decision-Feedback Equalization
WDDFSE	Widely-Linear Delayed Decision Feedback Sequence Estimation
WL	Widely Linear
WLE	Widely-Linear Linear Equalization
WPAN	Wireless Personal Area Network
WLAN	Wireless Local Area Network

Operators and Notation

$\mathsf{argmax}\{\cdot\}$	Argument maximizing the expression in the bracket
$\mathsf{argmin}\{\cdot\}$	Argument minimizing the expression in the bracket
$\lvert\cdot\rvert$	Absolute value of a complex number
$\cdot * \cdot$	Convolution

$\ln x$	Natural logarithm of x
$\mathsf{Re}\{\cdot\}$, $\mathrm{Im}\{\cdot\}$	Real and Imaginary part of a complex number
$z\{\cdot\}$	z-transform
$\delta(\cdot)$	Dirac delta function
$\|\|\cdot\|\|$	Frobenius norm
$\mathsf{sign}\{x\}$	Sign of $x \in \mathbb{R}$
$\mathsf{E}\{\cdot\}$	Expectation
$[\cdot]^*$	Complex conjugate
$[\cdot]^T$	Matrix or vector transposition
$[\cdot]^H$	Matrix or vector Hermitian transposition
$\mathbf{0}_m$	Zero vector with m elements
$\boldsymbol{I}_m$	Identity matrix with dimension $m \times m$

Acknowledgments

I would like to express my gratitude to Dr. Lutz Lampe for his invaluable guidance and continuous support at every stage of my research. His suggestions and constant encouragement helped me complete this challenging work. I am also indebted to Dr. Cyril Leung for providing much of the initial motivation to pursue this research work and for providing invaluable feedback that helped in improving the quality of this work.

I would also like to extend my sincere thanks to Dr. Robert Schober for his invaluable inputs and suggestions that were very helpful throughout this work.

Furthermore, I am thankful to my colleagues in the Communications Theory group for creating a stimulating and friendly environment.

This work was partially supported by the National Sciences and Engineering Research Council (NSERC) (Grants OGP0001731 and CRDPJ 320552) and by Bell University Laboratories.

Chapter 1

Introduction

Advances in wireless communications in the last decade have revolutionized our lives. The market for wireless devices such as mobile phones, laptops and personal digital assistants has grown extremely rapidly in the past several years. Wireless technologies such as wireless local area networks (WLANs) and Bluetooth, a wireless personal area network (WPAN) technology, have enabled high speed data transmission over shorter distances, whereas wireless metropolitan area network (commonly known as WiMAX) technology has enabled high-throughput broadband connections over longer distances. In the WPAN domain, Bluetooth technology promises data rates of up to 1 Mbps using the 2.4 GHz Industrial, Scientific and Medical (ISM) band [Blu03]. However, the growing demand for much higher data rates and the rising importance of WPANs, give rise to the need for new reliable wireless technologies enabling robust, low–cost, high–rate and low–power WPAN devices. With the approval of its application for commercial purposes in the U.S. and with similar trends being anticipated elsewhere in the world, the ultra-wideband (UWB) technology is well positioned to meet the evolving demands in wireless networking and to dominate the market place.

1.1 Ultra-wideband Technology

Traditionally, the term 'UWB signals' refers to very short duration pulses of the order of a few nanoseconds that do not require a carrier modulation. Until the late 1980s this technology was mainly known as 'impulse radio', 'baseband' or 'carrier free' technology. UWB pulses were first produced, in the late 1890s, using spark gap transmitters by Gugliemo Marconi, and were used to transmit Morse code across the Atlantic in 1901 [Fon04]. The potential of pulse based UWB technology for use in radars and communications was realized in the 1960s and 70s from the study of electromagnetic-wave propagation as viewed from the time-domain perspective [Fon04, BR78]. The term 'Ultra-wideband' was first used in 1989 by the Defense Advanced Research Projects Agency (DARPA), for differentiating impulse based radars from conventional ones [Fon04]. Until recently, this technology was restricted for use in defense applications such as radars and covert communications. The advances in semiconductors and microprocessors in the last few years, along with a more mature understanding of UWB system characteristics, have made it possible to build commercial applications based on UWB technology. In the U.S., the Federal Communications Commission (FCC) issued First Report and Order [FCC02] in February 2002, approving commercial use of UWB devices in the 3.1–10.6 GHz band with strict limits on power emission levels to allow co-existence of UWB systems with other wireless communication systems such as IEEE 802.11a WLAN, Universal Mobile Telecommunication System (UMTS) and Global Positioning System (GPS). The FCC spectral mask, shown in Fig. 1.1, allows communication devices to use 7.5 GHz of bandwidth between 3.1 GHz and 10.6 GHz, with power spectral density not exceeding -41.3 dBm/MHz (75 nW/MHz) [FCC02].

The FCC defines a UWB signal as any transmission with fractional bandwidth equal to or greater than 20 percent of the center frequency (f_c), or with -10 dB bandwidth occupying 500 MHz or more of the spectrum in 3.1 to 10.6 GHz band at all times of transmission. The

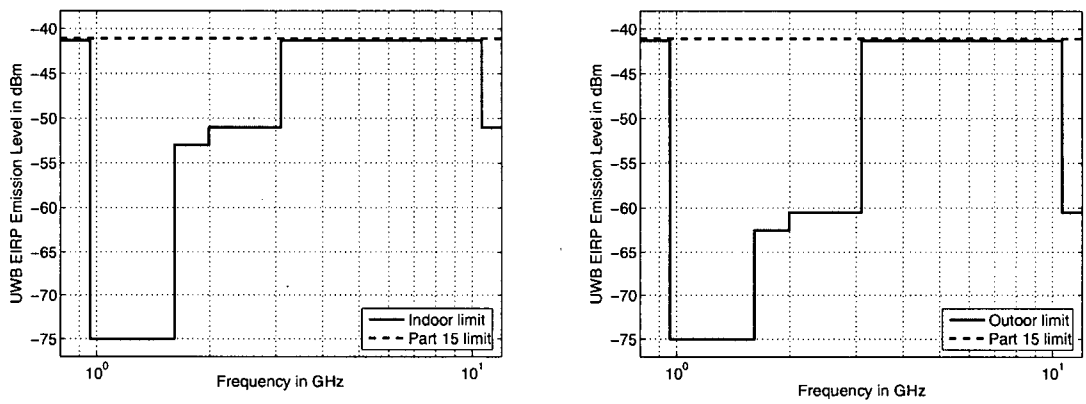

Figure 1.1: UWB spectral mask for indoor and outdoor communications systems.

fractional bandwidth (B_f) is defined as the ratio of -10 dB bandwidth (B) to the center frequency (f_c). Mathematically,

$$B_f = B/f_c = 2(f_h - f_l)/(f_h + f_l) \tag{1.1}$$

where f_l and f_h are the lowest and highest frequencies with signal 10 dB below the peak emission, respectively. The center frequency f_c is given by $(f_h + f_l)/2$ and the -10 dB bandwidth is $(f_h - f_l)$.

Given its extremely wide bandwidth UWB, promises improved channel capacity. The channel capacity (C), defined as the maximum achievable data rate over an additive white Gaussian noise (AWGN) channel is given by Shannon's formula [Sha48]

$$C = B\{\log_2(1 + SNR)\} \tag{1.2}$$

where, SNR is the signal to noise ratio. From (1.2), it is evident that the channel capacity increases linearly with B, whereas it increases logarithmically with the SNR. Thus, the wide bandwidth of UWB allows for the possibility of very high data rates even at relatively low SNR. However, due to FCC power restrictions the high data rate UWB devices can operate only over short ranges (< 10m). UWB devices are intended to operate in the 3.1–10.6 GHz band, on a license free basis, without causing harmful interference to existing

radio systems like IEEE 802.11a WLAN, UMTS and GPS, thereby increasing the spectrum utilization. Along with the aforementioned advantages, UWB has many unique properties such as robustness to fading, multipath diversity, low probability of detection and accurate positioning capabilities [PH03], that make it a very attractive technology for short range high rate WPANs and high precision positioning/tracking systems [YG04, OSR+04].

In the last few years UWB has received enormous attention from industry. Technology leaders like Motorola, Texas Instruments, Mitsubishi, Freescale and General Atomics have already started development of UWB based WPAN devices capable of providing data rates up to 500 Mbps. A large group of companies under the Zigbee Alliance [Zig] is working towards the development of UWB based devices that provide lower data rates (up to 250 kbps) and consume very low power, and so are characterized by long battery life. Market researchers are predicting that usage of UWB based systems will exceed 150 million devices by the end of 2008 [Sur05]. In order to harmonize interoperability of UWB devices, the IEEE 802.15.3a working group [WPA] is pursuing standardization of an alternative physical layer for WPANs based on UWB technology. In particular, the IEEE 802.15.3a committee is considering two standard proposals: direct-sequence spreading based UWB (DS-UWB) systems [FKMW05] and UWB systems based on multiband orthogonal frequency-division multiplexing (MB-OFDM) [P8004]. Both these proposals are different from the original UWB 'impulse radio' technology in the sense that these proposals use carrier based systems. In this research work we focus on DS-UWB systems. In the following section, the DS-UWB standard is briefly reviewed. Section 1.3 describes the specific challenges faced by DS-UWB systems that have been addressed in this research work. Section 1.4 provides a brief summary of contributions made in this work. Finally, Section 1.5 outlines the thesis organization.

1.2 DS-UWB Proposal for IEEE 802.15.3 WPAN Physical Layer Standard

The DS-UWB standard proposal [FKMW05] envisages two bands of operation: the lower band occupies 1.75 GHz of spectrum from 3.1 GHz to 4.85 GHz and the higher band occupies 3.5 GHz of spectrum from 6.2 GHz to 9.7 GHz. Each band supports up to six piconets. Any DS-UWB compliant device is required to support piconet channels 1–4, that lie in the lower band. Support for piconets 5–6 in the lower band and 7–12 in the upper band is optional. For each of these 12 piconets, the proposal specifies a fixed chip rate and a fixed center frequency. In order to support data rates ranging from 28 Mbps to 2 Gbps (depending on the code rate), the standard specifies spreading codes of lengths varying from 1 to 24 chips for each of the two modulation schemes (cf. [FKMW05, Table 6-8] for a list of spreading codes).

The DS-UWB physical layer proposal aims at utilizing the unique properties of UWB by using the wide bandwidth of the two bands and at the same time exploiting the multiple access capabilities offered by the standard code division multiple access(CDMA) technique. The DS-UWB technology, however is different from conventional spread spectrum in the sense that the purpose of employing the spreading codes is not to increase the signal bandwidth, but to reduce the interference from adjacent piconets by using the orthogonal property of these spreading codes [WMLM02]. The chip rate, which determines the bandwidth of the DS-UWB signal, remains fixed regardless of the length of the spreading code used.

The DS-UWB standard proposal specifies the use of binary phase-shift keying (BPSK) and 4-ary bi-orthogonal keying (4BOK) [Pro01] to modulate data symbols. Any DS-UWB compliant device is required to be able to transmit and receive BPSK signals, and to transmit 4BOK signals. Support for the ability to receive and demodulate 4BOK modulated signals is optional (for more details on BPSK and 4BOK see Sections 2.2.1 and 2.2.2, re-

spectively).The proposal specifies use of square root raised cosine (SRRC) pulse shaping. Use of convolutional codes of ratse 1/2 and 3/4 is specified, to provide forward error correction. In order to reduce the sensitivity of convolutional codes to error bursts, convolutional interleaving is used in conjunction with the encoder. In this work we do not consider the effect of convolutional coding and interleaving.

1.3 Challenges and Motivation

The multipath resolution of a signal that propagates over a channel is defined as the minimum delay between two paths that can be distinguished at the receiver as individual multipath components, and is given by the inverse of the bandwidth occupied by the transmitted signal. All the multipath components separated by more than the pulse duration can be resolved as individual paths with distinct propagation delays, whereas multipath components arriving within the resolution time of received signal cannot be resolved as individual paths and hence interfere constructively/destructively, resulting in fading. The very fine resolution provided by UWB due to the short duration of pulses (0.7 ns for DS-UWB systems in the lower band) offers advantages of robustness to fading and enhanced multipath diversity. Due to this very short duration of UWB pulses, fewer multipath components arrive within the resolution period, thereby reducing destructive interference and resulting in reduced signal fading. Moreover, a larger number of multipaths are resolvable, resulting in significant multipath diversity. RAKE receivers have been suggested for DS-UWB systems in order to exploit this diversity by coherently combining the multipaths [RMMW03, CWVM02, RSF03].

In indoor UWB channels signal propagation typically results in long root-mean-squared (rms) delay spreads, whereas the symbol durations in DS-UWB are comparatively very short. As an example, to achieve an uncoded data rate of 220 Mbps, the symbol duration

for DS-UWB is about 5.3 ns, whereas the typical rms delay spread at a distance of 10 m is between 14–26 ns. This results in significant ISI that spans a number of symbols. Thus, low-complexity equalizers are needed in order to effectively mitigate ISI at the output of RAKE combiner. Equalization for DS-UWB has been addressed in a number of recent publications. In [MWS03] fractionally-spaced RAKE receivers have been analyzed and in [ED05] the performance of decision-feedback and linear equalization techniques for DS-UWB systems employing Gaussian monocycles, a derivative of Gaussian pulse, is discussed. RAKE performance for carrierless pulse-based UWB transmission has been investigated in [RSF03]. However, most of these works either use pulse position modulation or Gaussian monocycle (which do not require a carrier), and hence do not provide a real evaluation of these equalization schemes when applied to DS-UWB systems that follow standard specifications (cf. Section 1.2, [FKMW05]).

In the 4BOK modulation scheme, a set of 4 bi-orthogonal signals is constructed by mapping two bits of information onto one of the four spreading sequences that include two orthogonal codewords and their negatives (Section 2.2.2, [Pro01]). Although the 4BOK modulation scheme has been specified in the DS-UWB standard proposal [FKMW05], equalization for 4BOK DS-UWB systems has received only little attention. Ishiyama and Ohtsuki [IO04] study frequency-domain equalization for 4BOK DS-UWB. Equalization is performed at the chip rate and relies on the use of a non standard-compliant cyclic prefix. Takizawa and Kohno [TK04] propose a suboptimum delayed decision feedback sequence estimation (DDFSE) [DHH89] scheme. However, since no prefilter is applied, state reduction will be problematic for non-minimum phase channels (cf. Section 3.1.2.4).

Another issue with 4BOK DS-UWB systems is the interference due to cross-correlation between spreading sequences. When the 4BOK modulated signal propagates through the multipath UWB channel the orthogonality of spreading codes is lost, resulting in severe interference due to cross-correlation between spreading sequences (cf. Chapter 4). This

interference degrades the performance of 4BOK DS-UWB systems even when long spreading sequences (24 chips) are used. In DS-UWB systems, higher data rates are achieved by reducing the length of spreading sequences while keeping the chip rate constant [FKMW05]. Therefore, at higher data rates the problem of interference due to the cross-correlation of the spreading sequences further intensifies, thereby seriously limiting the performance of 4BOK DS-UWB systems. Conventional equalization schemes such as linear equalization (LE) and decision feedback equalization (DFE) that could effectively reduce ISI in BPSK systems cannot be applied to 4BOK DS-UWB systems in their current form, since they ignore the aforementioned cross-correlation effects (cf. Section 4.2). Therefore, in this work we aim at developing equalization schemes specific to 4BOK DS-UWB systems that can effectively eliminate the interference and at the same time provide a good performance-complexity tradeoff.

1.4 Contributions

Since BPSK and 4BOK modulation schemes require a conceptually different analysis and lead to essentially different equalizer structures, the contributions of this research work are described in two parts.

1.4.1 Contributions for BPSK DS-UWB Systems

For BPSK DS-UWB systems we make the following contributions.

- We derive different versions of the MFB for DS-UWB. More specifically, besides the conventional MFB corresponding to the channel seen at the receiver input, which yields the absolute performance limit for any equalization scheme [Pro01], we consider MFBs which take into account the effect of (a) chip-matched filtering and chip-rate sampling and (b) RAKE combining with a limited number of RAKE fingers. The

evaluation of these MFBs for the IEEE 802.15.3a standard channel model for WPAN systems [P8002] shows that (a) a RAKE receiver combined with low-complexity equalization can well approach the performance of optimum equalization, (b) chip-matched filtering and chip-rate sampling yields a close-to-optimum performance and not much additional gain could be achievable with fractionally-spaced sampling, and (c) the number of RAKE fingers to sufficiently capture the useful received energy varies between about 8 and 30 depending on the underlying UWB channel.

- We develop an analytical expression for and investigate the distribution of the zeros of the channel transfer function effective at the RAKE combiner output. The distribution of the zeros provides useful information on the design of suboptimum equalizers, cf. [SG01, SG02]. In particular, we compare linear equalization (LE) and nonlinear equalization, where we focus on low-complexity decision-feedback equalization (DFE) [BP79] and delayed decision feedback sequence estimation (DDFSE) [DHH89] schemes. It is shown that LE is well suited for lower data rate modes (long spreading sequences), whereas DFE is favorably applied for high-data rate modes (short spreading sequences).

- DS-UWB with SRRC pulse shaping and carrier modulation is found to yield a second-order noncircular received signal [PB97]. We therefore propose the application of widely linear (WL) processing [PB97, PC95], i.e., WL equalization [GSL03] for DS-UWB. Requiring the same or even lower computational complexity than their "linear" counterparts, WL equalization schemes perform in the vicinity of the appropriate MFB.

1.4.2 Contributions for 4BOK DS-UWB Systems

For 4BOK DS-UWB systems we make the following contributions.

- We derive expressions for the bit-error rate (BER) limits according to the matched-filter bound (MFB) for 4BOK DS-UWB. In particular, we consider two variants of the MFB, which (a) take chip-matched filtering and chip-rate sampling and (b) subsequent RAKE combining into account. The BER expressions allow us to compare the performances of the devised low-complexity equalizers with the theoretically achievable limits.

- We develop new structures and methods for filter optimization for linear equalization (LE), decision feedback equalization (DFE) [BP79], and DDFSE [DHH89] for 4BOK DS-UWB. Different from conventional DS systems (e.g. BPSK DS-UWB), two spreading sequences are used in 4BOK DS-UWB, and one data bit determines which sequence is selected. The first considered equalizer design employs two separate feed-forward filters, each of which is optimized for only one of the spreading sequences. The second design is improved in that filter optimization takes the data-dependence of the spreading sequence into account. Due to the presence of two feedback filters in the case of DFE/DDFSE, we refer to these two approaches as single-input multiple-output (SIMO) filter optimization. Based on the insights from the second SIMO design, we develop an equivalent multiple-input multiple-output (MIMO) channel model for 4BOK DS-UWB, which leads to an efficient, third equalizer structure based on MIMO filter optimization techniques.

- As for the BPSK case, 4BOK DS-UWB is found to yield a second-order non-circular received signal [PC95]. We therefore propose the application of WL processing to equalization of 4BOK DS-UWB resulting in WL-MIMO equalization. It was found that the WL-MIMO equalization schemes offer considerable performance improvements.

1.5 Thesis Organization

The remainder of this thesis is organized as follows.

In Chapter 2, the DS-UWB transmission model is introduced. In particular, the two modulation schemes, BPSK and 4 BOK, are briefly reviewed and the IEEE 802.15.3 channel model [P8002] is described. Finally, the receiver structures for BPSK and 4BOK DS-UWB are discussed in this chapter.

In Chapter 3, equalization for BPSK DS-UWB systems is considered. Different MFB versions are derived and the distribution of the zeros of the effective transfer function is studied and analyzed for BPSK modulation. The LE, DFE, and DDFSE equalization schemes are then briefly reviewed, and the application of WL techniques to LE, DFE and DDFSE equalization techniques for BPSK DS-UWB is introduced.

In Chapter 4, equalization for 4BOK DS-UWB systems is discussed. First, equalization schemes based on SIMO filter optimization are derived. Subsequently, MIMO based LE, DFE and DDFSE are developed. Furthermore, the "widely linear" counterparts of MIMO LE, DFE and DDFSE are devised. This chapter also presents the three MFB versions derived, in order to compare the performance of the aforementioned equalizers with the theoretically achievable limits.

In Chapter 5, we present the simulation results for various equalization schemes considered. First, the results for BPSK DS-UWB systems are discussed. In particular, the distribution of zeros for different channel scenarios and data rates is presented and predictions are made for equalizer design. Subsequently, performance results for LE, DFE and DDFSE equalization schemes for BPSK DS-UWB are presented and compared with the predictions made from the study of distribution of zeros. Furthermore, the performances of "linear" equalization schemes are compared with the performances of their "widely linear" counterparts. Second, we discuss the results for 4BOK DS-UWB systems. More specifi-

cally, we present the results for performance differences between SIMO and MIMO filter optimization based equalization schemes, followed by the results for performance differences between the "linear" MIMO and "widely linear" MIMO schemes. Finally, the performance results obtained for the WL-MIMO equalization schemes are evaluated with respect to the different versions of MFB.

Finally, in Chapter 6, we summarize this work and draw some conclusions. We also make some suggestions for further extensions.

Chapter 2

Transmission System

2.1 Introduction

In this chapter, the transmission model for DS-UWB systems, including the modulation schemes, the pulse shaping filter, the channel model, the receive input filter and the demodulator is discussed. In this work, an equivalent baseband transmission model, i.e., complex-valued signals and systems [Pro01], has been adopted. The transmission model follows the specifications in the DS-UWB physical layer proposal [FKMW05]. In Section 2.2, the two proposed modulation schemes, BPSK and 4BOK, are briefly reviewed. Subsequently, the IEEE 802.15.3a channel model [P8002] for UWB based WPAN systems is described in Section 2.3. Finally, in Section 2.4 the receiver structures for BPSK and 4BOK modulation schemes are discussed.

2.2 Transmission Model

As mentioned in Section 1.2, the DS-UWB proposal [FKMW05] envisages two modulation formats: BPSK and 4BOK. This section briefly reviews these modulation schemes.

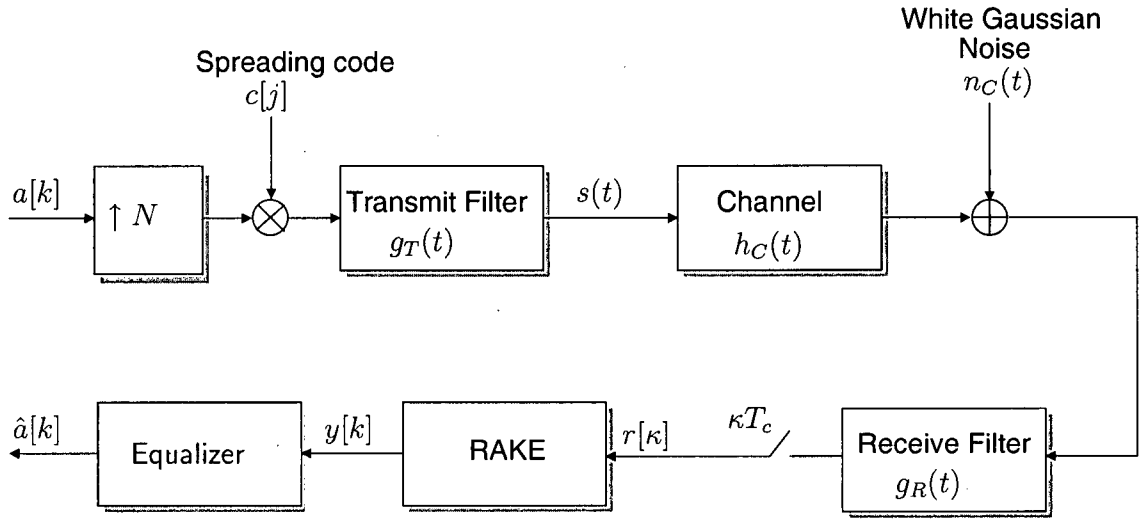

Figure 2.1: Block diagram of BPSK DS-UWB transmission system.

2.2.1 BPSK Modulation

The standard proposal [FKMW05] requires all DS-UWB systems to be able to transmit and receive BPSK modulated signals. Data rates ranging from 28 Mbps to 2 Gbps (depending on the code rate) are achievable by direct sequence spreading of BPSK symbols, using spreading sequences of lengths varying from 1 to 24 chips (for more details see [FKMW05, Table 6-7]).

The block diagram of the equivalent baseband system model for BPSK DS-UWB system is shown in Fig. 2.1. At the transmitter, BPSK symbols $a[k]$ are spread and modulated with chip pulses $g_T(t)$. The pulse shape is defined as

$$g(t) = \sum_{j=0}^{N-1} c[j] g_T(t - jT_c) \tag{2.1}$$

where $c[j]$ denotes the jth chip of the spreading code of length N and T_c is the chip duration. The pulse shaping filter $g_T(t)$ is SRRC [Rap96] with roll-off factor $\alpha = 0.3$

[FKMW05]. Finally, the transmit signal $s(t)$ can be written as

$$s(t) = \sum_{k=-\infty}^{\infty} a[k]g(t - kT_s) \tag{2.2}$$

with symbol duration $T_s = NT_c$.

2.2.2 4BOK Modulation

In the M-ary bi-orthogonal keying modulation (MBOK) scheme [Pro01, LS75] $K = \log_2 M$ bits of information are mapped onto one of the M spreading sequences chosen from the code set $\boldsymbol{C} = \{\boldsymbol{c}_1, \boldsymbol{c}_2, \ldots \boldsymbol{c}_{M/2}, -\boldsymbol{c}_1, -\boldsymbol{c}_2, \ldots - \boldsymbol{c}_{M/2}\}$, consisting of $M/2$ orthogonal codewords c_m, $1 \leqslant m \leqslant M/2$, and their negatives. For $M = 2$, MBOK reduces to BPSK, i.e., $\boldsymbol{C} = \{\boldsymbol{c}_1, -\boldsymbol{c}_1\}$.

The standard proposal uses a 4BOK ($M = 4$) modulation scheme and requires all compliant systems to allow for transmission of 4BOK modulated signals. However, the reception of these signals is optional [FKMW05]. In 4BOK signaling, the 4-ary data symbol at discrete-time k can be represented by the pair $(a[k], b[k])$, where $b[k] \in \{1, 2\}$ is an index which chooses one of the two spreading codes $\boldsymbol{c}_b = [c_b[0] \ldots c_b[N-1]]^T$ of length N, $b = \{1, 2\}$, $0 \leq j \leq N-1$, and $a[k] \in \{\pm 1\}$ is a BPSK symbol which modulates the spreading code $\boldsymbol{c}_b$. The block diagram of this equivalent baseband system model is shown in Fig. 2.2. The two pulse shapes can be defined as

$$g_b(t) = \sum_{j=0}^{N-1} c_b[j]g_T(t - jT_c) \ , \tag{2.3}$$

which correspond to the two spreading codes $\boldsymbol{c}_b$. As in the BPSK case, the pulse shaping filter $g_T(t)$ is SRRC with $\alpha = 0.3$. The transmit signal $s(t)$ can then be written as

$$s(t) = \sum_{k=-\infty}^{\infty} a[k]g_{b[k]}(t - kT_s) \ , \tag{2.4}$$

where $T_s = NT_c$ denotes the 4BOK symbol duration. 4BOK DS-UWB systems can achieve

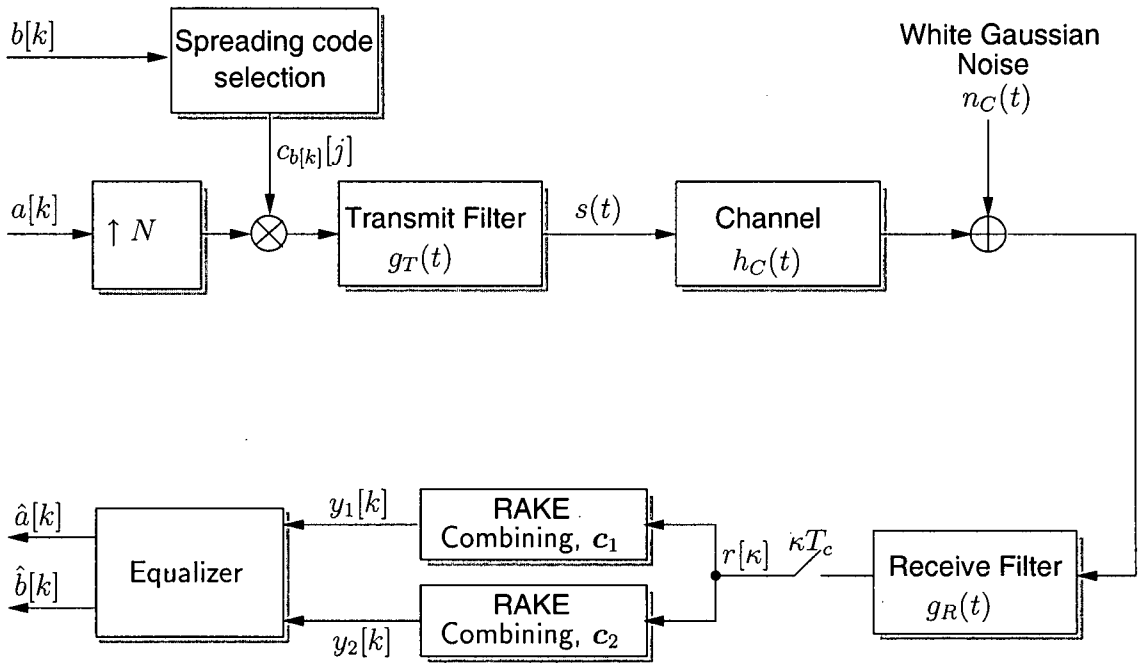

Figure 2.2: Block diagram of 4BOK DS-UWB transmission system.

data rates ranging from 110 Mbps to 2 Gbps using spreading sequences of lengths varying from 1 to 24 chips (depending on the code rate).

2.3 Channel Model

The channel model considered is the IEEE 802.15.3a model for UWB WPAN systems [P8002, MFP03]. This channel model is based on the Saleh-Valenzuela model [SV87] with some modifications to account for the properties of measured UWB channels. Multipath arrivals are grouped into two categories: cluster arrivals and ray arrivals within each cluster. The interarrival times between clusters or rays within a cluster are exponentially distributed. Lognormal fading is associated with clusters and also with rays within a cluster. The cluster and ray decay factors are based on a given power profile. Finally, the entire impulse response undergoes lognormal shadowing.

The impulse response of the multipath channel consists of L_c clusters of K_r rays and can be expressed as ($\delta(t)$ denotes the Dirac-delta function)

$$h'_C(t) = X \sum_{l=1}^{L_c} \sum_{k=1}^{K_r} \alpha_{k,l} \delta(t - T_l - \tau_{k,l}) \ , \tag{2.5}$$

where

- T_l is the delay of the lth cluster.
- $\tau_{k,l}$ is the delay of the kth multipath component relative to the lth cluster arrival time T_l.
- $\alpha_{k,l}$ is the multipath gain coefficient, where $\alpha_{k,l} = p_{k,l}\xi_l\beta_{k,l}$. The phase of $\alpha_{k,l}$ is given by the term $p_{k,l}$ which can be $+1$ or -1 with equal probability to account for signal inversion. ξ_l reflects the lognormal fading associated with the lth cluster and $\beta_{k,l}$ is the lognormal fading associated with the kth ray of the lth cluster. The variables ξ_l and $\beta_{k,l}$ are characterized as: $20\log_{10}(\xi_l\beta_{k,l}) \propto \text{Normal}(\mu_{k,l}, \sigma_1^2 + \sigma_1^2)$, where σ_1^2 and σ_2^2 are the standard deviations of the cluster and the ray lognormal fading term respectively. The term $\mu_{k,l}$ is given by

$$\mu_{k,l} = \frac{10\ln(\Omega_0) - 10T_l/\Gamma - 10\tau_{k,l}/\gamma}{\ln(10)} - \frac{(\sigma_1^2 + \sigma_2^2)\ln(10)}{20} \ , \tag{2.6}$$

  where Ω_0 is the mean energy of the first path of the first cluster. Γ and γ denote the cluster and ray decay factors, respectively. The total energy contained in the multipath gain coefficients for each realization is normalized to one.
- X is the lognormal shadowing and is characterized as $20\log_{10}(X) \propto \text{Normal}(0, \sigma_x^2)$, where σ_x^2 is the standard deviation of the lognormal fading term for the total multipath realization.

There are four different channel models (CMs) specified [P8002] with parameters designed to fit four different usage scenarios: CM1 for 0-4 m Line-of-Sight (LOS), CM2 for

Table 2.1: UWB channel parameters for different scenario models

Model Parameters	CM1	CM2	CM3	CM4
Λ [1/ns] (cluster arrival rate)	0.0233	0.4	0.0667	0.0667
λ [1/ns] (ray arrival rate)	2.5	0.5	2.1	2.1
Γ (cluster decay factor)	7.1	5.5	14.0	24.00
γ (ray decay factor)	4.3	6.7	7.9	12
σ_1 [dB] (stan. dev. of cluster lognormal fading term in [dB])	3.4	3.4	3.4	3.4
σ_2 [dB] (stan. dev. of ray lognormal fading term in [dB])	3.4	3.4	3.4	3.4
σ_2 [dB] (stan. dev. of lognormal fading term for total multipath realization in [dB])	3	3	3	3

0-4 m non-LOS (NLOS), CM3 for 4-10 m NLOS, and CM4 for NLOS with an extreme root-mean-square (rms) delay spread of 25 ns. For a particular CM, N_r channel realizations are randomly generated according to the parameter set. The channel model parameters for the different channel scenarios are described in Table 2.1 (for further details see [P8002, MFP03]). Fig. 2.3 shows the impulse response $h'_C(t)$ of a sample realization for channel CM1 and CM4.

The typical rms delay values range from 5 ns for channel CM1 to 25 ns for channel CM4 [P8002, MFP03], whereas the duration of transmitted DS-UWB signals, i.e, the chip period, is approximately 0.76 ns in the lower band and 0.38 ns in the higher band. This implies that the indoor UWB channel behaves in a highly frequency selective manner for DS-UWB systems. Due to the very fine multipath resolution of DS-UWB signals, resulting from the short duration of DS-UWB signals, and longer delay spreads associated with the UWB channel, a large number of multipaths can be resolved, thereby resulting in high multipath diversity. Since few multipath components arrive within one resolution period, DS-UWB signals do not undergo significant fading. Moreover, this results in the total received energy

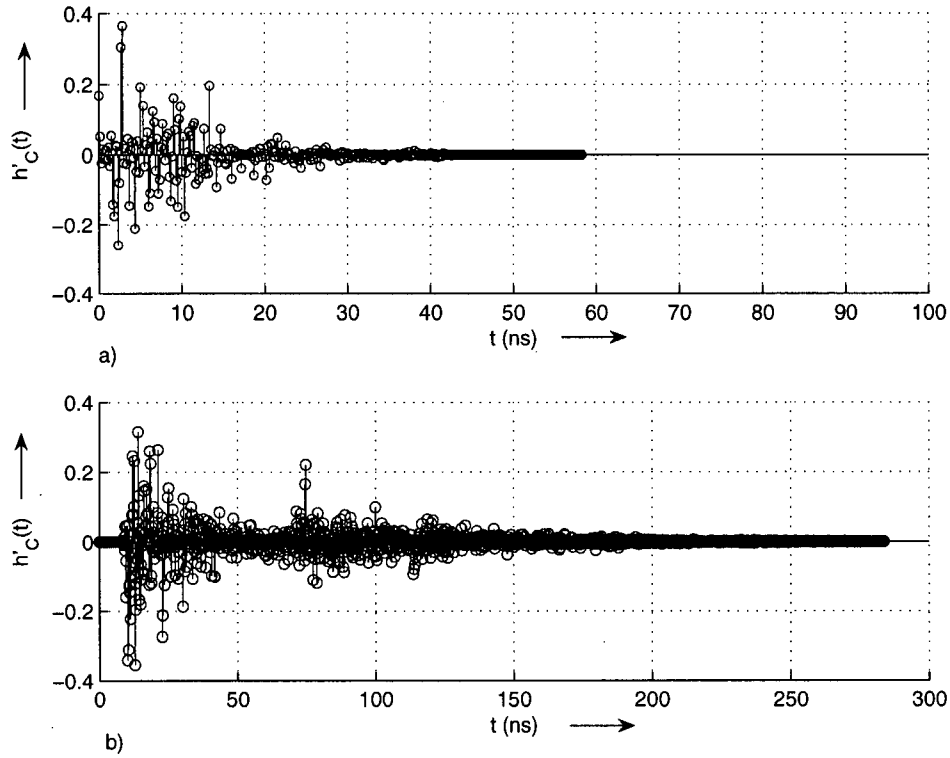

Figure 2.3: Impulse response of a sample realization for channel scenarios, a) CM1 b)CM4.

being distributed among a large number of paths, however, not every resolvable multipath contains a significant amount of energy [MFP03]. All these characteristics significantly impact the overall receiver design of DS-UWB systems as will be discussed in the following sections.

In the following, the equivalent baseband representation of $h'_C(t)$ (2.5), which is denoted by $h_C(t)$ (see Figs. 2.1 and 2.2) is considered.

2.4 Receiver

As mentioned previously, the high resolution characteristic of UWB signals results in enhanced multipath diversity. A RAKE combiner [Pro01] can be employed at the receiver in order to capture and coherently combine the received energy. The total number of resolved multipaths (N_p) is roughly proportional to the ratio of transmitted signal duration (chip duration T_c) to the excess delay τ_m, i.e, $N_p = \tau_m/T_c$ [Rap96]. Due to large excess delays for UWB indoor channels compared to the short chip duration (T_c) the value of N_p can be very high. A RAKE receiver employing a sufficiently large number of fingers to collect and coherently process all the multipath energy is equivalent to a matched filter receiver. Such a receiver provides an upper bound on the performance and serves as a measure to evaluate the limiting performance of DS-UWB receivers (see Section 3.1.1) but cannot be realized in practice. Therefore, a RAKE receiver that captures a reasonable fraction of energy by selectively combining a smaller number of paths needs to be employed. Selective RAKE receivers, which select the F paths with the largest amplitudes and then use maximum ratio combining for these paths, have been proposed and studied for UWB systems [CWVM02, RSF03, RSZ+04, WCS00]. Selective RAKE provides a good performance versus complexity trade-off by collecting a large amount of energy while employing relatively few fingers. However, due to the frequency selective nature of the UWB channel, significant ISI occurs even at the RAKE output. Thus, post-RAKE equalization is necessary in order to effectively mitigate this ISI.

In this research work, a RAKE with F fingers is considered, where F is a parameter chosen to trade-off performance and complexity (as will be shown in Section 5.1). The fingers are assigned to the F resolvable paths with the largest magnitudes. In the following, the demodulator architectures for BPSK and 4BOK DS-UWB systems are described. Equalization schemes for BPSK and 4BOK DS-UWB systems are developed and analyzed

in Chapters 3 and 4.

2.4.1 Receiver for BPSK

The equivalent complex baseband received BPSK signal $r(t)$ can be written as

$$r(t) = s(t) * h_C(t) + n_C(t) \tag{2.7}$$

where $s(t)$ is the transmitted BPSK signal, $h_C(t)$ is the equivalent baseband channel impulse response, $n_C(t)$ is an equivalent baseband noise process and is modelled as additive white Gaussian noise (AWGN) with two-sided power spectral density N_0, and "$*$" denotes convolution.

As shown in Fig. 2.1, the receiver front-end consists of a chip-matched filter $g_R(t) = g_T^*(-t)$ followed by chip-rate sampling ($(\cdot)^*$ denotes complex conjugation). The received signal after the matched filter ($r(t)$) is given by

$$r(t) = \sum_{k=-\infty}^{\infty} a[k] \sum_{j=0}^{N-1} c[j] h_o(t - kT_s - jT_c) + n_R(t) \tag{2.8}$$

where

$$n_R(t) = n_C(t) * g_R(t) \tag{2.9}$$

is the filtered AWGN $n_C(t)$ and

$$h_o(t) = g_T(t) * h_C(t) * g_R(t) \tag{2.10}$$

is the continuous-time overall impulse response including the effects of transmitter and receiver filters. Introducing the discrete-time overall impulse response

$$h_o[\kappa] = h_o(\kappa T_c) \ , \tag{2.11}$$

the discrete-time received signal after sampling with chip rate $1/T_c$ can be expressed as

$$r[\kappa] = \sum_{k=-\infty}^{\infty} a[k] \sum_{j=0}^{N-1} c[j]\, h_o[\kappa - kN - j] + n_R[\kappa] \ . \tag{2.12}$$

where

$$n_R[\kappa] = n_R(\kappa T_c) \tag{2.13}$$

is the sampled noise, which is AWGN.

As mentioned previously, an F finger RAKE is considered and the fingers are assigned to the F resolvable paths with largest amplitudes. The discrete-time receive signal $r[\kappa]$ is then fed into the RAKE combiner. The delayed versions of $r[\kappa]$ are despread and then maximum-ratio combined. The received sequence is delayed by d_i chip intervals by the ith finger. The corresponding RAKE output sequence can be written as

$$y[k] = \sum_{\nu=-\infty}^{\infty} a[\nu]h'[k-\nu] + n'[k] \,, \tag{2.14}$$

where $n'[k]$ is the noise sequence at the RAKE output and the following symbol-time impulse response $h'[.]$ is introduced

$$h'[k] = \sum_{i=1}^{F} h_o^*[d_i] \sum_{j=0}^{N-1} \sum_{m=0}^{N-1} c[j]c[m]\, h_o[kN + m + d_i - j] \,. \tag{2.15}$$

Finally, the RAKE output $y[k]$ is input to an equalizer to obtain the data estimate $\hat{a}[k]$ as shown in Fig. 2.1.

2.4.2 Receiver for 4BOK

The equivalent complex baseband received 4BOK signal $r(t)$ is given by

$$r(t) = s(t) * h_C(t) + n_C(t) \tag{2.16}$$

where $s(t)$ is the transmitted 4BOK signal as in (2.4), $h_C(t)$ is the equivalent baseband channel impulse response and $n_C(t)$ is AWGN with two-sided power spectral density N_0. Similar to the BPSK case, the 4BOK receiver front-end consists of a chip-matched filter $g_R(t) = g_T^*(-t)$ followed by chip-rate sampling. The received signal after the matched filter

$(r(t))$ is given by

$$r(t) = \sum_{k=-\infty}^{\infty} a[k] \sum_{j=0}^{N-1} c_{b[k]}[j] h_o(t - kT_s - jT_c) + n_R(t) \tag{2.17}$$

where the continuous-time overall impulse response $h_o(t)$ and noise $n_R(t)$ are defined as in (2.9) and (2.10).

The discrete-time received signal after sampling with chip rate $1/T_c$ is

$$r[\kappa] = \sum_{k=-\infty}^{\infty} a[k] \sum_{j=0}^{N-1} c_{b[k]}[j]\, h_o[\kappa - kN - j] + n_R[\kappa]\ . \tag{2.18}$$

where the definitions in (2.11) and (2.13) have been used. It should be noted that the sampled noise $n_R[\kappa] = n_R(\kappa T_c)$ is still AWGN.

Different from BPSK, in 4BOK two spreading sequences (and their negatives) are used as explained in Section 2.2.2. The receiver has no *a priori* information about the spreading code used at the transmitter to spread the data bits. Therefore, the received signal needs to be correlated separately by each of the two spreading sequences $\boldsymbol{c}_1$ and $\boldsymbol{c}_2$. This is implemented by employing two RAKE combiners, as shown in Fig. 2.2, at the receiver wherein the received signal is correlated with spreading sequence $\boldsymbol{c}_1$ in one RAKE and with spreading code $\boldsymbol{c}_2$ in the other. Both the RAKEs maximum-ratio combine (matched filters) the F strongest resolvable signal paths. One RAKE combiner selects the F strongest paths assuming $\boldsymbol{c}_1$ is transmitted and finger i delays the received sequence by $d_{1,i}$, while the other RAKE combiner assumes transmission with $\boldsymbol{c}_2$ for finger assignment and applies delays $d_{2,i}$. The despread signals can be written as

$$y_\nu[k] = \sum_{i=-\infty}^{\infty} a[i] h_{\nu b[i]}[k-i] + n_\nu[k]\ , \quad \nu \in \{1,2\}\ , \tag{2.19}$$

where $n_\nu[k]$ is the noise sequence after despreading with $\boldsymbol{c}_\nu$ and the following definition for symbol-time impulse response is introduced

$$h_{\nu\mu}[k] = \sum_{i=1}^{F} h_o^*[d_i] \sum_{j=0}^{N-1} \sum_{m=0}^{N-1} c_\mu[j] c_\nu[m]\, h_o[kN + m + d_{\nu,i} - j]\ . \tag{2.20}$$

Finally, the despreader outputs $y_\nu[k]$ are input to an equalizer to obtain the data estimate $(\hat{a}[k], \hat{b}[k])$ (see Fig. 2.2) as will be discussed in Section 4.2.

Chapter 3

Equalization for BPSK

In this chapter various suboptimum equalization schemes for BPSK DS-UWB systems are discussed. In order to evaluate the performance of various equalization schemes and also the performance of the overall receiver, different versions of the matched filter bound are derived in Section 3.1, taking into account practical constraints such as receiver filtering, sampling, and the number of RAKE fingers when RAKE preprocessing is applied at the receiver. The distribution of the zeros of the overall transfer function provides important information, with implications about the equalizer design [SG02]. An expression for the overall channel transfer function, which takes into account the effects of the spreading code, the SRRC transmit filter, the UWB channel, the receiver filter and the F finger RAKE, is derived and analytical expressions for density, marginal density and cumulative distribution of zeros are reviewed in Section 3.1.2. In Section 3.2.1, application of suboptimum equalization schemes such as LE, DFE and DDFSE to BPSK DS-UWB systems is discussed. Subsequently, equalization schemes with widely linear processing, which improves performance while not increasing equalizer complexity, are devised in Section 3.2.2.

3.1 Performance Measures for Equalization

Whether or not a certain equalization scheme achieves a favorable performance-complexity tradeoff depends strongly on the nature of the ISI channel. In particular, for suboptimum equalization techniques, such as LE, DFE, and DDFSE, the location of the zeros of the channel transfer function plays a crucial role [Pro01, SG01, SG02]. Therefore, we study and discuss the distribution of the zeros of the transfer function of the effective symbol-time channel (2.15) as an appropriate measure for the design of suboptimum equalizers in Section 3.1.2. Prior to that, the MFB, which is a performance bound for any equalization scheme, (cf., e.g., [Lin95]) is derived in Section 3.1.1.

3.1.1 Matched Filter Bound (MFB)

For the DS-UWB system under consideration, three versions of the MFB are developed, which, to different extents, account for suboptimalities of the receiver structure shown in Fig. 2.1. To obtain expressions for the bit-error rate (BER) for the respective MFBs, the signal-to-noise ratio is defined as

$$\gamma_r = \frac{E_b(r)}{N_0} , \tag{3.1}$$

where $E_b(r)$ is the received energy per bit for the rth UWB channel realization after the respective matched filter. The corresponding bit-error rate $\mathsf{BER}(\gamma_r)$ for BPSK and one particular channel realization is given by

$$\mathsf{BER}(\gamma_r) = \mathsf{Q}(\sqrt{2\gamma_r}) . \tag{3.2}$$

The average BER is obtained semi-analytically by averaging over N_r channel realizations

$$\mathsf{BER} = \frac{1}{N_r} \sum_{r=1}^{N_r} \mathsf{BER}(\gamma_r) . \tag{3.3}$$

3.1.1.1 MFB I

The first MFB, referred to as MFB I, is based on the continuous-time channel

$$h_{TC}(t) = g(t) * h_C(t) = \sum_{j=0}^{N-1} c[j] g_T(t - jT_c) * h_C(t) \tag{3.4}$$

including spreading, transmit filter, and channel impulse response. The optimum receiver input filter is the matched filter $h^*_{TC}(-t)$, which maximizes the SNR (3.1) and for which symbol-rate sampling provides a sufficient statistic. The received energy per bit for the rth channel is given by

$$E_b(r) = h_{TC}(t) * h^*_{TC}(-t)\big|_{t=0} \,. \tag{3.5}$$

It should be noted that MFB I is the ultimate performance bound, as optimum preprocessing (matched filtering) is assumed. More specifically, this bound shows the performance of a matched filter which assumes that all multipath energy can be captured, that the time duration between transmitted symbols is large enough such that no ISI occurs, and that the channel is perfectly known to the receiver. No realizable equalization scheme or receiver design can exceed this performance bound [Lin95].

3.1.1.2 MFB II

The second MFB, referred to as MFB II, takes the suboptimality of chip-spaced sampling after chip-matched filtering with $g_R(t)$ into account. This means that it is based on the discrete-time channel impulse response

$$h_{TCR}[\kappa] = h_{TC}(t) * g_R(t)\big|_{t=\kappa T_c} \,, \tag{3.6}$$

and the normalized received energy per bit after matched filtering with respect to $h_{TCR}[\kappa]$ follows as

$$E_b(r) = \frac{\sum_{\kappa=-\infty}^{\infty} |h_{TRC}[\kappa]|^2}{g_R(t) * g^*_R(-t)\big|_{t=0}} \,. \tag{3.7}$$

where the denominator term represents the normalization factor for received energy per bit since the noise variance is still considered to be N_o (see (3.1)).

The BER of MFB II is a lower bound on the performance of any receiver that employs a front end filter with chip rate sampling. A comparison of MFB I and MFB II also provides information about the potential performance gain that could be achieved by sampling at rates higher than chip rate sampling. Based on comparison of MFB I and MFB II, it was found that for BPSK DS-UWB systems chip rate sampling does not result in significant performance degradation, as will be shown in Chapter 5.

3.1.1.3 MFB III

The third MFB, referred to as MFB III, also considers the discarding of energy of the useful received signal by using a finite number F of RAKE fingers, where, for complexity reasons, F is chosen smaller than the total number of resolvable channel paths.

In general, $n'[k]$ in (2.19) is correlated Gaussian noise, which is directly accounted for in the equalizer design. However, for derivation of MFB III and analysis of distribution of zeros in Section 3.1 it is convenient to apply a noise whitening filter $f_w[k]$ and to consider the effective impulse response

$$h[k] = h'[k] * f_w[k] \,. \tag{3.8}$$

The coefficients $f_w[k]$ of the whitening filter are normalized such that

$$n[k] = n'[k] * f_w[k] \tag{3.9}$$

is AWGN with variance N_0. The effective impulse response $h[k]$ allows us to fairly compare the requirements for the equalizer design for different system parameters and channel models. The total received energy per bit for the rth UWB channel realization at the output

of the F finger RAKE is given by

$$E_b(r) = \sum_{k=-\infty}^{\infty} |h[k]|^2 \,. \tag{3.10}$$

Using (3.10) in (3.1), (3.2) and (3.3) gives the bit error rate corresponding to MFB III. For the BPSK DS-UWB receiver that employs a chip-matched filter as the receiver front end, followed by an F finger RAKE, the BER of MFB III is the lower bound on the BER achievable by any post-RAKE equalization scheme. Moreover, a comparison of performance of MFB III with that of MFB II serves as an indicator of the performance loss that occurs on account of the use of a finite number F of RAKE fingers.

3.1.2 Densities of Zeros of the Overall Transfer Function

The application of the distribution of zeros of the channel transfer function to equalizer design was introduced by Schober and Gerstacker in [SG01, SG02]. Based on the theory developed in [SG01, SG02], in the following, we study the distribution of zeros of the effective transfer function $H(z) = \mathcal{Z}\{h[k]\}$ for DS-UWB with RAKE combining.

3.1.2.1 Overall Transfer Function

The effective discrete-time impulse response $h[k]$ (3.8) depends on the spreading code, the transmit filter, the UWB channel, the receiver input filter, and the RAKE combiner. For the following considerations, it is appropriate to limit the length of $h[k]$ to some finite value L. In particular, a window $k_s \leq k < k_s + L$ is applied such that the L taps contain the fraction $\eta = 0.99$ of the total energy of the impulse response of all the N_r realizations. For ease of notation, the truncated version of the effective impulse response is still denoted by $h[k]$.

The transfer function $H(z)$ is then obtained as

$$H(z) = \mathcal{Z}\{h[k]\} = \sum_{k=k_s}^{k_s+L-1} h[k]z^{-k} = z^{-(k_s+L-1)}\boldsymbol{h}^T\boldsymbol{v}(z)\ , \tag{3.11}$$

where the definitions $\boldsymbol{h} = \left[h[k_s+L-1]\, h[k_s+L-2]\, \ldots\, h[k_s]\right]^T$ and $\boldsymbol{v}(z) = [1\, z\, \ldots\, z^{L-1}]^T$ are used.

3.1.2.2 Density of Zeros

In order to derive an analytical expression for the density of the zeros of $H(z)$ in the complex plane, it is assumed that the elements of $\boldsymbol{h}$ are non-zero mean Gaussian distributed with (a) uncorrelated real and imaginary parts, (b) identical covariance matrices for real and imaginary parts, (c) mean $\boldsymbol{\mu_h} = \mathsf{E}\{\boldsymbol{h}\}$, (d) correlation matrix $\boldsymbol{\Phi_{hh}} = \mathsf{E}\{\boldsymbol{h}\boldsymbol{h}^H\}$, and (e) covariance matrix $\boldsymbol{C_{hh}}[0] = (\boldsymbol{\Phi_{hh}} - \boldsymbol{\mu_h}\boldsymbol{\mu_h}^H)$, cf. [SG02].

Although assumptions (a) and (b) hold only approximately for the UWB channel models, the performance results (shown in Section 5.1.3) are in perfect agreement with the equalizer design implications from the analysis of distribution of zeros obtained from simulating the density (shown in Section 5.1.2).

With the above assumptions, the density of zeros of $H(z)$ in the complex plane is given by [SG02]

$$f_z(z) = \frac{1}{\pi l_0(z)} \exp\left(-\frac{|\boldsymbol{v}^T(z)\boldsymbol{\mu_h}|^2}{l_0(z)}\right) \cdot \left(\boldsymbol{v}'(z) - \frac{l_1(z)}{z\, l_0(z)}\boldsymbol{v}(z)\right)^T \boldsymbol{\Phi_{hh}} \left(\boldsymbol{v}'(z^*) - \frac{l_1^*}{z^*\, l_0^*(z)}\boldsymbol{v}(z^*)\right) \tag{3.12}$$

with the componentwise derivative $\boldsymbol{v}'(z) = [0\, 1\, \ldots\, (L-1)z^{L-2}]^T$ and

$$l_\xi(z) = \boldsymbol{v}^T(z)\boldsymbol{C_{hh}}[\xi]\, \boldsymbol{v}(z^*), \qquad \xi \in \{0,1\}\ . \tag{3.13}$$

For $\xi = 1$ the elements $c_{\mu\nu}[1]$ of matrix $\boldsymbol{C_{hh}}[1]$ are given by $c_{\mu\nu}[1] = \mu c_{\mu\nu}[0]$, where $c_{\mu\nu}[0]$ are the elements of the covariance matrix $\boldsymbol{C_{hh}}[0]$.

3.1.2.3 Marginal Density and Cumulative Distribution

For channel equalization, the important figure of merit is the density of the magnitude of the zeros. Therefore, the density of zeros is expressed in polar coordinates r, φ, i.e., $z = r \cdot \mathrm{e}^{\mathrm{j}\varphi}$, $0 \leq r < \infty$, $0 \leq \varphi < 2\pi$. The marginal density $f_r(r)$ is given by

$$f_r(r) = r \int_0^{2\pi} f_z(r\cos(\varphi) + \mathrm{j}r\sin(\varphi))\, d\varphi \,. \tag{3.14}$$

From (3.14), the expected number of zeros inside the disc $|z| = r \leq R$ is given by

$$n(R) = \int_0^R f_r(r)\, dr \,. \tag{3.15}$$

As the total number of zeros is $L-1$, we have $\lim_{R\to\infty} n(R) = L-1$.

3.1.2.4 Application to Equalizer Design for DS-UWB

The distribution of zeros of the overall transfer function in the complex plane gives important information useful for equalizer design. If many zeros lie close to the unit circle, LE[1] will perform poorly, since the presence of zeros on unit circle leads to enhancement of noise power in the case of LE. Otherwise, LE is recommended as low-complexity equalization scheme. In the case of non-linear equalization, the expected number of zeros outside the unit circle $x(\infty) = n(\infty) - n(1)$ is important. If $x(\infty) > 0$, the impulse response $h[k]$ is not minimum phase with some probability. The absence of a minimum phase equivalent of the impulse response $h[k]$ results in performance degradation for non-linear equalization techniques, since the energy of the minimum phase channel $h_{min}[k]$ is concentrated in the first few taps, i.e., $\sum_{k=0}^{\eta} h_{min}[k] \geqslant \sum_{k=0}^{\eta} h[k]$ for $1 \leqslant \eta \leqslant L$, which leads to a increase in minimum euclidean distance in the case of DDFSE [GH96]. Therefore, allpass pre-filtering,

[1]It should be noted that when studying zeros of the channel transfer function, we consider classical linear and non-linear equalization without widely linear processing.

which is approximated by an MMSE feedforward filter (FFF), is required to transform $h[k]$ into its minimum-phase equivalent $h_{min}[k]$.

Results for the distribution of zeros of $h[k]$ for combinations of different channel scenarios and spreading lengths and their application to the equalizer design for the BPSK DS-UWB systems will be discussed in Section 5.1.

3.2 Equalization Strategies

In the following, the classical LE, DFE, and DDFSE are briefly reviewed in the context of DS-UWB. The minimum mean-square error (MMSE) criterion is applied for filter optimization [Pro01]. Subsequently, equalization with WL processing for BPSK DS-UWB is introduced and the respective schemes are referred to as WLE, WDFE, and WDDFSE.

3.2.1 Classical Equalization Schemes

3.2.1.1 Linear Equalization

LE is a suboptimum equalization scheme that finds widespread application on account of its low implementation complexity. The LE employed for BPSK DS-UWB systems consists of a linear filter with coefficients $f[k]$ optimized according to the MMSE criterion. Introducing the following definition for filter vector $\boldsymbol{f}$

$$\boldsymbol{f} = \begin{bmatrix} f[0] & f[1] & \dots & f[q_f] \end{bmatrix}^H \tag{3.16}$$

with order q_f, and taking into account the correlated Gaussian noise $n'[k]$ in (2.19), the optimized filter coefficients are given by

$$\boldsymbol{f} = (\boldsymbol{A}\boldsymbol{A}^H + \zeta \boldsymbol{\Phi}_{n'n'})^{-1} \boldsymbol{h}' , \tag{3.17}$$

where ζ denotes the SNR at the RAKE output, $\mathbf{\Phi}_{n'n'}$ denotes the autocorrelation of noise $n'[k]$ given by

$$\mathbf{\Phi}_{n'n'} = \mathsf{E}[\boldsymbol{n'}[k]\boldsymbol{n'}^H[k]] \,, \tag{3.18}$$

and the following definitions are used

$$\boldsymbol{h'} = \begin{bmatrix} h'[k_o] & h'[k_o-1] & \dots & h'[k_o-q_f] \end{bmatrix}^T \,, \tag{3.19}$$

$$\boldsymbol{A} = \begin{bmatrix} h'[0] & h'[1] & \dots & h'[L] & 0 & \dots & 0 \\ 0 & h'[0] & h'[1] & \dots & h'[L] & \ddots & 0 \\ \vdots & \ddots & \ddots & \ddots & \ddots & \ddots & 0 \\ 0 & \dots & 0 & h'[0] & h'[1] & \dots & h'[L] \end{bmatrix} . \tag{3.20}$$

In the above k_0 denotes decision delay. The output $d[k]$ of the MMSE linear equalizer is given by

$$d[k] = \boldsymbol{f}^H \boldsymbol{y}_{q_f}[k] \,, \tag{3.21}$$

where

$$\boldsymbol{y}_{q_f}[k] = \left[y[k] \dots y[k-q_f]\right]^T \tag{3.22}$$

is a vector for RAKE output sequence $y[\cdot]$ given by (2.19). Since the modulation scheme considered here is BPSK, the data estimate $\hat{a}[k-k_o]$ can be obtained simply by considering the sign of the real part of the LE output $d[k]$. Mathematically,

$$\hat{a}[k-k_0] = \mathsf{sign}\{\mathsf{Re}\{d[k]\}\} \,. \tag{3.23}$$

3.2.1.2 Decision Feedback Equalization (DFE)

The DFE equalizer consists of a feedforward filter (FFF) and a feedback filter (FBF) with taps spaced T_s (symbol duration) time apart. The RAKE output $y[k]$, as in (2.19), is fed to the FFF. The FBF eliminates the post-cursor interference, i.e., the interference caused by previous data symbols to the currently estimated symbol. The filters are jointly optimized

according to the MMSE criterion [BP79]. For MMSE DFE, the FFF coefficients $f_F[k]$ and the FBF coefficients $f_B[k]$ are given by

$$\begin{aligned} \boldsymbol{f}_F &= ((\boldsymbol{A}\boldsymbol{A}^H - \boldsymbol{H}\boldsymbol{H}^H) + \zeta\boldsymbol{\Phi}_{n'n'})^{-1}\boldsymbol{h}' , \\ \boldsymbol{f}_B &= \boldsymbol{H}^H\boldsymbol{f}_B , \end{aligned} \tag{3.24}$$

where $\boldsymbol{A}$, $\boldsymbol{h}'$ are defined in (3.20), (3.19), respectively, $\boldsymbol{\Phi}_{n'n'}$ is the autocorrelation of noise $n'[k]$ given by (3.18), and the following definitions are used

$$\boldsymbol{f_F} = \begin{bmatrix} f_F[0] & f_F[1] & \dots & f_F[q_F] \end{bmatrix}^H , \tag{3.25}$$

$$\boldsymbol{f_B} = \begin{bmatrix} f_B[1] & f_B[2] & \dots & f_B[q_B] \end{bmatrix}^H , \tag{3.26}$$

$$\boldsymbol{H} = \begin{bmatrix} h'[k_0+1] & h'[k_0+2] & \dots & h'[k_0+q_B] \\ h'[k_0] & h'[k_0+1] & \dots & h'[k_0+q_B-1] \\ \vdots & \vdots & \vdots & \vdots \\ h[k_0+1-q_F] & h[k_0+2-q_F] & \dots & h[k_0+q_B-q_F] \end{bmatrix} . \tag{3.27}$$

where q_F and q_B denote the order of FFF and FBF, respectively and k_o is the decision delay which has to be optimized (cf. [VLC96]). The equalizer output $d[k]$ can be expressed as

$$d[k] = \boldsymbol{f}_F^H \boldsymbol{y}_{q_F}[k] - \boldsymbol{f}_B^H \hat{\boldsymbol{a}}_B[k] . \tag{3.28}$$

Data decisions $\hat{a}[k-k_0]$ are obtained as in (3.23), and fed back to the FBF as vector $\hat{\boldsymbol{a}}_B[k] = \left[\hat{a}[k-k_0-1] \dots \hat{a}[k-k_0-q_B]\right]^T$. The output of the FBF is a weighted sum of these past decisions $\hat{\boldsymbol{a}}_B[k]$ and the FBF coefficients $\boldsymbol{f}_B^H$, which results in total elimination of ISI caused by previous symbols to the currently estimated symbol (assuming that all the past decisions were correct).

3.2.1.3 Delayed Decision-Feedback Sequence Estimation (DDFSE)

The optimum equalization scheme for any ISI wireless channel is maximum likelihood sequence estimation (MLSE), which is implemented using a Viterbi algorithm (VA). The

complexity of the VA is dependent on the number of states employed by the VA, which increases exponentially with the channel memory. For a channel with finite memory length L, the number of states employed in the VA performing MLSE is exponential in L. The long excess delay in UWB channels compared to the short symbol duration results in long channel memory. Moreover, as data rates are increased in the DS-UWB system, the symbol duration decreases, further increasing the L. In particular, for higher data rate DS-UWB systems L could be as high as 30. Then, for MLSE, the number of states in VA would be 2^{30}, which is not feasible for practical implementation. Therefore, we consider DDFSE [DHH89], a hybrid algorithm between MLSE and DFE, which provides a direct trade-off between complexity and performance. DDFSE is based on a trellis with a reduced number of states as compared to MLSE. More specifically, for a channel with memory length L, DDFSE employes a VA that performs MLSE for the initial q_{tr} past symbols where $0 < q_{tr} < L$, and at the same time performs DFE to remove ISI due to the remaining $L - q_{tr}$ past symbols, where the feedback information provided by the best path leading to a state is used.

For the BPSK DS-UWB system, the DDFSE uses a VA with $2^{q_{tr}}$ states $\boldsymbol{s}[k] = [\tilde{a}[k - k_0 - 1] \ldots \tilde{a}[k - k_0 - q_{tr}]]^T$. An MMSE-FFF is applied prior to the reduced state VA in order to change the channel to its minimum phase equivalent, thereby avoiding any performance losses that could occur due to the non-minimum phase channel, see Section 3.1.2.4, [GH96]. Defining the decision-feedback symbol vector for state $\boldsymbol{s}[k]$ by $\hat{\boldsymbol{a}}_{B,s}[k]$ as

$$\hat{\boldsymbol{a}}_{B,s}[k] = \left[\begin{array}{cccc} \hat{a}[k - k_0 - 2 - q_{tr}] & \hat{a}[k - k_0 - 1 - q_{tr} & \ldots \hat{a}[k - k_0 - q_B] \end{array} \right]^T \quad (3.29)$$

and introducing the following definitions

$$\begin{aligned} \boldsymbol{f}_B^{q_{tr}} &= \left[\begin{array}{cccc} f_B[1] & f_B[2] & \ldots & f_B[q_{tr}] \end{array} \right]^H , \\ \boldsymbol{f}_B^{q_B - q_{tr}} &= \left[\begin{array}{cccc} f_B[q_{tr}+1] & f_B[q_{tr}+2] & \ldots & f_B[q_B] \end{array} \right]^H , \end{aligned} \quad (3.30)$$

where $f_B[k]$ is given by (3.24) and (3.26), the DDFSE branch metric for state $\boldsymbol{s}[k]$ and trial

symbol $\tilde{a}[k-k_0]$ is given by

$$\lambda(\tilde{a}[k-k_0], \boldsymbol{s}[k]) = |\boldsymbol{f}_F^H \boldsymbol{y}_{q_F}[k] - \tilde{a}[k-k_0] - (\boldsymbol{f}_B^{q_{tr}})^H \boldsymbol{s}[k] - (\boldsymbol{f}_B^{q_B-q_{tr}})^H \hat{\boldsymbol{a}}_{B,s}[k]|^2 . \quad (3.31)$$

It should be noted that for $q_{tr} = 0$ DDFSE reduces to DFE. Also, DDFSE approximates MLSE as $q_{tr} \rightarrow L$.

3.2.2 Equalization Schemes with WL Processing

In order to completely describe the second-order statistics of a complex signal $x[k] = x_I[k] + jx_Q[k]$ where $x_I[k] = \mathsf{Re}\{x[k]\}$ and $x_Q[k] = \mathrm{Im}\{x[k]\}$, it is necessary to consider the pseudo-correlation $\mathsf{E}\{x[k+m]x[k]\}$ in addition to the correlation $\mathsf{E}\{x[k+m]x^*[k]\}$ [PB97, NM93]. The complex signal $x[k]$ is said to be second-order noncircular[2] (or improper) if its pseudo-autocorrelation is not zero. Mathematically,

$$\mathsf{E}\{x[k+m]x[k]\} \neq 0 \quad \text{for some m} \in \mathbb{Z} \quad (3.32)$$

For complex valued signals a widely linear (WL) approach to mean square estimation (MSE) has been proposed in [PC95], wherein the estimation of a random process $w[k]$ is done by considering not only the original observed signal $x[k]$ but also the complex conjugate of the observed signal $x^*[k]$. If the observed signal $x[k]$ is non-circular (as characterized by (3.32)) or if the observed signal is circular $x[k]$ but its pseudo-crosscorrelation with the estimated process $w[k]$ is non-zero, i.e., both $\mathsf{E}\{x[k+m]x[k]\} = 0 \; \forall \; m \in \mathbb{Z}$, and $\mathsf{E}\{x[k+m]w[k]\} \neq 0$ for some m $\in \mathbb{Z}$, are valid, then, "widely linear" MSE results in improved estimation of the random process $w[k]$ as compared to the conventional "linear" MSE [PC95]. When both the pseudo-autocorrelation and pseudo-crosscorrelation are zero, i.e., $\mathsf{E}\{x[k+m]x[k]\} = \mathsf{E}\{x[k+m]w[k]\} = 0 \; \forall \; m \in \mathbb{Z}$, then "widely linear" MSE reduces to conventional "linear" MSE.

[2]In the following, we will use the term 'non-circular' to denote 'second-order non-circular' for the sake of conciseness.

From the fact that BPSK signaling and carrier modulation are applied, i.e., complex $y[k]$ (2.14), we observe that the pseudo-autocorrelation function

$$\mathsf{E}\{y[k+m]y[k]\} = \sum_{\nu=-\infty}^{\infty} h'[\nu]h'[\nu+m] \tag{3.33}$$

for the RAKE output signal $y[k]$ (2.19) is nonzero in general. Hence, $y[k]$ is noncircular. As a result, WL processing, i.e., joint processing of $y[k]$ and its complex-conjugated version $y^*[k]$, should be applied. It should be noted that for carrierless UWB modulation (often considered with Gaussian monocycles, cf. e.g. [MWS03, ED05, RSF03, IO04]), WL processing is identical to conventional "linear" processing since no equivalent complex baseband signal is generated.

WL equalization schemes for frequency-selective channels have recently been proposed in [GSL03]. In particular, MMSE-WLE and MMSE-WDFE schemes have been developed as extensions to conventional MMSE-LE and MMSE-DFE, respectively. In the following section, we discuss WL processing based equalization schemes for BPSK DS-UWB systems.

In the remainder of this chapter, the correlated noise at the output of RAKE $n'[k]$ is considered to be circular i.e., $\mathsf{E}\{n'[k+m]n'[k]\} = 0$. As in the Section 3.2.1, the noise autocorrelation is denoted by $\mathbf{\Phi}_{n'n'}$.

3.2.2.1 Widely Linear Equalization (WLE)

For MMSE-WLE the RAKE output signal $y[k]$ and its complex conjugate $y^*[k]$ are filtered using linear filters $f_{WL}[k]$ and $g_{WL}[k]$ and their outputs are linearly combined. Therefore, the final output $d[k]$ can be expressed as

$$d[k] = \boldsymbol{f}_{WL}^H \boldsymbol{y}_{q_f}[k] + \boldsymbol{g}_{WL}^H \boldsymbol{y}_{q_f}^*[k] \,, \tag{3.34}$$

where $\boldsymbol{f}_{WL} = [f_{WL}[0] \dots f_{WL}[q_f]]^H$ and $\boldsymbol{g}_{WL} = [g_{WL}[0] \dots g_{WL}[q_f]]^H$ are filter vectors of order q_f and $\boldsymbol{y}_{q_f}$ is given by (3.22). Modifying the optimization presented in [GSL03] in

order to directly account for correlation of the noise $n'[k]$ in (2.19), we obtain

$$\begin{aligned} \boldsymbol{f}_{WL} &= [(\boldsymbol{A}\boldsymbol{A}^H + \zeta\boldsymbol{\Phi}_{n'n'}) - (\boldsymbol{A}\boldsymbol{A}^T)\cdot(\boldsymbol{A}^*\boldsymbol{A}^T + \zeta\boldsymbol{\Phi}^*_{n'n'})^{-1}\cdot(\boldsymbol{A}^*\boldsymbol{A}^H)]^{-1} \\ &\quad \cdot[\boldsymbol{h}' - \boldsymbol{A}\boldsymbol{A}^T\cdot(\boldsymbol{A}^*\boldsymbol{A}^T + \zeta\boldsymbol{\Phi}^*_{n'n'})^{-1}\boldsymbol{h}'^*] , \qquad (3.35) \\ \boldsymbol{g}_{WL} &= \boldsymbol{f}^*_{WL} , \qquad (3.36) \end{aligned}$$

where the definitions (3.19), (3.20) and (3.27) are used. The WLE output $d[k]$ can now be expressed as

$$d[k] = 2\mathrm{Re}\{\boldsymbol{f}^H_{WL}\boldsymbol{y}_{q_f}[k]\} . \qquad (3.37)$$

It should be noted that the WLE output $d[k]$ is real valued. The data estimate $\hat{a}[k-k_o]$ is given by

$$\hat{a}[k-k_0] = \mathrm{sign}\{d[k]\} . \qquad (3.38)$$

3.2.2.2 Widely Linear Decision Feedback Equalization (WDFE)

In MMSE-WDFE in addition to WL processing of the RAKE output signal $y[k]$, feedback filtering is applied. The WDFE output $d[k]$ can be expressed as

$$d[k] = \boldsymbol{f}^H_{F,WL}\boldsymbol{y}_{q_f}[k] + \boldsymbol{g}^H_{F,WL}\boldsymbol{y}^*_{q_f}[k] - \boldsymbol{f}^H_{B,WL}\hat{\boldsymbol{a}}_B[k] , \qquad (3.39)$$

where $\boldsymbol{f}_{F,WL} = [f_{F,WL}[0]\ldots f_{F,WL}[q_F]]^H$ and $\boldsymbol{g}_{F,WL} = [g_{B,WL}[0]\ldots g_{B,WL}[q_F]]^H$ are the FFF vectors of order q_F, and $\boldsymbol{f}_{B,WL} = [f_{B,WL}[0]\ldots f_{B,WL}[q_B]]^H$ is the FBF vector with order q_B. The filters are jointly optimized according to the WL MMSE criterion as in [GSL03]. Taking into account the noise autocorrelation $\boldsymbol{\Phi}_{n'n'}$, the filter coefficients are given by

$$\begin{aligned} \boldsymbol{f}_{F,WL} &= [(\boldsymbol{A}\boldsymbol{A}^H - \boldsymbol{H}\boldsymbol{H}^H + \zeta\boldsymbol{\Phi}_{n'n'}) - (\boldsymbol{A}\boldsymbol{A}^T - \boldsymbol{H}\boldsymbol{H}^T) \\ &\quad \cdot(\boldsymbol{A}^*\boldsymbol{A}^T - \boldsymbol{H}^*\boldsymbol{H}^T + \zeta\boldsymbol{\Phi}^*_{n'n'})^{-1}\cdot(\boldsymbol{A}^*\boldsymbol{A}^H - \boldsymbol{H}^*\boldsymbol{H}^H)]^{-1} \\ &\quad \cdot[\boldsymbol{h} - (\boldsymbol{A}\boldsymbol{A}^T - \boldsymbol{H}\boldsymbol{H}^T)\cdot(\boldsymbol{A}^*\boldsymbol{A}^T - \boldsymbol{H}^*\boldsymbol{H}^T + \zeta\boldsymbol{\Phi}^*_{n'n'})^{-1}\boldsymbol{h}'^*] , \qquad (3.40) \\ \boldsymbol{g}_{F,WL} &= \boldsymbol{f}^*_{F,WL} , \qquad (3.41) \\ \boldsymbol{f}_{B,WL} &= \boldsymbol{H}^H\boldsymbol{f}_{F,WL} + \boldsymbol{H}^T\boldsymbol{f}^*_{F,WL} = 2\mathrm{Re}\{\boldsymbol{H}^H\boldsymbol{f}_{F,WL}\} . \qquad (3.42) \end{aligned}$$

Substituting (3.40) and (3.41) in (3.39), the equalizer output can be expressed as

$$d[k] = 2\mathrm{Re}\{\boldsymbol{f}_{F,WL}^{H}\boldsymbol{y}_{q_F}[k]\} - \boldsymbol{f}_{B,WL}^{H}\,\hat{\boldsymbol{a}}_B[k]\,. \tag{3.43}$$

Data decisions $\hat{a}[k-k_0]$ are obtained as in (3.38), and fed back to the FBF as vector $\hat{\boldsymbol{a}}_B[k] = \left[\hat{a}[k-k_0-1]\ \ldots\ \hat{a}[k-k_0-q_B]\right]^T$.

3.2.2.3 Widely Linear DDFSE (WDDFSE)

The WDDFSE scheme is an extension of the conventional DDFSE (described in Section 3.2.1.3) with the difference that the FFF is optimized according to the WL MMSE criterion. Observing that the minimum phase channel coefficients $f_{B,WL}[k]$ (see (3.42)) are real, the WDDFSE branch metric $\lambda(\tilde{a}[k-k_0], \boldsymbol{s}[k])$ can be expressed as

$$\lambda(\tilde{a}[k-k_0], \boldsymbol{s}[k]) = (2\mathrm{Re}\{\boldsymbol{f}_F^H\boldsymbol{y}_{q_F}[k]\} - \tilde{a}[k-k_0] - (\boldsymbol{f}_{B,WL}^{q_{tr}})^H\,\boldsymbol{s}[k] - (\boldsymbol{f}_{B,WL}^{q_B-q_{tr}})^H\,\hat{\boldsymbol{a}}_{B,s}[k])^2\,, \tag{3.44}$$

where $\boldsymbol{f}_{B,WL}^{q_{tr}} = [f_{B,WL}[1]\ldots f_{B,WL}[q_{tr}]]^H$ and $\boldsymbol{f}_{B,WL}^{q_B-q_{tr}} = [[f_{B,WL}[q_{tr}+1]\ldots f_{B,WL}[q_B]]^H$.

It should be noted that the FBFs used in WDFE and WDDFSE are real-valued, which yields a small complexity advantage of WL equalization over conventional equalization.

Chapter 4

Equalization for 4BOK

In the previous chapter, we discussed equalization for BPSK DS-UWB systems. As explained in Chapter 2, in 4BOK DS-UWB systems, different from the BPSK case, two spreading sequences are employed at the transmitter, and at the receiver two RAKEs are used in order to despread the received data separately with each of the two spreading sequences. Since the corresponding demodulator structure for 4BOK is conceptually different from that of BPSK, the equalization schemes discussed for BPSK DS-UWB systems, in their current form, cannot be applied to the 4BOK case. Therefore, in this chapter, we discuss the equalizer designs developed specifically for 4BOK DS-UWB systems. In particular, we first derive the MFBs in Section 4.1. In Section 4.2.1, two SIMO filter optimization methods are described and the corresponding equalizer structures are discussed. Subsequently, in Section 4.2.2, MIMO filter optimization is discussed and LE, DFE and DDFSE based on this optimization method are described. Furthermore, widely linear processing is applied to the MIMO filter optimization and WL-MIMO equalization schemes are developed in Section 4.2.3.

4.1 Performance Bound for 4BOK Equalization

Before considering particular equalizer implementations, it is useful to determine the performance limit for any equalizer. It is well known that this performance limit is given by the MFB, cf. e.g. [Lin95]. Therefore, we apply the MFB concept to 4BOK transmission and consider the error probability when a single symbol pair (a, b) is transmitted. Since four different pairs $(a, b)_m$, $1 \leq m \leq 4$, are possible, we will first determine the pairwise error probability (PEP) $P_e(m, n)$ that $(a, b)_m$ is transmitted and $(a, b)_n$ with $n \neq m$ is detected. An upper bound for the BER is then obtained from the union bound over the PEPs, whereas a lower bound, and thus a true performance limit, results from only considering the dominant PEP.

In order to also analyze the potential performance losses due to the RAKE as equalizer front end, two versions of the MFB are considered. First, the MFB based on the chip-matched filtered and chip-rate sampled received signal $r[\kappa]$ is determined. This MFB is referred to as MFB I in the following. Subsequently, we obtain the MFB given the RAKE outputs $y_\nu[k]$, $\nu \in \{1, 2\}$, which is referred to as MFB II. Since for BPSK DS-UWB in Section 3.1.1.2 it was found that chip-matched filtering and chip-rate sampling cause only negligible performance degradations compared to optimum matched filtering, we concentrate on the corresponding MFBs for the 4BOK case.

4.1.1 MFB I

If only a single symbol pair (a, b) is transmitted, the sampled received signal is (see (2.18))

$$r[\kappa] = a \sum_{j=0}^{N-1} c_b[j]\, h_o[\kappa - j] + n_R[\kappa] \,, \tag{4.1}$$

where $n_R[\kappa]$ is AWGN with variance σ_n^2. Furthermore, it is appropriate to consider a window $\kappa_s \leq \kappa < \kappa_s + L$ of L taps of the impulse response $h_o[\kappa]$, such that this window captures the

fraction η of the total energy of $h_o[\kappa]$, where η is chosen (arbitrarily) close to one. Defining the corresponding vectors $\boldsymbol{h} = [h_o[\kappa_s] \ldots h_o[\kappa_s + L - 1]]^T$, $\boldsymbol{r} = [r[\kappa_s] \ldots r[\kappa_s + N + L - 1]]^T$, and $\boldsymbol{n} = [n_R[\kappa_s] \ldots n_R[\kappa_s + N + L - 1]]^T$, (4.1) can be compactly written as

$$\boldsymbol{r} = \boldsymbol{C}(a, b)\boldsymbol{h} + \boldsymbol{n} \ , \tag{4.2}$$

where the data dependent $(N + L - 1) \times L$ circulant matrix $\boldsymbol{C}(a, b)$ is defined as

$$\boldsymbol{C}(a,b) = \begin{bmatrix} ac_b[0] & 0 & \ldots & 0 & 0 \\ \vdots & ac_b[0] & \ddots & 0 & 0 \\ ac_b[N-1] & \vdots & \ddots & \ddots & 0 \\ 0 & ac_b[N-1] & \ddots & \ddots & \vdots \\ \vdots & \ddots & \ddots & ac_b[0] & 0 \\ 0 & 0 & \ddots & \vdots & ac_b[0] \\ 0 & 0 & \ddots & ac_b[N-1] & \vdots \\ 0 & 0 & \ldots & 0 & ac_b[N-1] \end{bmatrix} . \tag{4.3}$$

Since the elements of $\boldsymbol{n}$ are independent complex zero-mean Gaussian random variables, the (optimum) maximum-likelihood (ML) decision rule is given by

$$(\hat{a}, \hat{b}) = \underset{(a,b)}{\mathsf{argmin}}\{||\boldsymbol{r} - \boldsymbol{C}(a, b)\boldsymbol{h}||^2\} \ . \tag{4.4}$$

Based on (4.4), the PEP for channel realization $\boldsymbol{h}$ can be written as (we use $\boldsymbol{C}(x)$ as short-hand for $\boldsymbol{C}((a, b)_x)$)

$$\begin{aligned} P_e(m, n|\boldsymbol{h}) &= \Pr\{||\boldsymbol{r} - \boldsymbol{C}(m)\boldsymbol{h}||^2 > ||\boldsymbol{r} - \boldsymbol{C}(n)\boldsymbol{h}||^2\} \\ &= \Pr\{0 > ||(\boldsymbol{C}(n) - \boldsymbol{C}(m))\boldsymbol{h}||^2 - 2\mathsf{Re}\{\boldsymbol{n}^H(\boldsymbol{C}(n) - \boldsymbol{C}(m))\boldsymbol{h}\}\} \ , \end{aligned} \tag{4.5}$$

which immediately leads to

$$P_e(m, n|\boldsymbol{h}) = \mathsf{Q}\left(||(\boldsymbol{C}(n) - \boldsymbol{C}(m))\boldsymbol{h}||/\sigma_n\right) \ . \tag{4.6}$$

It should be noted that since the calculation of actual MFB is not possible, so we consider a lower bound and an upper bound on the actual MFB. Applying the union bound

to $P_e(m,n|\boldsymbol{h})$ in (4.6), an upper bound $\mathsf{BER}^{\mathsf{u}}_{\mathsf{MFB}}(\boldsymbol{h})$ on the MFB is obtained

$$\mathsf{BER}^{\mathsf{u}}_{\mathsf{MFB}}(\boldsymbol{h}) = \frac{1}{4}\sum_{m=1}^{4}\sum_{\substack{n=1\\ n\neq m}}^{4}\frac{g(m,n)}{2}P_e(m,n|\boldsymbol{h}) \ , \tag{4.7}$$

where $g(m,n) \in \{1,2\}$ denotes the number of bit errors if $(a,b)_m$ is transmitted and $(a,b)_n$ is detected. A lower BER bound $\mathsf{BER}^{\mathsf{l}}_{\mathsf{MFB}}(\boldsymbol{h})$ results if only the dominant error event is considered:

$$\mathsf{BER}^{\mathsf{l}}_{\mathsf{MFB}}(\boldsymbol{h}) = \max_{\substack{m,n\\ n\neq m}}\left\{\frac{g(m,n)}{2}P_e(m,n|\boldsymbol{h})\right\} \ . \tag{4.8}$$

Finally, the average BERs are obtained semi-analytically by averaging over N_r channel realizations

$$\mathsf{BER}^{\mathsf{x}}_{\mathsf{MFB}} = \frac{1}{N_r}\sum_{N_r}\mathsf{BER}^{\mathsf{x}}_{\mathsf{MFB}}(\boldsymbol{h}) \ , \quad \mathsf{x}\in\{\mathsf{l},\mathsf{u}\} \ . \tag{4.9}$$

As for the BPSK case, the performance of this MFB is an upper bound on the performance of any 4BOK DS-UWB receiver that employs a front end filter with chip rate sampling.

4.1.2 MFB II

For the second MFB based on $y_\nu[k]$ (2.19) it is convenient to define the $N\times N$ matrix $\boldsymbol{H}_\nu[k]$ with element $\sum_{i=1}^{F} h_o^*[d_{\nu,i}]h_o[kN+d_{\nu,i}+m-j]$ in row m and column j, $1\le j,m\le N$. Then, the symbol-time impulse response from (2.20) can be rewritten as

$$h_{\nu\mu}[k] = \boldsymbol{c}_\nu^T\boldsymbol{H}_\nu[k]\boldsymbol{c}_\mu \ , \quad \mu,\nu\in\{1,2\} \ . \tag{4.10}$$

Using (4.10) and assuming a single symbol pair (a,b) is transmitted, the RAKE output $y_\nu[k]$ (2.19) is given by

$$y_\nu[k] = a\boldsymbol{c}_\nu^T\boldsymbol{H}_\nu[k]\boldsymbol{c}_b + n_\nu[k] \ , \quad \nu\in\{1,2\} \ . \tag{4.11}$$

We again consider an appropriately chosen window $k_s \le k < k_s + L$ of length L, such that this window captures a sufficient fraction η of the total energy of the impulse responses

$h_{\mu\nu}[\kappa]$, $\mu, \nu \in \{1, 2\}$. It is important to note that L is chosen such that $L = \max\{L_{\mu\nu}\}$, $\mu, \nu \in \{1, 2\}$ where $L_{\mu\nu}$ is the length that captures a fraction η of total energy of the impulse responses $h_{\mu\nu}[\kappa]$, $\mu, \nu \in \{1, 2\}$. Defining the following $2L$-dimensional vectors

$$\begin{aligned} \boldsymbol{H} &= [\boldsymbol{H}_1^T[k_s]\boldsymbol{c}_1 \ldots \boldsymbol{H}_1^T[k_s + L - 1]\boldsymbol{c}_1 \, \boldsymbol{H}_2^T[k_s]\boldsymbol{c}_2 \ldots \boldsymbol{H}_2^T[k_s + L - 1]\boldsymbol{c}_2]^T, \\ \boldsymbol{y} &= [y_1[k_s] \ldots y_2[k_s + L - 1] \, y_2[k_s] \ldots y_2[k_s + L - 1]]^T, \\ \boldsymbol{n} &= [n_1[k_s] \ldots n_2[k_s + L - 1] \, n_2[k_s] \ldots n_2[k_s + L - 1]]^T, \end{aligned} \tag{4.12}$$

we obtain the compact expression

$$\boldsymbol{y} = a\boldsymbol{H}\boldsymbol{c}_b + \boldsymbol{n} \, . \tag{4.13}$$

The noise $\boldsymbol{n}$ is jointly Gaussian with zero mean and covariance matrix $\boldsymbol{R}_{\boldsymbol{nn}}$, which depends on the RAKE finger delays $d_{\nu,i}$ and the auto- and cross-correlation functions of the spreading sequences $\boldsymbol{c}_1$ and $\boldsymbol{c}_2$.

From (4.13) and using the Cholesky decomposition $\boldsymbol{R}_{\boldsymbol{nn}} = \boldsymbol{L}\boldsymbol{L}^H$, we have the ML decision rule

$$(\hat{a}, \hat{b}) = \underset{(a,b)}{\mathsf{argmin}}\{||\boldsymbol{L}^{-1}(\boldsymbol{y} - a\boldsymbol{H}\boldsymbol{c}_b)||^2\} \, . \tag{4.14}$$

Finally, writing $\boldsymbol{c}(m) = a\boldsymbol{c}_b$ for the pair $(a, b)_m$, the PEP $P_e(m, n|\boldsymbol{h})$ follows as

$$P_e(m, n|\boldsymbol{h}) = \mathsf{Q}\left(||\boldsymbol{L}^{-1}\boldsymbol{H}(\boldsymbol{c}(n) - \boldsymbol{c}(m))||\right) \, . \tag{4.15}$$

Substituting $P_e(m, n|\boldsymbol{h})$ from (4.15) into (4.7) and (4.8) gives the corresponding upper and lower BER bound, respectively.

For the 4BOK DS-UWB receiver that employs chip rate sampling and F RAKE fingers for each of the two RAKEs (see Fig.2.2), the performance of this lower BER bound is the upper limit on the performance achievable by any post-rake equalization scheme.

4.2 Equalization Strategies

In this section the design of equalizers, which process the despread signals $y_\nu[k]$ (2.19), $\nu \in \{1,2\}$ is discussed,[1] to obtain decisions $(\hat{a}[k], \hat{b}[k])$. We aim at low-complexity solutions and therefore consider LE, DFE, and DDFSE. First, in Section 4.2.1, equalization strategies with separate feedforward filtering for $y_1[k]$ and $y_2[k]$ are devised. These strategies apply two feedback filters per despreading branch and are therefore referred to as equalization with SIMO filter optimization. It turns out, however, that 4BOK transmission is conveniently modelled by an equivalent MIMO system, for which a MIMO equalization strategy is devised in Section 4.2.2. Finally, by recognizing the non-circularity of the signals $y_\nu[k]$, WL processing for DS-UWB MIMO equalization is introduced in Section 4.2.3.

Throughout this section, we focus on DFE for the development of equalizer structures and filter optimization, and we briefly describe the necessary modifications for LE and DDFSE. We exclusively consider equalizer filter optimization according to the minimum mean-square error (MMSE) criterion, and, for the sake of conciseness, the prefix "MMSE" is omitted, when referring to the respective equalizers.

4.2.1 4BOK Equalization with SIMO Filter Optimization

Fig. 4.1 illustrates the straightforward approach to DFE for 4BOK. Assuming strong self-interference suppression, i.e., signal components spread with $\boldsymbol{c}_\mu$ are largely suppressed after despreading with $\boldsymbol{c}_\nu$, $\nu \neq \mu$, $\mu, \nu \in \{1,2\}$, the two despreader outputs $y_\nu[k]$ are processed by two separate feedforward filters (FFF) $f_{F,\nu}[k]$. Since the appropriate feedback filter (FBF) depends on the effective channel seen at the FFF output, i.e., it depends on $\boldsymbol{c}_{b[k]}$, two feedback filters $f_{B,\nu\mu}[k]$ per branch ν are needed. Therefore, this structure is referred to as DFE with SIMO filter optimization. It should be noted that, different from conventional

[1] Throughout this section, indices μ and ν are from the set $\{1,2\}$ and for the sake of readability, we omit repeated stating of $\mu \in \{1,2\}$ and $\nu \in \{1,2\}$, respectively.

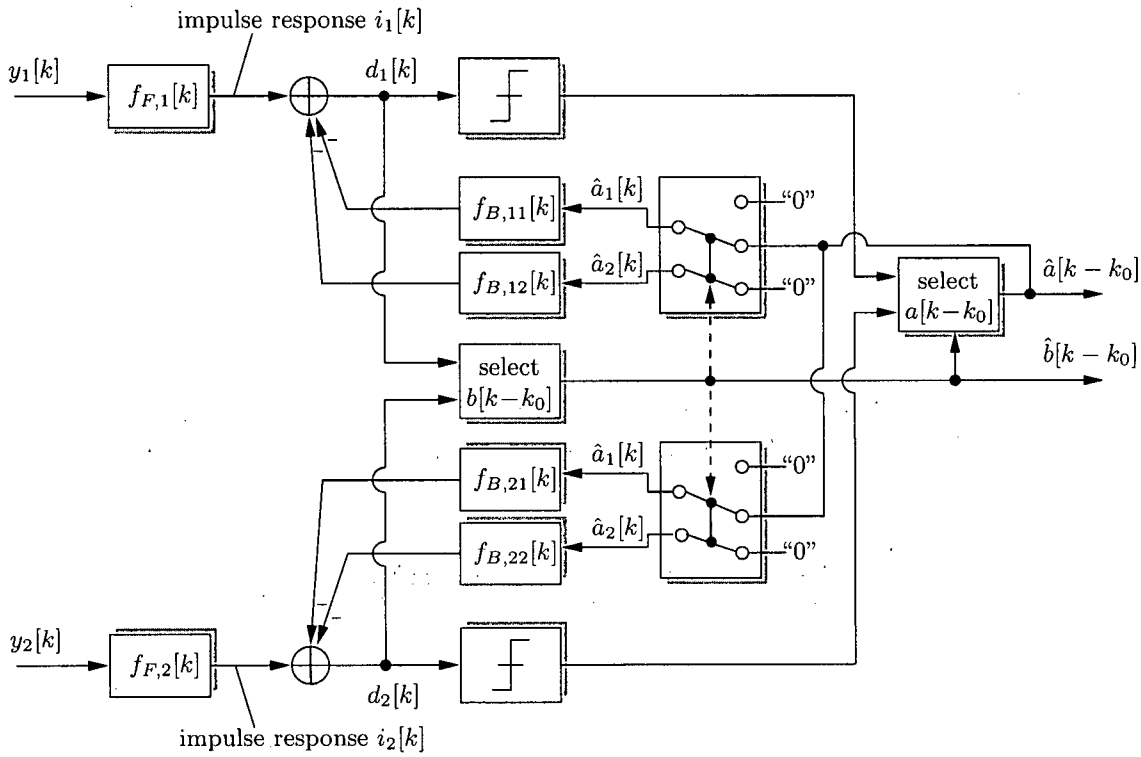

Figure 4.1: Block diagram of DFE with SIMO filter optimization for 4BOK DS-UWB.

DFE where the effective channel is known, a switch is required that selects the appropriate feedback filter according to the assumed effective channel depending on the estimated spreading code $\boldsymbol{c}_{\hat{b}[k]}$.

In order to appropriately model the data-dependent spreading codes of 4BOK, it is convenient to introduce a ternary data symbol

$$a_\mu[k] = \begin{cases} a[k] & \text{if } b[k] = \mu \\ 0 & \text{otherwise} \end{cases}, \tag{4.16}$$

which (a) accounts both for BPSK modulation and spreading code selection and (b) leads to a time-invariant overall channel impulse response. More specifically, the transmission channel between input $a_\mu[k]$ and ν_{th} RAKE output $y_\nu[k]$ can be formulated as (cf. (2.19)

and (2.20))

$$y_\nu[k] = a_1[k] * h_{\nu 1}[k] + a_2[k] * h_{\nu 2}[k] + n[k] \,. \tag{4.17}$$

The RAKE outputs $y_1[k]$ and $y_2[k]$ are fed to FFFs $f_{F,1}[k]$ and $f_{F,2}[k]$, respectively. The feedback part of the equalizer is used to eliminate ISI caused by previous symbols to the currently estimated symbols. For each equalizer branch, to cancel interference caused by the ith previous symbol, one of the two FBFs is chosen based on the previous decision $\hat{a}[k-i]$, assuming that the previous decision was correct. For example, if the previous symbol detected was $a_1[k-i]$ then for branch 1, FBF $f_{B,11}[k]$ is used and for branch two, FBF $f_{B,21}[k]$ is used to cancel ISI due to this symbol. On the other hand, if the previous symbol detected was $a_2[k-i]$ then for branch 1, FBF $f_{B,12}[k]$ is used and for branch two, FBF $f_{B,22}[k]$ is used. For each branch, the output of the feedback part, which is a weighted linear combination of the previous symbol decisions, is subtracted from the output of the FFF filter to give decision variable $d_\nu[k]$.

Defining the FFFs $\boldsymbol{f}_{F,\nu}$ and FBFs $\boldsymbol{f}_{B,\nu}$ as

$$\begin{aligned} \boldsymbol{f}_{F,\nu} &= \begin{bmatrix} f_{F,\nu}[0] & f_{F,\nu}[1] & \dots & f_{F,\nu}[q_F] \end{bmatrix}^H , \\ \boldsymbol{f}_{B,\nu\mu} &= \begin{bmatrix} f_{B,\nu\mu}[1] & f_{B,\nu\mu}[1] & \dots & f_{B,\nu\mu}[q_B] \end{bmatrix}^H , \end{aligned} \tag{4.18}$$

where q_F and q_B denote the order of FFFs and FBFs, respectively, the output of the DFE equalizer branch ν can be compactly written as (see Fig. 4.1)

$$d_\nu[k] = \boldsymbol{f}_{F,\nu}^H \boldsymbol{y}_\nu[k] - \boldsymbol{f}_{B,\nu\nu}^H \hat{\boldsymbol{a}}_{B,\nu}[k] - \boldsymbol{f}_{B,\nu\mu}^H \hat{\boldsymbol{a}}_{B,\mu}[k] \,, \quad \mu \neq \nu \,, \tag{4.19}$$

where the following definitions have been used

$$\begin{aligned} \boldsymbol{y}_\nu &= \begin{bmatrix} y_\nu[k] & y_\nu[k-1] & \dots & y_\nu[k-q_F] \end{bmatrix}^T , \\ \boldsymbol{h}_{\nu\mu} &= \begin{bmatrix} h_{\nu\mu}[k_0] & h_{\nu\mu}[k_0-1] & \dots & h_{\nu\mu}[k_0-q_F] \end{bmatrix}^T , \\ \hat{\boldsymbol{a}}_{B,\nu} &= \begin{bmatrix} \hat{a}_\nu[k-k_0-1] & \hat{a}_\nu[k-k_0-2] & \dots & \hat{a}_\nu[k-k_0-q_B] \end{bmatrix}^T . \end{aligned} \tag{4.20}$$

It should be noted that the estimates $\hat{a}_\mu[k]$ are the outputs of the switch in the feedback path (see Fig. 4.1). The data estimates for $b[k]$ and $a[k]$ are obtained as

$$\begin{aligned} \hat{b}[k-k_0] &= \underset{b=1,2}{\mathsf{argmax}}\{|\mathsf{Re}\{d_b[k]\}|\} \\ \hat{a}[k-k_0] &= \mathsf{sign}\{\mathsf{Re}\{d_{\hat{b}[k-k_0]}[k]\}\} \ , \end{aligned} \tag{4.21}$$

where k_0 is the decision delay, which has to be optimized, as was done for conventional DFE (cf. [VLC96]).

For the optimization of FFFs and FBFs according to the MMSE criterion, the equalizer error signal

$$e_\nu[k] = d_\nu[k] - a[k-k_0] \tag{4.22}$$

is considered. Two different approaches are pursued, which are referred to as Filter Design I and II.

4.2.1.1 Filter Design I

In Filter Design I for optimization of FFF $f_{F,\nu}$ we make the following assumption: due to the orthogonality between spreading sequence $\boldsymbol{c}_\mu$ and $\boldsymbol{c}_\nu$, signal components spread with $\boldsymbol{c}_\mu$ are largely suppressed after despreading with $\boldsymbol{c}_\nu$, $\nu \neq \mu$, i.e., $h_{\nu\mu}[k] \approx 0, \nu \neq \mu$. Therefore, ignoring the term $a_\nu[k] * h_{\nu\mu}[k]$, $\nu \neq \mu$, in (4.17), the received signal in equalizer branch ν is well approximated by

$$y_\nu[k] = a_\nu[k] * h_{\nu\nu}[k] + n[k] \ . \tag{4.23}$$

This means that the simplified error signal $e_\nu[k] = \boldsymbol{f}_{F,\nu}^H \boldsymbol{y}_\nu[k] - \boldsymbol{f}_{B,\nu\nu}^H \hat{\boldsymbol{a}}_{B,\nu}[k] - a[k-k_0]$ is used for filter optimization. Assuming, as usual, correct feedback decisions $\hat{a}[k] = a[k]$ [Pro01] and taking into account the correlation $\boldsymbol{\Phi}_{nn} = \mathsf{E}\{\boldsymbol{n}[k]\boldsymbol{n}^H[k]\}$ of noise $\boldsymbol{n}[k] = [n[k_0] \ \ldots \ n[k_0 - q_F]]$, the optimized FFFs are obtained as

$$\boldsymbol{f}_{F,\nu} = (\boldsymbol{A}_{\nu\nu}\boldsymbol{A}_{\nu\nu}^H - \boldsymbol{H}_{\nu\nu}\boldsymbol{H}_{\nu\nu}^H + \zeta\boldsymbol{\Phi}_{nn})^{-1}\boldsymbol{h}_{\nu\nu} \ , \tag{4.24}$$

where ζ denotes the SNR at the RAKE output and the following definitions are used

$$\boldsymbol{H}_{\nu\mu} = \begin{bmatrix} h_{\nu\mu}[k_0+1] & h_{\nu\mu}[k_0+2] & \dots & h_{\nu\mu}[k_0+q_B] \\ h_{\nu\mu}[k_0] & h_{\nu\mu}[k_0+1] & \dots & h_{\nu\mu}[k_0+q_B-1] \\ \vdots & \vdots & \vdots & \vdots \\ h_{\nu\mu}[k_0+1-q_F] & h_{\nu\mu}[k_0+2-q_F] & \dots & h_{\nu\mu}[k_0+q_B-q_F] \end{bmatrix}, \tag{4.25}$$

$$\boldsymbol{A}_{\nu\mu} = \begin{bmatrix} h_{\nu\mu}[0] & h_{\nu\mu}[1] & \dots & h_{\nu\mu}[L] & 0 & \dots & 0 \\ 0 & h_{\nu\mu}[0] & h_{\nu\mu}[1] & \dots & h_{\nu\mu}[L] & \ddots & 0 \\ \vdots & \ddots & \ddots & \ddots & \ddots & \ddots & 0 \\ 0 & \dots & 0 & h_{\nu\mu}[0] & h_{\nu\mu}[1] & \dots & h_{\nu\mu}[L] \end{bmatrix}. \tag{4.26}$$

The matrix $\boldsymbol{H}_{\nu\mu}$ and $\boldsymbol{A}_{\nu\mu}$ has dimensions $(q_F+1)\times q_B$ and $(q_F+1)\times(q_F+L+1)$.

Since, different from the design assumption for $\boldsymbol{f}_{F,\nu}$, the impulse responses $h_{\nu\mu}[k]$, $\mu \neq \nu$, are non-zero in general, the two feedback filters

$$\boldsymbol{f}_{B,\nu\mu} = \boldsymbol{H}_{\nu\mu}^H \boldsymbol{f}_{F,\nu} \tag{4.27}$$

are used to achieve postcursor cancellation (cf. (4.19) and Fig. 4.1).

Assuming $b[k] = 1$, Fig. 4.2 shows the magnitudes of the impulse responses $i_\nu[k] = f_{F,\nu}[k] * h_{\nu 1}[k]$ at the FFF outputs (circles) and of the corresponding the FBF coefficients $f_{B,\nu 1}[k]$ (stars) for an exemplary CM4 channel realization and spreading with code length $N = 6$ (cf. also Fig. 4.1). It can be seen that $i_1[k]$ is minimum phase with negligible precursors due to the MMSE optimization. For $\nu = 2 \neq b[k]$ we observe that (a) $i_2[k]$ is non-zero, i.e., orthogonality of the spreading codes is lost due to the UWB ISI channel, and (b) stronger precursors occur as $b[k] = 1$ is not accounted for in the design of $f_{F,2}[k]$. Postcursors are fully cancelled through the use of the two feedback filters $f_{B,\nu 1}[k] = i_\nu[k]$ for $k > k_0$.

4.2.1.2 Filter Design II

As illustrated in Fig. 4.2, a shortcoming of Filter Design I is the conceptual separation of the 4BOK transmission (4.17) into two parallel BPSK transmissions (4.23) for optimization

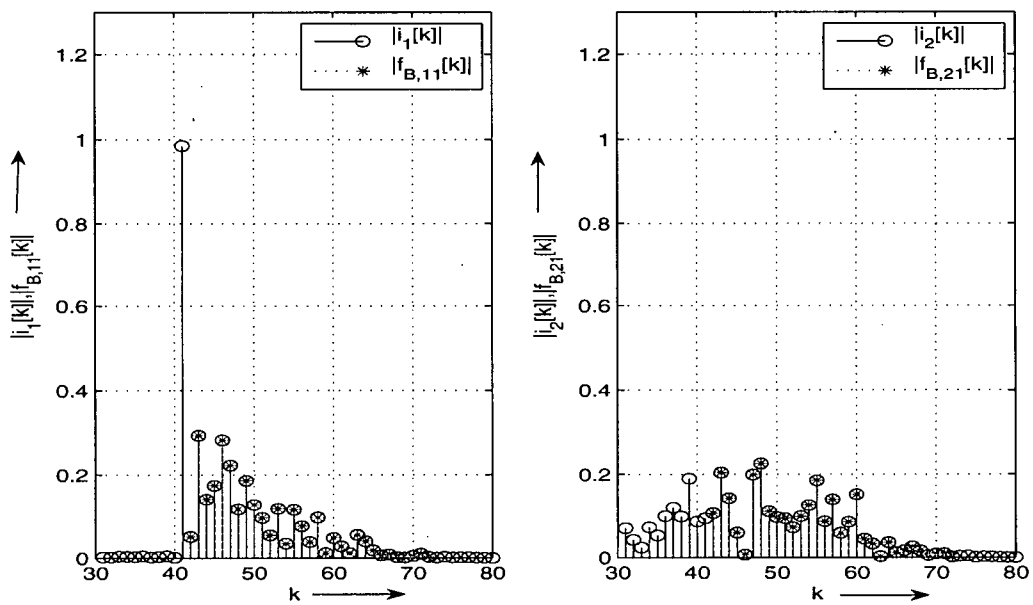

Figure 4.2: SIMO Filter Design I: Magnitudes of the impulse responses $i_\nu[k] = f_{F,\nu}[k] * h_{\nu 1}[k]$ at the FFF outputs (circles) and of the FBF coefficients $f_{B,\nu 1}[k]$ (stars) (see also Figs. 4.1 and 4.4) for an exemplary CM4 channel realization and spreading with code length $N = 6$.

of the FFFs $\boldsymbol{f}_{F,\nu}$ due to the assumption that $h_{\nu\mu}[k] \approx 0, \nu \neq \mu$. To overcome this problem, Filter Design II is directly based on (4.17), i.e, the error signal in (4.22) with $d_\nu[k]$ from (4.19) is used. Noting that

$$\mathsf{E}\left\{[a_1[k+\kappa]\, a_2[k+\kappa]]^T [a_1[k]\, a_2[k]]^*\right\} = \begin{bmatrix} \frac{1}{2}\delta[\kappa] & 0 \\ 0 & \frac{1}{2}\delta[\kappa] \end{bmatrix}, \tag{4.28}$$

the optimized FFF coefficients are given by

$$\boldsymbol{f}_{F,\nu} = (\frac{1}{2}(\boldsymbol{A}_{\nu 1}\boldsymbol{A}_{\nu 1}^H + \boldsymbol{A}_{\nu 2}\boldsymbol{A}_{\nu 2}^H - \boldsymbol{H}_{\nu 1}\boldsymbol{H}_{\nu 1}^H - \boldsymbol{H}_{\nu 2}\boldsymbol{H}_{\nu 2}^H) + \zeta\boldsymbol{\Phi}_{nn})^{-1}\boldsymbol{h}_{\nu\nu}\,. \tag{4.29}$$

The FBFs are given by (4.27) with $\boldsymbol{f}_{F,\nu}$ from (4.29).

Fig. 4.3 shows the magnitudes of the impulse responses $i_\nu[k]$ (circles) and of the FBF coefficients $f_{B,\nu 1}[k]$ (stars) with the FFFs according to (4.29). We observe that, different

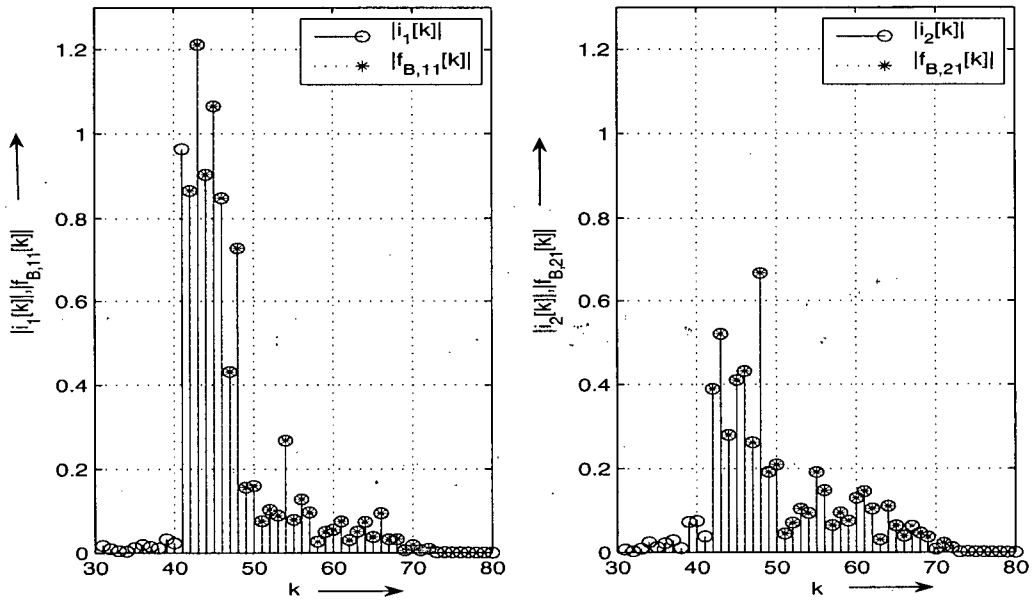

Figure 4.3: SIMO Filter Design II: Magnitudes of the impulse responses $i_\nu[k] = f_{F,\nu}[k] * h_{\nu 1}[k]$ at the FFF outputs (circles) and of the FBF coefficients $f_{B,\nu 1}[k]$ (stars) (see also Figs. 4.1 and 4.4) for an exemplary CM4 channel realization and spreading with code length $N = 6$.

from Filter Design I in Fig. 4.2, precursors of $i_2[k]$ are much better suppressed at the expense of slightly larger precursors in $i_1[k]$. This is due the fact that $\boldsymbol{f}_{F,\nu}$ from (4.29) is optimized such that both spreading sequences $\boldsymbol{c}_\nu$ are taken into account (compare with (4.24)). Clearly, the design of two separate FFFs cannot accomplish full precursor suppression in $i_1[k]$ and $i_2[k]$ at the same time. It can also be seen that $i_1[k]$ is not minimum phase, which causes increased error propagation for DFE and DDFSE.

4.2.1.3 LE based on Filter I and Filter II

In the case of LE, the decision variable reads

$$d_\nu[k] = \boldsymbol{f}_{f,\nu}^H \boldsymbol{y}_\nu[k] \,, \tag{4.30}$$

where $\boldsymbol{f}_{f,\nu}$ is optimized according to the MMSE criterion and follows as a special case of $\boldsymbol{f}_{F,\nu}$ for DFE with $q_F = q_f$ and $q_B = 0$. The optimized filter for SIMO filter I design can be expressed as

$$\boldsymbol{f}_\nu = (\boldsymbol{A}_{\nu\nu}\boldsymbol{A}_{\nu\nu}^H + \zeta\boldsymbol{\Phi}_{n_\nu n_\nu})^{-1}\boldsymbol{h}_{\nu\nu} \ , \tag{4.31}$$

and for SIMO filter II is given by

$$\boldsymbol{f}_\nu = (\frac{1}{2}(\boldsymbol{A}_{\nu 1}\boldsymbol{A}_{\nu 1}^H + \boldsymbol{A}_{\nu 2}\boldsymbol{A}_{\nu 2}^H) + \zeta\boldsymbol{\Phi}_{n_\nu n_\nu})^{-1}\boldsymbol{h}_{\nu\nu} \ . \tag{4.32}$$

The data estimates for $b[k]$ and $a[k]$ are obtained as in (4.21).

4.2.1.4 DDFSE based on Filter I and Filter II

In the case of DDFSE, we employ the Viterbi algorithm with $4^{q_{tr}}$ states $\boldsymbol{s}[k] = [\tilde{a}_1[k - k_0 - 1]\,\tilde{a}_2[k - k_0 - 1] \ldots \tilde{a}_1[k - k_0 - q_{tr}]\,\tilde{a}_2[k - k_0 - q_{tr}]]$. We apply the filters obtained from the optimization for DFE (cf. e.g. [GH96] for single-input single-output DDFSE), and the Viterbi branch metric variables are $(|d_1[k] - \tilde{a}_1[k - k_0]|^2 + |d_2[k] - \tilde{a}_2[k - k_0]|^2)$ with $d_\nu[k]$ from (4.19) and the $2q_{tr}$ feedback symbols $\hat{a}_\nu[k - k_0 - m]$, $1 \leq m \leq q_{tr}$, are replaced by the trial symbols in $\boldsymbol{s}[k]$. Introducing the following definitions

$$\begin{aligned} \boldsymbol{f}_{B,\nu\mu}^{q_{tr}} &= \begin{bmatrix} f_{B,\nu\mu}[1] & f_B\nu\mu[2] & \ldots & f_{B.\nu\mu}[q_{tr}] \end{bmatrix}^H , \\ \boldsymbol{f}_{B,\nu\mu}^{q_B - q_{tr}} &= \begin{bmatrix} f_{B,\nu\mu}[q_{tr}+1] & f_{B,\nu\mu}[q_{tr}+2] & \ldots & f_{B,\nu\mu}[q_B] \end{bmatrix}^H , \end{aligned} \tag{4.33}$$

The state metric $\lambda(\tilde{a}[k - k_0], \boldsymbol{s}[k])$ can be obtained as

$$\begin{aligned} \lambda(\tilde{a}[k - k_0], \boldsymbol{s}[k]) &= |\boldsymbol{f}_{F,1}^H \boldsymbol{y}_1[k] - \tilde{a}_1[k - k_0] - (\boldsymbol{f}_{B,1s}^{q_{tr}})^H \boldsymbol{s}[k] - (\boldsymbol{f}_{B,11}^{q_B - q_{tr}})^H \hat{\boldsymbol{a}}_{B,s}[k] \\ &\quad -(\boldsymbol{f}_{B,12}^{q_B - q_{tr}})^H \hat{\boldsymbol{a}}_{B,s}[k]|^2 \\ &\quad +|\boldsymbol{f}_{F,2}^H \boldsymbol{y}_2[k] - \tilde{a}_2[k - k_0] - (\boldsymbol{f}_{B,2s}^{q_{tr}})^H \boldsymbol{s}[k] - (\boldsymbol{f}_{B,22}^{q_B - q_{tr}})^H \hat{\boldsymbol{a}}_{B,s}[k] \\ &\quad -(\boldsymbol{f}_{B,21}^{q_B - q_{tr}})^H \hat{\boldsymbol{a}}_{B,s}[k]|^2 \end{aligned} \tag{4.34}$$

4.2.2 4BOK Equalization with MIMO Filter Optimization

From (4.17) we see that 4BOK with RAKE combining can be regarded as a MIMO transmission system. Therefore, defining the rake output vector as $\boldsymbol{y}[k] = [y_1[k]\, y_2[k]]^T$ and using equations (4.17) and (2.19) we arrive at the following expression

$$\boldsymbol{y}[k] = \sum_m \boldsymbol{H}[m]\boldsymbol{a}[k-m] + \boldsymbol{n}[k] = \boldsymbol{H}[k] * \boldsymbol{a}[k] + \boldsymbol{n}[k] \,, \tag{4.35}$$

with the (2×2) channel matrix

$$\boldsymbol{H}[k] = \begin{bmatrix} h_{11}[k] & h_{12}[k] \\ h_{21}[k] & h_{22}[k] \end{bmatrix} \tag{4.36}$$

and two-dimensional data vector $\boldsymbol{a}[k] = [a_1[k]\, a_2[k]]^T$ and noise vector $\boldsymbol{n}[k] = [n_1[k]\, n_2[k]]^T$. Note that the components of $\boldsymbol{a}[k]$ are drawn from a ternary alphabet according to (4.16) with autocorrelation as given in (4.28). We therefore conclude that MIMO equalization strategies, cf. e.g. [DH92, YR94], can be applied to 4BOK systems.

Fig. 4.4 shows the block diagram for MIMO-DFE. We define the vector $\underline{\boldsymbol{y}}[k]$ of despread signal samples, the vector $\underline{\hat{\boldsymbol{a}}}_B[k]$ of data estimates, and the vector $\underline{\boldsymbol{n}}[k]$ of noise samples as

$$\begin{aligned} \underline{\boldsymbol{y}}[k] &= \begin{bmatrix} \boldsymbol{y}^T[k] & \boldsymbol{y}^T[k-1] & \dots & \boldsymbol{y}^T[k-q_F] \end{bmatrix}^T , \\ \underline{\hat{\boldsymbol{a}}}_B[k] &= \begin{bmatrix} \hat{\boldsymbol{a}}^T[k-k_0-1] & \hat{\boldsymbol{a}}^T[k-k_0-2] & \dots & \hat{\boldsymbol{a}}^T[k-k_0-q_B] \end{bmatrix}^T , \\ \underline{\boldsymbol{n}}[k] &= \begin{bmatrix} \boldsymbol{n}^T[k] & \boldsymbol{n}^T[k-1] & \dots & \boldsymbol{n}^T[k-q_F] \end{bmatrix}^T , \end{aligned} \tag{4.37}$$

and the feedforward matrix filter $\underline{\boldsymbol{F}}_F^H$ and feedback matrix filter $\underline{\boldsymbol{F}}_B^H$ as

$$\begin{aligned} \underline{\boldsymbol{F}}_F^H &= \begin{bmatrix} \boldsymbol{F}_F^H[0] & \boldsymbol{F}_F^H[1] & \dots & \boldsymbol{F}_F^H[q_F] \end{bmatrix} , \\ \underline{\boldsymbol{F}}_B^H &= \begin{bmatrix} \boldsymbol{F}_B^H[1] & \boldsymbol{F}_B^H[2] & \dots & \boldsymbol{F}_B^H[q_B] \end{bmatrix} , \end{aligned} \tag{4.38}$$

with (2×2) component matrices $\boldsymbol{F}_F[k]$ and $\boldsymbol{F}_B[k]$ given by

$$\begin{aligned} \boldsymbol{F}_F[k] &= \begin{bmatrix} f_{F,11}[k] & f_{F,12}[k] \\ f_{F,21}[k] & f_{F,22}[k] \end{bmatrix} , \\ \boldsymbol{F}_B[k] &= \begin{bmatrix} f_{B,11}[k] & f_{B,12}[k] \\ f_{B,21}[k] & f_{B,22}[k] \end{bmatrix} , \end{aligned} \tag{4.39}$$

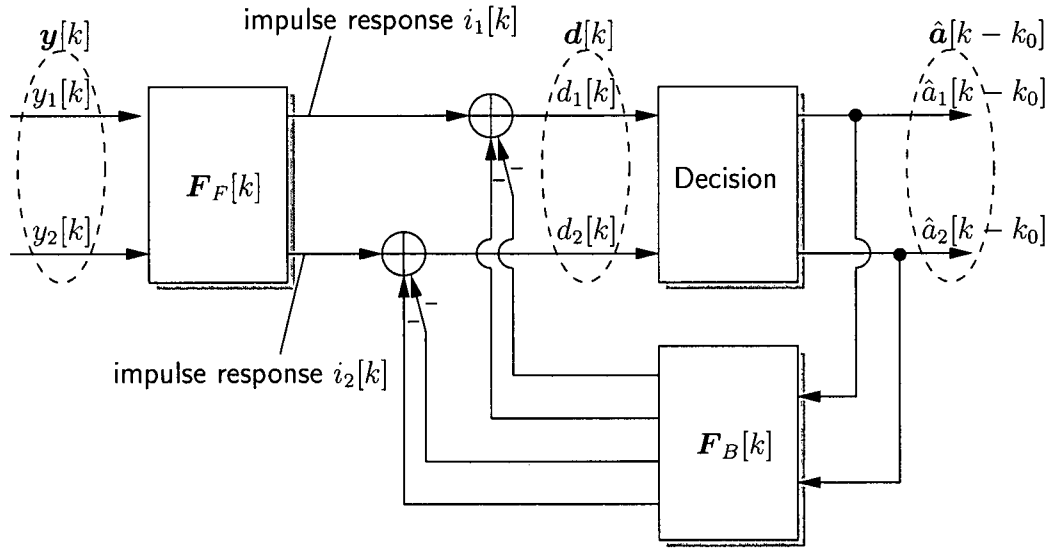

Figure 4.4: Block diagram of DFE with MIMO filter optimization for 4BOK DS-UWB.

where $f_{F,ij}$ and $f_{F,ij}$, $1 \leq i,j \leq 2$ denote the FFF and FBF coefficients, respectively (see Fig. 4.4). The MIMO-DFE decision variable $\boldsymbol{d}[k] = [d_1[k]\, d_2[k]]^T$ can now be written as

$$\boldsymbol{d}[k] = \underline{\boldsymbol{F}}_F^H \underline{\boldsymbol{y}}[k] - \underline{\boldsymbol{F}}_B^H \hat{\underline{\boldsymbol{a}}}_B[k] \,. \tag{4.40}$$

It should be noted that the matrix FFF $\underline{\boldsymbol{F}}_F$ for MIMO-DFE contains four scalar filters with, compared to the SIMO case, two additional cross-FFFs between $y_1[k]$ and $d_2[k]$ and between $y_2[k]$ and $d_1[k]$, respectively (cf. Figs. 4.1 and 4.4). Since the complexity of DFE is dominated by feedforward filtering, MIMO-DFE is approximately twice as complex as DFE with SIMO filter optimization from Section 4.2.1.

For optimization of the matrix filters $\underline{\boldsymbol{F}}_F$ and $\underline{\boldsymbol{F}}_B$, we again apply the MMSE criterion and follow the derivation in [ADS00]. Using the definitions in (4.37), the RAKE output $\underline{\boldsymbol{y}}[k]$ can be expressed as

$$\underline{\boldsymbol{y}}[k] = \underline{\boldsymbol{H}}\, \underline{\boldsymbol{a}}[k] + \underline{\boldsymbol{n}}[k] \,, \tag{4.41}$$

where $\underline{\boldsymbol{H}}$ is given by

$$\underline{\boldsymbol{H}} = \begin{bmatrix} \boldsymbol{H}[0] & \boldsymbol{H}[1] & \dots & \boldsymbol{H}[L] & 0 & \dots & 0 \\ 0 & \boldsymbol{H}[0] & \boldsymbol{H}[1] & \dots & \boldsymbol{H}[L] & \ddots & 0 \\ \vdots & \ddots & \ddots & \ddots & \ddots & \ddots & 0 \\ 0 & \dots & 0 & \boldsymbol{H}[0] & \boldsymbol{H}[1] & \dots & \boldsymbol{H}[L] \end{bmatrix} . \tag{4.42}$$

Then, the input-output cross-correlation matrix $\boldsymbol{R}_{\underline{\boldsymbol{ay}}}$ and output auto-correlation matrix $\boldsymbol{R}_{\underline{\boldsymbol{yy}}}$ are given by

$$\begin{aligned} \boldsymbol{R}_{\underline{\boldsymbol{ay}}} &= E\{\underline{\boldsymbol{a}}[k]\underline{\boldsymbol{y}}^H[k]\} = \boldsymbol{R}_{\underline{\boldsymbol{aa}}}\underline{\boldsymbol{H}}^H \\ \boldsymbol{R}_{\underline{\boldsymbol{yy}}} &= E\{\underline{\boldsymbol{y}}[k]\underline{\boldsymbol{y}}^H[k]\} = \underline{\boldsymbol{H}}\boldsymbol{R}_{\underline{\boldsymbol{aa}}}\underline{\boldsymbol{H}}^H + \boldsymbol{R}_{\underline{\boldsymbol{nn}}} \end{aligned} \tag{4.43}$$

where $\boldsymbol{R}_{\underline{\boldsymbol{aa}}}$ denotes the input auto-correlation matrix $\boldsymbol{R}_{\underline{\boldsymbol{aa}}} = E\{\underline{\boldsymbol{a}}[k]\underline{\boldsymbol{a}}^H[k]\}$ and a $\boldsymbol{R}_{\underline{\boldsymbol{nn}}}$ is the noise auto-correlation matrix $\boldsymbol{R}_{\underline{\boldsymbol{nn}}} = E\{\underline{\boldsymbol{n}}[k]\underline{\boldsymbol{n}}^H[k]\}$.

Defining the matrix $\boldsymbol{R}$ as

$$\boldsymbol{R} = \boldsymbol{R}_{\underline{\boldsymbol{aa}}}^{-1} + \underline{\boldsymbol{H}}^H\boldsymbol{R}_{\underline{\boldsymbol{nn}}}^{-1}\underline{\boldsymbol{H}} \tag{4.44}$$

and introducing the following definitions for matrix $\boldsymbol{\varphi}$, and $\boldsymbol{C}$

$$\begin{aligned} \boldsymbol{\varphi} &= \begin{bmatrix} \boldsymbol{I}_{2k_0\times 2(k_0+1)} \\ \boldsymbol{0}_{2\times 2k_0} \end{bmatrix} \\ \boldsymbol{C}^H &= \begin{bmatrix} \boldsymbol{0}_{2\times 2(k_0+1)} & \boldsymbol{I}_2 \end{bmatrix} , \end{aligned} \tag{4.45}$$

the optimized FBFs $\underline{\boldsymbol{F}}_B$ are obtained from [ADS00]

$$\begin{aligned} \underline{\underline{\boldsymbol{F}}}_B^H &= \boldsymbol{R}\boldsymbol{\varphi}(\boldsymbol{\varphi}^H\boldsymbol{R}\boldsymbol{\varphi})^{-1}\boldsymbol{C} \\ \underline{\underline{\boldsymbol{F}}}_B^H &= \begin{bmatrix} \boldsymbol{0}_{2\times 2k_0} & \boldsymbol{I}_2 & \underline{\boldsymbol{F}}_B^H \end{bmatrix} . \end{aligned} \tag{4.46}$$

As can be seen, $\underline{\boldsymbol{F}}_B$ is obtained from $\underline{\underline{\boldsymbol{F}}}_B^H$ after discarding a block of leading zeros and the matrix $\boldsymbol{I}_2$.

The optimized FFFs $\underline{\boldsymbol{F}}_F$ are then given by [ADS00],

$$\underline{\boldsymbol{F}}_F^H = \underline{\underline{\boldsymbol{F}}}_B^H\boldsymbol{R}_{\underline{\boldsymbol{ay}}}\boldsymbol{R}_{\underline{\boldsymbol{yy}}}^{-1} . \tag{4.47}$$

Assuming correct previous decisions, the decision vector $\boldsymbol{d}[k] = [d_1[k]\, d_2[k]]^T$ can be written as

$$\boldsymbol{d}[k] = \boldsymbol{a}[k-k_0] + \boldsymbol{e}[k]\,. \tag{4.48}$$

The error vector $\boldsymbol{e}[k]$ has the autocorrelation matrix $\boldsymbol{R}_{ee,\min}$ given by (cf. [ADS00])

$$\boldsymbol{R}_{ee,\min} = \boldsymbol{C}^H(\boldsymbol{\varphi}^H\boldsymbol{R}\boldsymbol{\varphi})^{-1}\boldsymbol{C}. \tag{4.49}$$

Assuming $\boldsymbol{e}[k]$ is approximately Gaussian distributed, the decision rule

$$\hat{\boldsymbol{a}}[k-k_0] = \underset{\boldsymbol{a}[k-k_0]}{\operatorname{argmin}} \left\{(\boldsymbol{d}[k] - \boldsymbol{a}[k-k_0])^H \boldsymbol{R}_{ee,\min}^{-1}(\boldsymbol{d}[k] - \boldsymbol{a}[k-k_0])\right\} \tag{4.50}$$

is obtained. It should be noted that the optimization in (4.50) is performed for the 4-ary vector signal set $\boldsymbol{a}[k] \in \{\binom{1}{0}, \binom{-1}{0}, \binom{0}{-1}, \binom{0}{1}\}$ (see (4.16)).

The decision metric (4.50) considerably simplifies if we assume that $e_1[k]$ and $e_2[k]$ are uncorrelated and have identical variance σ_e^2, i.e., $\boldsymbol{R}_{ee,\min} = \sigma_e^2\boldsymbol{I}_2$. Then, we have

$$\hat{\boldsymbol{a}}[k-k_0] = \underset{\boldsymbol{a}[k-k_0]}{\operatorname{argmax}} \left\{\mathrm{Re}\{\boldsymbol{d}^H[k]\boldsymbol{a}[k-k_0]\}\right\}\,. \tag{4.51}$$

Considering the particular 4-ary signal set of $\boldsymbol{a}[k]$, (4.51) can be simplified to the two-stage decision in (4.21).

Fig. 4.5 depicts the magnitudes of the impulse responses $i_\nu[k]$ (circles) and FBF coefficients $f_{B,\nu 1}[k]$ (stars) with the MIMO FFFs. Compared to the SIMO filter optimization cases in Figs. 4.2 and 4.3, improved precursor suppression is achieved and the impulse responses more closely resemble[2] minimum-phase responses, which is crucial for efficient DFE and DDFSE.

[2]The minimum–phase criterion for $\boldsymbol{J}[k] = \sum_{m=0}^{q_F} \boldsymbol{F}_F^H[m]\boldsymbol{H}[k-m]$ does not imply that the scalar elements of $\boldsymbol{J}[k]$ are minimum-phase responses (cf. e.g. [GT04]).

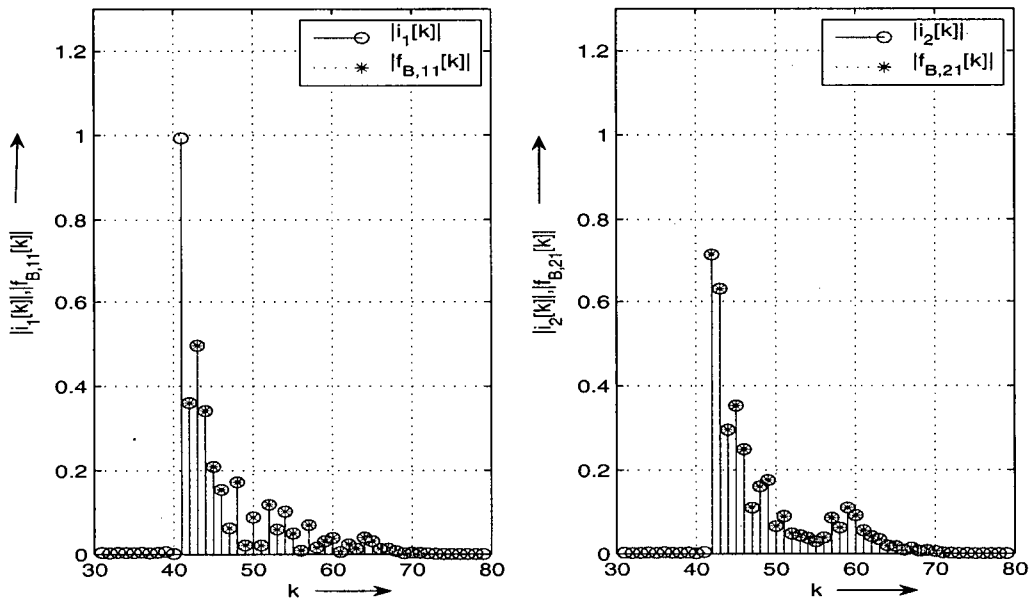

Figure 4.5: MIMO Filter Design: Magnitudes of the impulse responses $i_\nu[k] = f_{F,\nu}[k] * h_{\nu 1}[k]$ at the FFF outputs (circles) and of the FBF coefficients $f_{B,\nu 1}[k]$ (stars) (see also Figs. 4.1 and 4.4) for an exemplary CM4 channel realization and spreading with code length $N = 6$.

4.2.2.1 MIMO Optimization based LE and DDFSE

As for the SIMO filter optimization case, we use the DFE filters also for, respectively, LE and DDFSE with MIMO FFF. In case of LE, the decision variable reads

$$\boldsymbol{d}[k] = \underline{\boldsymbol{F}}_f^H \underline{\boldsymbol{y}}[k] \,, \tag{4.52}$$

where $\underline{\boldsymbol{F}}_f = \underline{\boldsymbol{F}}_F$ for DFE with $q_F = q_f$ and $q_B = 0$. For DDFSE the Viterbi algorithm has $4^{q_{tr}}$ states $\boldsymbol{S}[k] = [\tilde{\boldsymbol{a}}^T[k-k_0-1] \ldots \tilde{\boldsymbol{a}}^T[k-k_0-q_{tr}]]^T$, and the Viterbi branch metric variables are $||\boldsymbol{d}[k] - \tilde{\boldsymbol{a}}[k-k_0]||^2$ from (4.40) with q_{tr} feedback symbols $\hat{\boldsymbol{a}}[k-k_0-m]$, $1 \leq m \leq q_{tr}$, replaced by the trial symbols in $\boldsymbol{S}[k]$. Mathematically, the branch metric can be expressed as

$$\lambda(\hat{\boldsymbol{a}}[k-k_0], \boldsymbol{S}[k]) = ||\underline{\boldsymbol{F}}_F^H \underline{y}[k] - \hat{\boldsymbol{a}}[k-k_0] - (\underline{\boldsymbol{F}}_B^{q_{tr}})^H \boldsymbol{S}[k] - (\underline{\boldsymbol{F}}_B^{q_B - q_{tr}})^H \underline{\hat{\boldsymbol{a}}}_{B,S[k]}||^2. \tag{4.53}$$

4.2.3 4BOK Equalization with WL-MIMO Filter Optimization

From (4.16) it is easy to see that the correlation between $\boldsymbol{a}[k]$ and $\boldsymbol{a}^*[k]$ is non-zero:

$$\mathsf{E}\{\boldsymbol{a}[k+\kappa]\boldsymbol{a}^T[k]\} = \begin{bmatrix} \frac{1}{2}\delta[\kappa] & 0 \\ 0 & \frac{1}{2}\delta[\kappa] \end{bmatrix} . \tag{4.54}$$

Furthermore, the pseudo-autocorrelation function [NM93] of the received sequence $\boldsymbol{y}[k]$

$$\mathsf{E}\{\boldsymbol{y}[k+\kappa]\boldsymbol{y}^T[k]\} = \frac{1}{2}\boldsymbol{H}[\kappa] * \boldsymbol{H}[\kappa] \tag{4.55}$$

is also nonzero, implying that $\boldsymbol{y}[k]$ is non-circular. As explained in Section 3.2.2, for a non-circular $\boldsymbol{y}[k]$, WL processing can be applied to the MMSE based equalization schemes. WL MMSE equalization schemes, in particular WLE and WDFE schemes, for SISO channels have been developed by in [GSL03]. Furthermore, in [MPS05] these schemes have been extended to the MIMO channel case considering complex baseband transmission with a mixture of real- and complex-valued modulations. In the following, we discuss 4BOK equalization schemes based on the application of widely linear processing to the MIMO filter optimization discussed in the previous section.

In order to cast the receiver processing and the filter optimization for 4BOK equalization with WL-MIMO-DFE in a form analogous to the "linear" case discussed in the previous section, it is useful to introduce the transformation

$$\boldsymbol{X} \xrightarrow{\mathcal{T}} \bar{\boldsymbol{X}} : \quad \bar{\boldsymbol{X}} = \frac{1}{\sqrt{2}}\left[\boldsymbol{X}^T\, \boldsymbol{X}^H\right]^T \tag{4.56}$$

for a general matrix (vector) $\boldsymbol{X}$. Applying this transformation to the variables in (4.35), we obtain the augmented MIMO channel description

$$\bar{\boldsymbol{y}}[k] = \bar{\boldsymbol{H}}[k] * \boldsymbol{a}[k] + \bar{\boldsymbol{n}}[k] . \tag{4.57}$$

Substituting this MIMO channel description for (4.35), we can immediately use the results of [ADS00] for WL-MIMO-DFE filter optimization. Using (4.56) and (4.41), we obtain

$$\underline{\bar{\boldsymbol{y}}}[k] = \underline{\bar{\boldsymbol{H}}}\, \underline{\boldsymbol{a}}[k] + \underline{\bar{\boldsymbol{n}}}[k] , \tag{4.58}$$

where $\underline{\bar{y}}[k]$, $\underline{a}[k]$, and $\underline{\bar{n}}[k]$ are defined using (4.56) and (4.37) and the matrix $\underline{\bar{H}}$ can be obtained by replacing $\boldsymbol{H}[k]$ by $\bar{\boldsymbol{H}}[k]$ in (4.42). The definitions of noise autocorrelation matrix $\boldsymbol{R}_{\underline{a\bar{y}}}$, the input-output cross-correlation matrix $\boldsymbol{R}_{\underline{a\bar{y}}}$ and output auto-correlation matrix $\boldsymbol{R}_{\underline{\bar{y}\bar{y}}}$ are given by

$$\begin{aligned}
\boldsymbol{R}_{\underline{\bar{n}\bar{n}}} &= E\{\underline{\bar{n}}[k]\underline{\bar{n}}^H[k]\} = \frac{1}{2}\begin{bmatrix} \boldsymbol{R}_{\underline{nn}} & 0 \\ 0 & \boldsymbol{R}_{\underline{nn}} \end{bmatrix}, \\
\boldsymbol{R}_{\underline{a\bar{y}}} &= E\{\underline{a}[k]\underline{\bar{y}}^H[k]\} = \boldsymbol{R}_{\underline{aa}}\underline{\bar{H}}^H, \\
\boldsymbol{R}_{\underline{\bar{y}\bar{y}}} &= E\{\underline{\bar{y}}[k]\underline{\bar{y}}^H[k]\} = \underline{\bar{H}}\boldsymbol{R}_{\underline{aa}}\underline{\bar{H}}^H + \boldsymbol{R}_{\underline{\bar{n}\bar{n}}}. \qquad (4.59)
\end{aligned}$$

It should be noted that the correlated noise at the RAKE output $\bar{\boldsymbol{n}}[k]$ is circular i.e., $\mathsf{E}\{\bar{\boldsymbol{n}}[k]\bar{\boldsymbol{n}}^T[k]\} = 0$. Furthermore, defining the matrix $\boldsymbol{R}_{WL}$ as

$$\boldsymbol{R}_{WL} = \boldsymbol{R}_{\underline{aa}} + \underline{\bar{H}}^H\boldsymbol{R}_{\underline{\bar{n}\bar{n}}}\underline{\bar{H}}, \qquad (4.60)$$

the FFF matrix $\underline{\boldsymbol{F}}_{F,WL}$and FBF matrix $\underline{\boldsymbol{F}}_{B,WL}$, which can be defined by (4.38) and (4.39) by using variables $\boldsymbol{F}_{x,WL}[k]$ and $f_{x,WL,ij}$,, $x \in \{F,B\}$, $1 \le i,j \le 2$ instead of $\boldsymbol{F}_x[k]$ and $f_{x,ij}$, , $x \in \{F,B\}$, $1 \le i,j \le 2$, is given by (see (4.46))

$$\begin{aligned}
\underline{\underline{\boldsymbol{F}}}^H_{B,WL} &= \boldsymbol{R}_{WL}\boldsymbol{\varphi}(\boldsymbol{\varphi}^H\boldsymbol{R}_{WL}\boldsymbol{\varphi})^{-1}\boldsymbol{C} \\
\underline{\underline{\boldsymbol{F}}}^H_{B,WL} &= \begin{bmatrix} \boldsymbol{0}_{2\times 2k_0} & \boldsymbol{I}_2 & \underline{\boldsymbol{F}}^H_{B,WL} \end{bmatrix}, \qquad (4.61)
\end{aligned}$$

where $\boldsymbol{\varphi}$ and $\boldsymbol{C}$ are defined in (4.45). Again, as in the "linear" MIMO-DFE case,the FBF matrix $\underline{\boldsymbol{F}}^H_{B,WL}$ is obtained from $\underline{\underline{\boldsymbol{F}}}^H_{B,WL}$ after discarding a block of leading zeros and the matrix $\boldsymbol{I}_2$. Also, it should be noted that all FBF coefficients $f_{B,WL,ij}$, $1 \le i,j \le 2$, are real valued.

The feedforward matrix filter $\underline{\bar{\boldsymbol{F}}}_{F,WL} = [\underline{\boldsymbol{F}}^T_{F,WL}\underline{\boldsymbol{F}}^H_{F,WL}]^T$ is given by [ADS00]

$$\underline{\bar{\boldsymbol{F}}}^H_{F,WL} = \underline{\underline{\boldsymbol{F}}}^H_{B,WL}\boldsymbol{R}_{\underline{a\bar{y}}}\boldsymbol{R}^{-1}_{\underline{\bar{y}\bar{y}}}. \qquad (4.62)$$

The WL-MIMO-DFE decision variable reads (compare with (4.40))

$$\bar{\boldsymbol{d}}[k] = \underline{\bar{\boldsymbol{F}}}^H_F\underline{\bar{\boldsymbol{y}}}[k] - \underline{\boldsymbol{F}}^T_B\underline{\hat{\boldsymbol{a}}}_B[k] = 2\mathsf{Re}\{\underline{\boldsymbol{F}}^H_F\underline{\boldsymbol{y}}[k]\} - \underline{\boldsymbol{F}}^T_B\underline{\hat{\boldsymbol{a}}}_B[k]. \qquad (4.63)$$

The data estimates are obtained by following the decision rule in (4.21). It should be noted that the complexity of WL-MIMO-DFE is slightly lower than that of MIMO-DFE (4.40), since the coefficients of the feedback filter $\underline{\boldsymbol{F}}_B^T$ are real valued.

4.2.3.1 WL-MIMO-LE and WL-MIMO-DDFSE

WL-MIMO-LE uses the same FFF as WL-MIMO-DFE assuming $q_B = 0$ and the decision variable is $\bar{\boldsymbol{d}}[k] = \mathsf{Re}\{\underline{\boldsymbol{F}}_F^H \underline{\boldsymbol{y}}[k]\}$. WL-MIMO-DDFSE applies the WL-MIMO-DFE FFFs and FBFs and the Viterbi algorithm with $4^{q_{tr}}$ states as described for MIMO-DDFSE. The WL-MIMO-DDFSE branch metric $\lambda(\hat{\boldsymbol{a}}[k-k_0], \boldsymbol{S}[k])$ is given by

$$\lambda(\hat{\boldsymbol{a}}[k-k_0], \boldsymbol{S}[k]) = (2\mathsf{Re}\{\underline{\boldsymbol{F}}_{F,WL}^H \underline{\boldsymbol{y}}[k]\} - \hat{\boldsymbol{a}}[k-k_0] - (\underline{\boldsymbol{F}}_{B,WL}^{q_{tr}})^H \boldsymbol{S}[k] - (\underline{\boldsymbol{F}}_{B,WL}^{q_B-q_{tr}})^H \underline{\hat{\boldsymbol{a}}}_{B,S[k]})^2 \,. \tag{4.64}$$

From a comparison of (4.64) and (4.53), it can be concluded that the complexity of WL-MIMO-DDFSE is slightly lower than that of MIMO-DDFSE (4.40), since the components of vectors $\underline{\boldsymbol{F}}_{B,WL}^{q_{tr}}$ and $\underline{\boldsymbol{F}}_{B,WL}^{q_B-q_{tr}}$ are real valued.

Chapter 5

Results and Discussion

In this chapter, the simulation results for the various equalization schemes considered for BPSK and 4BOK DS-UWB systems are presented. First we present results for BPSK DS-UWB systems in Section 5.1. In Chapter 3, the analysis of the distribution of zeros for DS-UWB systems was discussed. Based on this, in Section 5.1.2, we present the results for distribution of zeros for three different scenarios corresponding to different channels and data rates. Subsequently, based on information from these distribution results, we analyse the equalizer designs for BPSK DS-UWB systems. These predictions about the equalizer designs are then compared with the actual performance results obtained for LE, DFE and DDFSE equalization schemes for BPSK DS-UWB systems in Section 5.1.3. Furthermore, performance results obtained from the application of widely linear processing to LE, DFE and DDFSE are compared with the performance of the corresponding "linear" equalization schemes. Second, we present results for 4BOK DS-UWB systems in Section5.2. In Section 5.2.2 equalization techniques based on SIMO filter optimization are compared with those based on MIMO. Also, MIMO-LE and MIMO-DFE schemes are compared with MIMO-WLE and MIMO-WDFE, respectively. Finally, the absolute performance results for 4BOK WL-MIMO equalization schemes are presented.

5.1 Performance Results and Discussion for BPSK DS-UWB Systems

In this section we provide results obtained for the distribution of zeros of the overall channel transfer function and the performance results for the LE, DFE and DDFSE equalization schemes for BPSK DS-UWB systems. Furthermore, results for comparison of the performances of "linear" and "widely linear" schemes are also shown. First, we describe the system parameters used in simulations.

5.1.1 Simulation Parameters

We consider the lower UWB operating band from 3.1 to 4.85 GHz. The system parameters are as specified in Table 5.1, except for the case when we study the effect of varying the number of RAKE fingers F in Section 5.1.3.3. For the results showing the performance of the various equalization schemes, simulations are performed over $N_r = 100$ channel realizations of CM1 and CM4. The results show the performance averaged over the best 90 out of 100 channel realizations, cf. [P8002]. For all simulations it is assumed that perfect channel state information is available at the receiver. For a fair comparison of (W)LE[1] and (W)DFE, we choose $q_f = q_F$. This is because the feedback part of (W)DFE does not involve any multiplications, but only sign-changes and subtractions, and hence practically does not contribute to the overall complexity of (W)DFE. For all equalization schemes a favorable delay parameter k_0 is found by testing various k_0 within a reasonable range [VLC96].

The BER results are plotted as functions of $10\log_{10}(E_b/N_0)$, where E_b is the average received energy per data bit $a[k]$ assuming optimum matched filtering, i.e., $E_b = \mathsf{E}\{E_b(r)\}$ with $E_b(r)$ from (3.5). As discussed in Sections 3.2.1.3 and 3.2.2.3, (W)DDFSE uses the same FFF as (W)DFE and the number of states is two, i.e., $q_{tr} = 1$ is applied.

[1]The notation (W)LE/DFE/DDFSE is used when we refer to both "linear" LE/DFE/DDFSE and "widely linear" LE/DFE/DDFSE.

Table 5.1: Parameters for the considered BPSK DS-UWB systems.

BPSK Spreading Codes [FKMW05]	$N = 24$: $[-1, 0, 1, -1, -1, -1, 1, 1, 0, 1, 1, 1, 1, -1, 1, -1, 1, 1, 1, -1, 1, -1, -1, 1]$ $N = 6$: $[1, 0, 0, 0, 0, 0]$
Channel Models	CM1 and CM4, lower band from 3.1 to 4.85 GHz (see Section 2.3 and [P8002])
Pulse shape	Square root-raised cosine ($\alpha = 0.3$) [FKMW05]
Data rates	57 Mbps ($N = 24$) and 220 Mbps ($N = 6$) [FKMW05]
Number of RAKE fingers	$F = 16$ [TK04] (except in Section 5.1.3.3)

5.1.2 Application of Distribution of Zeros to Equalizer Design for DS-UWB

In section 3.1.2, an expression for the overall channel transfer function for BPSK DS-UWB systems, which takes into account the effect of the spreading code, the RRC transmit filter, the UWB channel, the receiver filter and the F finger RAKE, is derived and analytical expressions for probability density function and cumulative distribution function for the zeros were reviewed. In the following, the results for the distribution of zeros for different channel scenarios and spreading sequence lengths are discussed. In particular, we have evaluated the expressions (3.12), (3.14), (3.15) for the DS-UWB system with spreading codes of lengths $N = 24$ (lower data-rate mode) and $N = 6$ (high data-rate mode) and channel models CM1 and CM4, which constitute the two extreme cases in terms of rms delay spread [P8002].

For DS-UWB with $N = 24$ and CM1, Figs. 5.1(a)-(c) show the normalized density $f_z(z)/(L-1)$, the normalized marginal density $f_r(r)/(L-1)$, and the normalized number of zeros $n(R)/(L-1)$ inside the disc $|z| \leq R$, respectively. It can be seen that all the zeros are located inside $|z| < 0.3$. Based on the discussion in Section 3.1.2.4, we conclude that

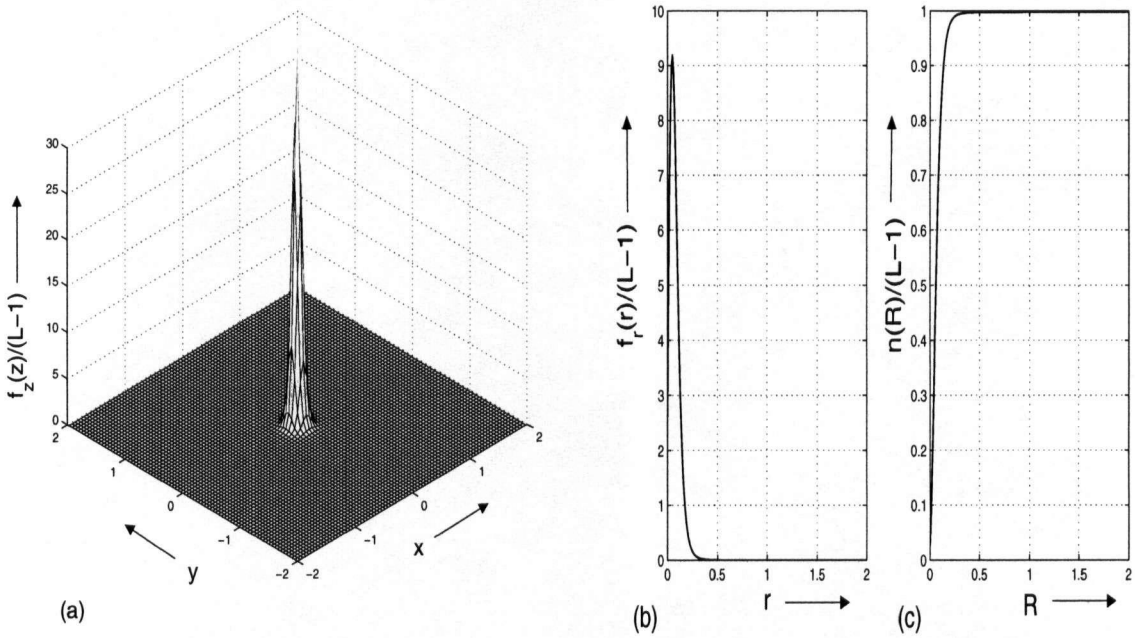

Figure 5.1: UWB CM1 and $N = 24$. $z = x + \mathrm{j}y$. (a) Normalized density $f_z(z)/(L-1)$ of zeros of effective transfer function $H(z)$. (b) Normalized marginal density $f_r(r)/(L-1)$ of zeros of $H(z)$. (c) Normalized average number $n(R)/(L-1)$ of zeros of $H(z)$ inside the disc $|z| \leq R$.

LE should perform well for CM1 and $N = 24$, and that DFE/DDFSE will yield only very small improvements.

Figs. 5.2(a)-(c) depict the mentioned functions considering the same spreading code length $N = 24$ but CM4. We observe that all zeros lie inside $|z| < 0.6$. Thus, for CM4 with significant multipath components and relatively large delays, we expect that LE after RAKE combining works well and that DFE/DDFSE lead to only small performance improvements. However, we expect larger gains with DFE/DDFSE than for the CM1, $N = 24$ case.

For higher data-rate DS-UWB systems, shorter spreading code lengths are used. For $N = 6$ and CM4, Figs. 5.3(a)-(c) show the distribution of zeros. As can be seen, the distribution is quite different from those for the long spreading code with $N = 24$. For

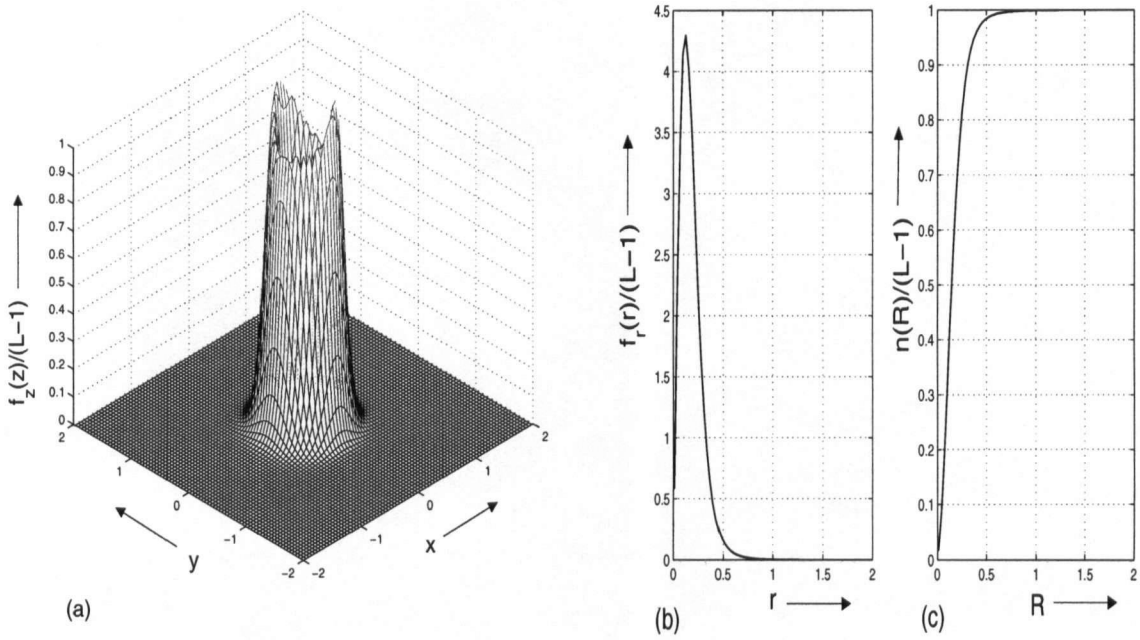

Figure 5.2: UWB CM4 and $N = 24$. $z = x + jy$. (a) Normalized density $f_z(z)/(L-1)$ of zeros of effective transfer function $H(z)$. (b) Normalized marginal density $f_r(r)/(L-1)$ of zeros of $H(z)$. (c) Normalized average number $n(R)/(L-1)$ of zeros of $H(z)$ inside the disc $|z| \leq R$.

this high-rate (220 Mbps) DS-UWB system, a considerable fraction of zeros lies close to and outside the unit circle. In particular, from Fig 5.3(b) we observe that about $x(\infty) \approx 0.35(L-1)$ zeros lie outside the unit circle. We thus anticipate that a FFF has to be applied for DFE and DDFSE to avoid a considerable performance loss due to the non-minimum-phase impulse response. Since there are also zeros very close to the unit circle, LE is expected to suffer from a significant performance degradation.

5.1.3 Simulation Results for BPSK DS-UWB Systems

In this section, the performance results for the proposed equalization schemes for DS-UWB systems using BPSK modulation are presented and compared with (a) the three MFBs

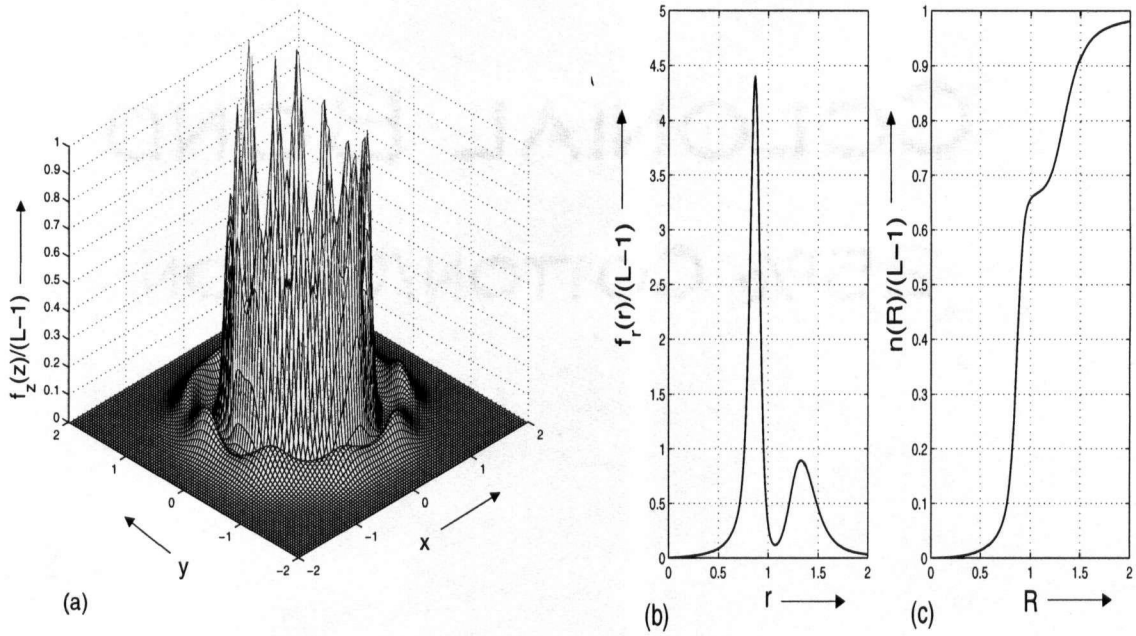

Figure 5.3: UWB CM4 and $N = 6$. $z = x + \mathrm{j}y$. (a) Normalized density $f_z(z)/(L-1)$ of zeros of effective transfer function $H(z)$. (b) Normalized marginal density $f_r(r)/(L-1)$ of zeros of $H(z)$. (c) Normalized average number $n(R)/(L-1)$ of zeros of $H(z)$ inside the disc $|z| \leq R$.

developed in Section 3.1.1, and (b) the findings from studying the distribution of the zeros of $H(z)$ in Section 5.1.2. First, the BER results for the different equalization strategies without WL processing and with $F = 16$ RAKE fingers are presented. Subsequently, the improvement due to WL processing (Section 5.1.3.2) and the effect of a finite number F of RAKE fingers (Section 5.1.3.3) are considered.

5.1.3.1 Equalization Strategies and MFBs

Fig. 5.4 shows the BER performance of the DS-UWB system for spreading code length $N = 24$ and CM1 as function of $10\log_{10}(E_b/N_0)$. We compare MMSE-LE with a two-tap filter $\boldsymbol{f}$ and MMSE-DFE also with a two-tap FFF $\boldsymbol{f}_F$ and a single-tap FBF $\boldsymbol{f}_B$. Although

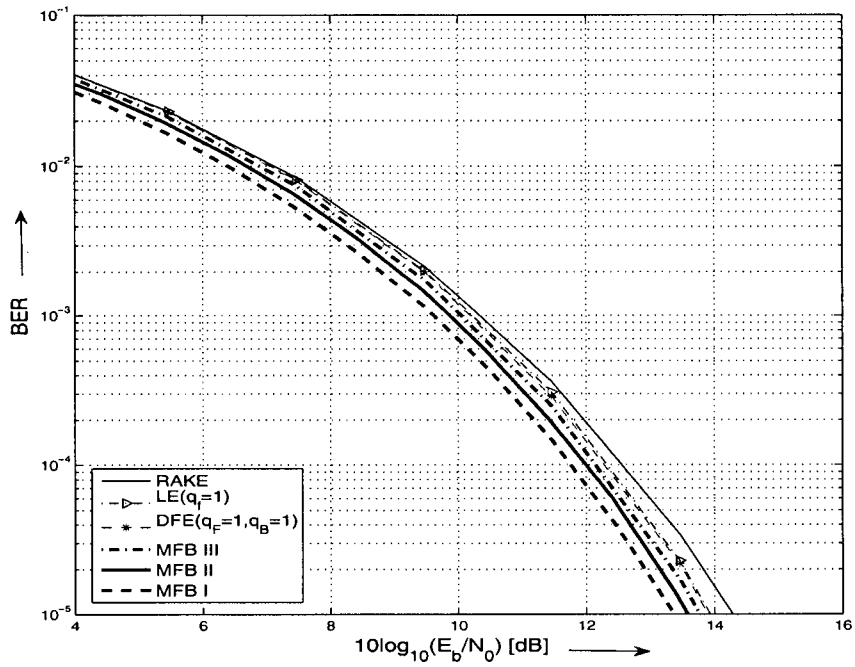

Figure 5.4: BER versus $10\log_{10}(E_b/N_0)$ *for MMSE-LE and MMSE-DFE for CM1 and* $N = 24$. *Also shown: RAKE combining without equalization and MFBs I-III (cf. Section 3.1.1).*

the effective channels are minimum phase (cf. Section 3.1.2.4), the short FFF is beneficial for DFE with this short FBF length. The BER curves without equalization (labeled as RAKE) and the MFBs I-III are also plotted in Fig. 5.4.

As anticipated from the analysis in Section 5.1.2 (cf. Figs. 5.1(a)-(c)), LE and DFE achieve practically identical performances. The loss in power efficiency compared to MFB III is only about 0.15 dB at $\mathsf{BER} = 10^{-5}$ and hence, DDFSE (not shown) does not yield a significant performance improvement. In fact, simple RAKE combining without additional equalization already approaches MFB III within 0.5 dB at $\mathsf{BER} = 10^{-5}$. This can be attributed to the facts that (a) the delay spread for CM1 is relatively short, and (b) a long spreading code is applied. MFB II and MFB III are almost identical, which means that 16 RAKE fingers are (more than) sufficient for CM1. Interestingly, the gap between MFB I

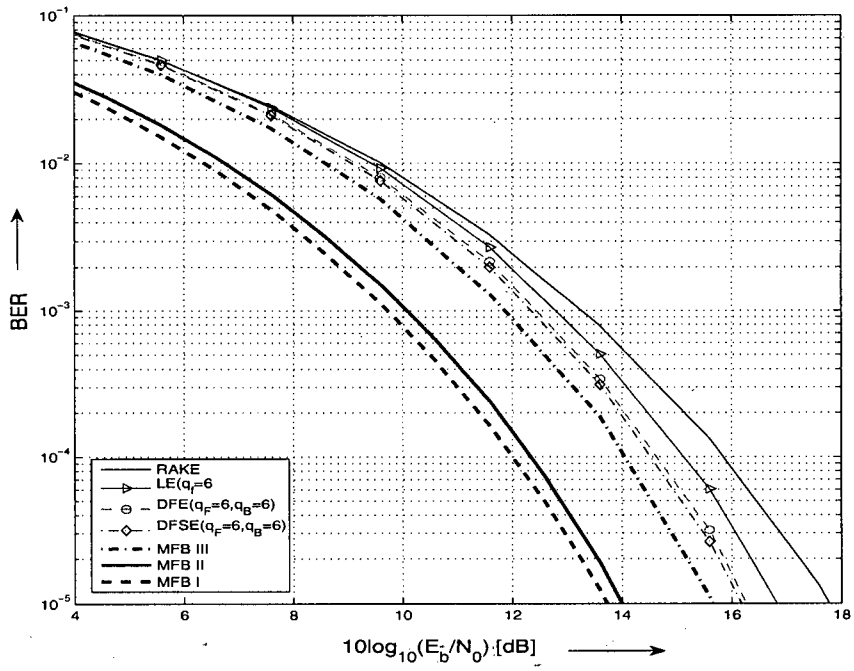

Figure 5.5: BER versus $10\log_{10}(E_b/N_0)$ *for MMSE-LE, MMSE-DFE, and MMSE-DDFSE for CM4 and* $N = 24$. *Also shown: RAKE combining without equalization and MFBs I-III (cf. Section 3.1.1).*

and MFB II is about 0.25 dB at BER $= 10^{-5}$, which indicates that only little can be gained by sampling faster than the chip rate.

Fig. 5.5 presents the BER curves for the DS-UWB system with $N = 24$ and CM4 channels. Filters of order 6 are used for MMSE-LE and as FFF of MMSE-DFE and MMSE-DDFSE. Due to the longer impulse responses $h'[k]$ for CM4, the performance with pure RAKE combining deteriorates for low error rates. Different from that, the BER curves for MMSE-LE and MMSE-DFE are almost parallel to that of MFB III even for this short filter length. In accordance with the findings in Section 5.1.2, LE and DFE show a similar performance, but the gap in power efficiency between LE and DFE is larger than for CM1 and $N = 24$ in Fig. 5.4 (cf. Figs. 5.2(a)-(c) and 5.1(a)-(c)). Since DFE already approaches MFB III closely, the additional gain with DDFSE is rather small. On the other hand, we

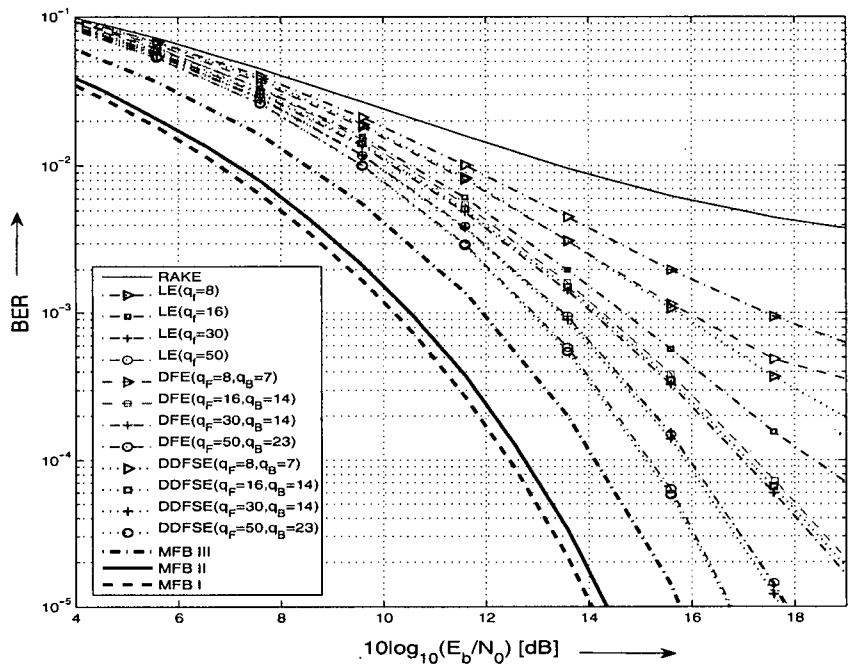

Figure 5.6: BER versus $10\log_{10}(E_b/N_0)$ *for MMSE-LE, MMSE-DFE, and MMSE-DDFSE with different filter lengths for CM4 and* $N = 6$*. Also shown: RAKE combining without equalization and MFBs I-III (cf. Section 3.1.1).*

observe a gap between MFB III and MFB II of about 1.6 dB, which can only be bridged by using more RAKE fingers (cf. Section 5.1.3.3). Again, the curves for MFB I and MFB II are relatively close.

As third scenario, we consider the simulation results for spreading with $N = 6$ and CM4 channels in Fig. 5.6. Equalizers of different filter lengths are chosen to illustrate the performance-complexity tradeoff. Clearly, RAKE combining without further equalization is not a viable solution in this case. We observe that MMSE-DFE significantly outperforms MMSE-LE for the same filter orders $q_f = q_F$ as was (qualitatively) to be expected from the results in Section 5.1.2 (cf. Figs. 5.3(a)-(c)). DDFSE provides only small gains over DFE, as the latter already approaches MFB III within 0.9 dB for $q_F = 50$ and $q_B = 23$. Compared to the low-rate case with $N = 24$ in Fig. 5.5, much longer filters are needed for efficient

equalization, which is in accordance with the predictions in Section 5.1.2. The gap of about 1.4 dB between MFB III and MFB II indicates that the use of more than $F = 16$ RAKE fingers could yield further performance improvement. We further observe that, as for the other two scenarios discussed above, the curves for MFB I and MFB II are very close. This leads to the general conclusion that almost no additional gain can be achieved by sampling faster than the chip rate, which renders chip-rate sampling an attractive alternative when aiming at low receiver complexity. It is interesting to note that an oversampling factor of 10 was found necessary for DS-UWB systems employing Gaussian monocycles in [MWS03].

Finally, the comparison of performance results in Fig. 5.6 with those of [ED05, Fig. 2] leads to the conclusion that DS-UWB with RRC pulse shaping and carrier modulation is more power efficient than carrierless UWB with Gaussian monocycles for high-rate transmission.

5.1.3.2 Linear vs. WL Processing

From Fig. 5.7, which corresponds to the lower data rate (57 Mbps) scenario with $N = 24$, it can be seen that WLE provides a performance gain of around 0.2 dB and WDFE, with a reduced complexity FBF design, also performs better than DFE.

For the more important high data rate scenario corresponding to CM4 and $N = 6$ (as in Fig: 5.6) the benefits of WL processing over conventional "linear" processing are illustrated in Figs. 5.8 and 5.9, where BER curves for LE and DFE are compared with those for WLE and WDFE, respectively. For a further comparison, the curve for DFE with $q_F = 50$ and $q_B = 23$ is also included.

As can be seen, WLE consistently outperforms LE for low BERs by about 1 dB, whereas the gains of WDFE over DFE are in the order of 0.3 dB. It should be noted that these improvements in power efficiency come at no cost in complexity (for LE vs. WLE) or even

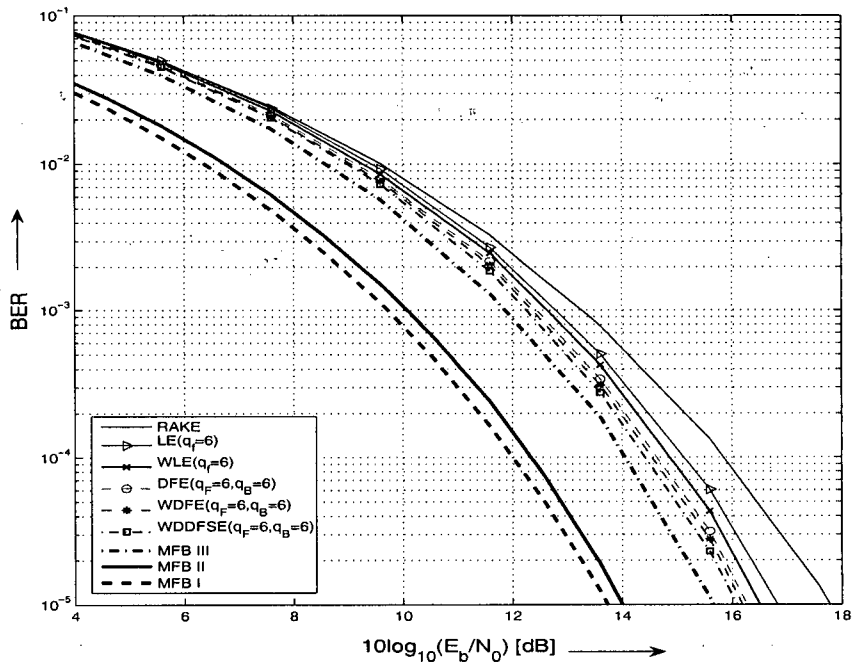

Figure 5.7: BER versus $10\log_{10}(E_b/N_0)$ *for MMSE-(W)LE and MMSE-(W)DFE for CM4 and* $N = 24$*. Also shown: MMSE-WDDFSE, RAKE combining without equalization, and MFBs I-III (cf. Section 3.1.1).*

with reduced complexity (for DFE vs. WDFE). Moreover, we found that WLE achieves similar BERs as DFE with identical FFF order. As an example, Fig. 5.8 shows the corresponding BERs for $q_f = q_F = 50$. Hence, for fixed power efficiency, WL processing achieves a similar gain over LE as decision-feedback processing, but it is less complex and, different from DFE, it can easily be combined with error-correcting decoders as no decision feedback is required.

5.1.3.3 Number of RAKE Fingers

In order to assess the effect of the number F of RAKE fingers independent of a possibly applied equalization strategy, we study the loss in average SNR for $F < F_\infty$, where F_∞ denotes the number of taps of the overall impulse response $h_o[\kappa]$ (2.11) after chip-rate

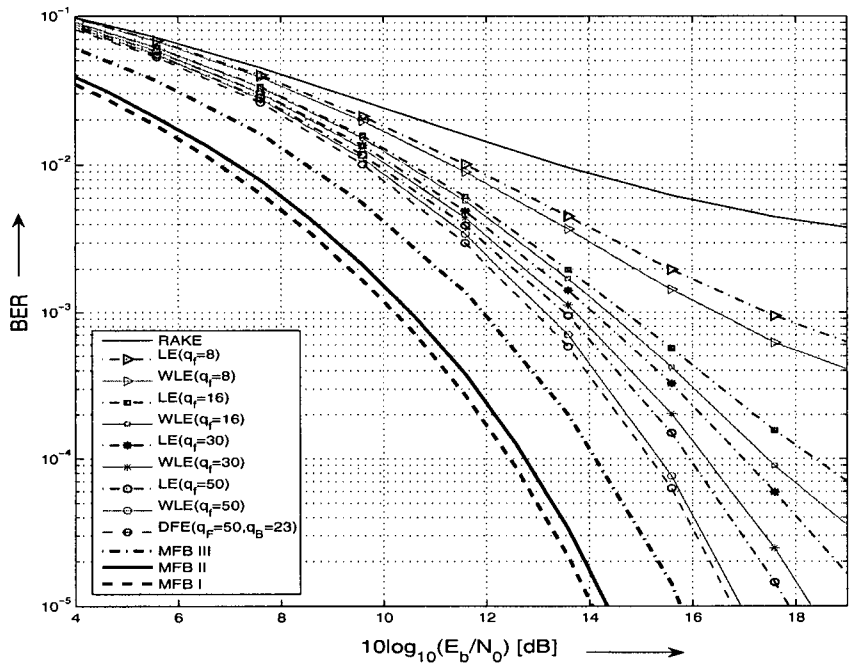

Figure 5.8: BER versus $10\log_{10}(E_b/N_0)$ *for MMSE-LE and MMSE-WLE with different filter lengths for CM4 and* $N = 6$*. Also shown: MMSE-DFE with* $q_F = 50$ *and* $q_B = 23$*, RAKE combining without equalization, and MFBs I-III (cf. Section 3.1.1).*

sampling. This average SNR loss is defined as

$$\Delta\text{SNR}(F) = 10\log_{10}\left(\frac{1}{N_r}\sum_{r=1}^{N_r}\frac{\gamma_r(F)}{\gamma_r(F_\infty)}\right), \tag{5.1}$$

where $\gamma_r(F)$ is the SNR (3.1) with $E_b(r)$ from (3.10) for F RAKE fingers. We note that the average SNR loss $\Delta\text{SNR}(F)$ is closely related to but not identical with the difference in E_b/N_0 between MFB II and MFB III, since BERs are averaged to obtain MFBs but SNR ratios are averaged to obtain $\Delta\text{SNR}(F)$.

Fig. 5.10 shows $\Delta\text{SNR}(F)$ as function of F for the three scenarios (CM1, $N = 24$), (CM4, $N = 24$), and (CM4, $N = 6$). We observe that for CM1, $F = 16$ RAKE fingers incur only a very small SNR loss of $\Delta\text{SNR}(16) = 0.3$ dB, which is in accordance with the BER simulations in Fig. 5.4. From this curve we also conclude that for CM1 a good capture of the useful received energy is accomplished with $F \geq 8$ fingers.

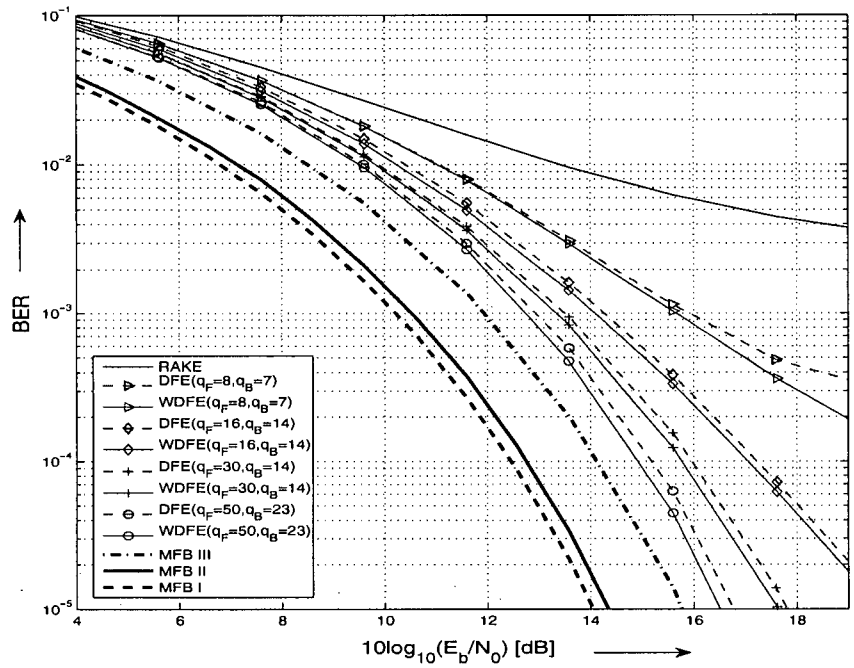

Figure 5.9: BER versus $10\log_{10}(E_b/N_0)$ *for MMSE-DFE and MMSE-WDFE with different filter lengths for CM4 and* $N = 6$*. Also shown: RAKE combining without equalization, and MFBs I-III (cf. Section 3.1.1).*

In the case of CM4, on the other hand, non-negligible SNR losses occur for small to moderately large numbers of fingers $F < 20$. This result, which has already been observed in Figs. 5.5-5.9 for $F = 16$, is due to the long delay spread associated with CM4 and it is (almost) independent of the spreading code length N. A rather large number of RAKE fingers ($F \geq 30$) would be required to approach the optimum performance, which seems impractical for implementation.

5.2 Performance Results and Discussion for 4BOK DS-UWB Systems

In this section, we provide a performance comparison of the equalization strategies proposed in Section 4.2 based on simulated BER results. We also compare the simulation results with

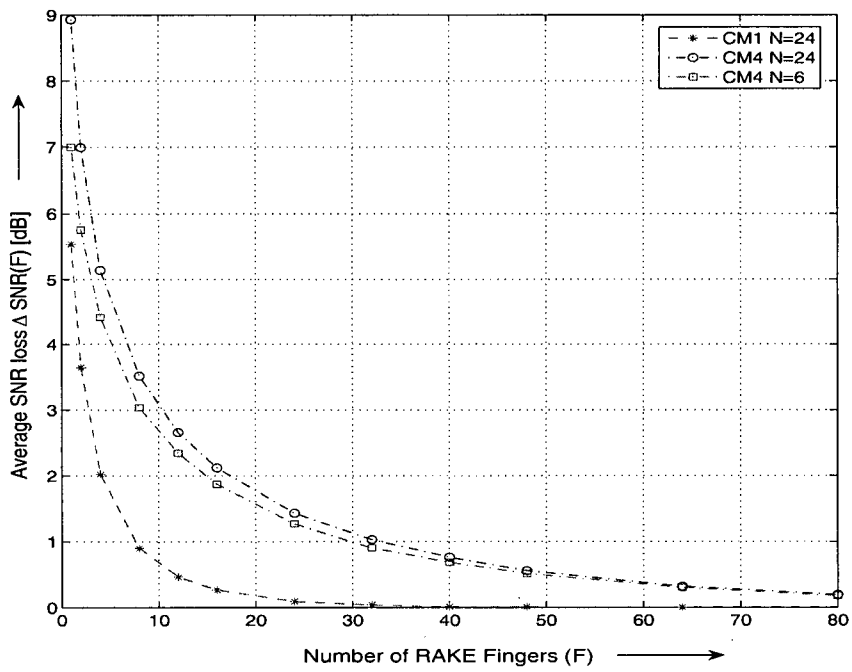

Figure 5.10: Average SNR loss $\Delta\mathrm{SNR}(F)$ *as function of the number of RAKE fingers* F *for the three scenarios (CM1,* $N = 24$*), (CM4,* $N = 24$*), and (CM4,* $N = 6$*).*

the BER bounds from Section 4.1.

5.2.1 Simulation Parameters

As for the BPSK case, we consider the lower UWB operating band from 3.1 to 4.85 GHz. Simulations are performed over $N_r = 100$ channel realizations of CM1 and CM4, which constitute the extreme cases of the UWB channel model. The BER results are obtained as an average over the best 90 out of 100 channel realizations, cf. [P8002]. 4BOK DS-UWB transmission with spreading codes of length $N = 24$ (corresponding to a data rate of 110 Mbps) and $N = 6$ (corresponding to data rates 440 Mbps), respectively, are exemplarily chosen [FKMW05]. At the receiver side, RAKE combining with $F = 16$ fingers is applied (cf. e.g. [TK04]) and we assume that the channel realizations are perfectly estimated at the receiver. For the MIMO equalization case we consider the simplified decision rule (4.21).

Table 5.2: Parameters for the considered 4BOK DS-UWB systems.

4BOK Spreading Codes [FKMW05]	$N = 24$: $[-1, 1, -1, -1, 1, -1, -1, 1, -1, 0, -1, 0, -1, -1, 1, 1, 1, -1, 1, 1, 1, -1, -1, -1]$ $N = 24$: $[0, -1, -1, 0, 1, -1, -1, 1, -1, -1, 1, 1, 1, 1, -1, -1, 1, -1, 1, -1, 1, 1, 1, 1]$ $N = 6$: $[1, 0, 0, 0, 0, 0]$ $N = 6$: $[0, 0, 0, 1, 0, 0]$
Channel Models	CM1 and CM4, lower band from 3.1 to 4.85 GHz (see Section 2.3 and [P8002])
Pulse shape	Square root-raised cosine ($\alpha = 0.3$) [FKMW05]
Data rates	110 Mbps ($N = 24$) and 440 Mbps ($N = 6$) [FKMW05]
Number of RAKE fingers	$F = 16$ [TK04]

Since the complexity of LE and DFE is dominated by feedforward filtering, we choose $q_f = q_F$. DDFSE uses the same FFF as DFE and the number of states is four, i.e., $q_{tr} = 1$ is considered. For all equalization schemes a favorable delay parameter k_0 is found by testing various k_0 within a reasonable range. The system parameters are summarized in Table 5.2.

5.2.2 Simulation Results

First, the performance differences due to (a) SIMO vs. MIMO filter optimization, and (b) MIMO vs. WL-MIMO filter optimization, are discussed in Section 5.2.2.1. Then, in Section 5.2.2.2, we consider the absolute performance of 4BOK equalization for different transmission scenarios and compare these with the respective MFBs.

5.2.2.1 Filter Optimization

We consider LE and DFE, and, for the sake of brevity, we use SIMO-x-Y, MIMO-Y, and WL-MIMO-Y, x $\in \{\mathrm{I}, \mathrm{II}\}$, Y $\in \{\mathrm{LE}, \mathrm{DFE}\}$, to refer to LE and DFE with SIMO Filter De-

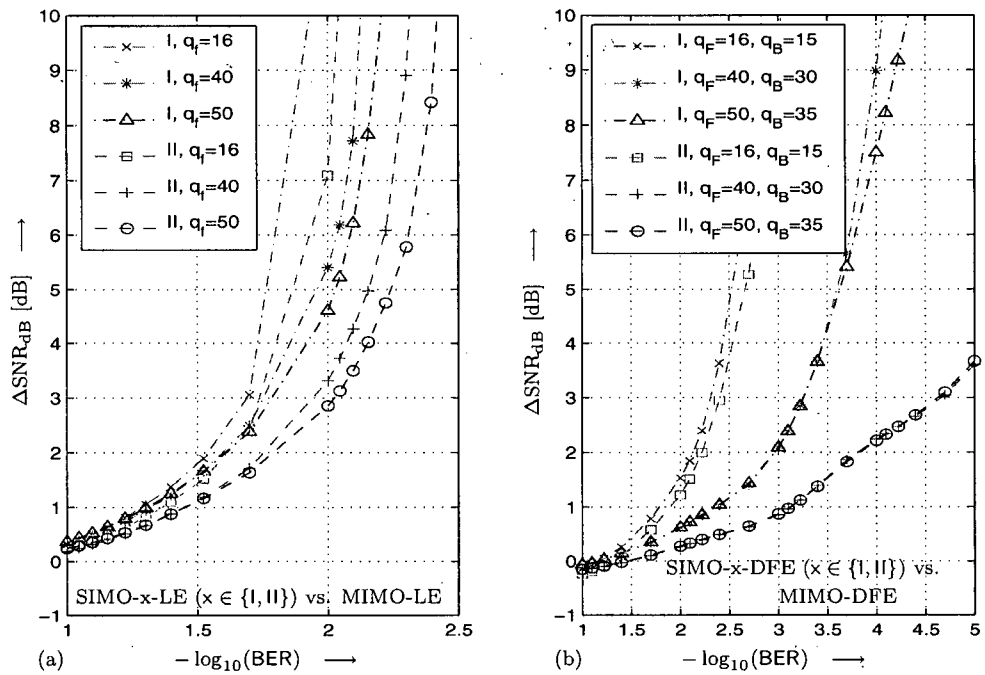

Figure 5.11: Performance comparison for equalization with SIMO and MIMO filter optimization. CM4 and $N = 6$. (a) LE: $\Delta\mathrm{SNR}_{\mathrm{dB}} = 10\log_{10}(\mathrm{SNR}(\textit{SIMO-x-LE})) - 10\log_{10}(\mathrm{SNR}(\textit{MIMO-LE}))$, $\mathrm{x} \in \{\mathrm{I}, \mathrm{II}\}$, *(b) DFE:* $\Delta\mathrm{SNR}_{\mathrm{dB}} = 10\log_{10}(\mathrm{SNR}(\textit{SIMO-x-DFE})) - 10\log_{10}(\mathrm{SNR}(\textit{MIMO-DFE}))$, $\mathrm{x} \in \{\mathrm{I}, \mathrm{II}\}$. *Filter orders $q_f = 16$, $q_f = 40$, and $q_f = 50$ for LE and ($q_F = 16$, $q_B = 15$), ($q_F = 40$, $q_B = 30$), and ($q_F = 50$, $q_B = 35$) for DFE.*

sign I and II, and MIMO and WL-MIMO filter optimization, respectively. *SIMO vs. MIMO Filter Optimization:* Fig. 5.11 compares the performances of different filter optimization techniques for LE (Fig. 5.11(a)) and DFE ((Fig. 5.11(b)) assuming different filter orders and the example of CM4 and $N = 6$. More specifically, the signal-to-noise ratio (SNR) difference

$$\Delta\mathrm{SNR}_{\mathrm{dB}} = 10\log_{10}(\mathrm{SNR}(\mathrm{SIMO\text{-}x\text{-}Y})) - 10\log_{10}(\mathrm{SNR}(\mathrm{MIMO\text{-}Y}))\ ,\ \mathrm{x} \in \{\mathrm{I}, \mathrm{II}\}\ ,\quad \mathrm{Y} \in \{\mathrm{LE}, \mathrm{DFE}\}\ , \tag{5.2}$$

between SIMO and MIMO equalization required to achieve a certain BER assuming identical filter orders (q_f, q_F, q_B) is plotted vs. $-\log_{10}(\mathrm{BER})$. Since $\Delta\mathrm{SNR}_{\mathrm{dB}}$ is always positive

for LE (Fig. 5.11(a)) and for $\mathsf{BER} > 10^{-1.5}$ in case of DFE (Fig. 5.11(b)), we conclude that MIMO equalization is practically always superior to SIMO equalization, which was anticipated from the findings in Section 4.2 (cf. also the impulse responses in Figs. 4.2, 4.5 and 4.5). The SNR gains due to MIMO filter optimization are more pronounced for LE, where SIMO-I-LE and SIMO-II-LE show a relatively high error floor at $\mathsf{BER} \approx 10^{-2.0} \ldots 10^{-2.5}$ depending on the filter order q_f, i.e., $\Delta\mathrm{SNR}_{\mathrm{dB}}$ grows unboundedly for LE and $\mathsf{BER} < 10^{-2.5}$. It should be mentioned that no error floor was observed for MIMO-LE with $q_f = 50$ and $\mathsf{BER} \gtrsim 10^{-5}$. Also, for DFE the differences in power efficiency increase for lower target BER, e.g., MIMO-DFE with $(q_F = 40, q_B = 30)$ outperforms SIMO-II-DFE with the same filter orders by 0.9 dB and 3.7 dB for $\mathsf{BER} = 10^{-3}$ and 10^{-5}, respectively. Furthermore, SIMO-II-DFE with shorter filters and SIMO-I-DFE cause a higher error floor than MIMO-DFE with identical filter orders. When comparing the two SIMO filter optimization schemes, we note that SIMO–II has considerable performance improvements over SIMO–I, especially for DFE and lower target BER, where the effect of error propagation is insignificant (cf. Section 4.2.1).

Fig. 5.12 (a) compares the performance of different filter optimization techniques for LE and DFE for the lower data rate scenario of CM4 and $N = 24$. Interestingly, even for this low data rate scenario, MIMO equalization schemes perform better than the corresponding SIMO equalization schemes. More specifically, MIMO-LE outperforms SIMO-I-LE and SIMO-II-LE by 3.75 dB and 2.75 dB, respectively and MIMO-DFE outperforms SIMO-I-DFE and SIMO-II-DFE by 1.1 dB and 1.25 dB, respectively, for $\mathsf{BER} = 10^{-5}$. Moreover, this performance gap increases for higher target BER.

MIMO vs. WL-MIMO Filter Optimization: In Figs. 5.12(b) and 5.13 the performances for MIMO and WL-MIMO equalization are compared in terms of $\Delta\mathrm{SNR}_{\mathrm{dB}}$ vs. $-\log_{10}(\mathsf{BER})$ for CM4 and $N = 6$ and $N = 24$, respectively. The SNR difference for a fixed target BER

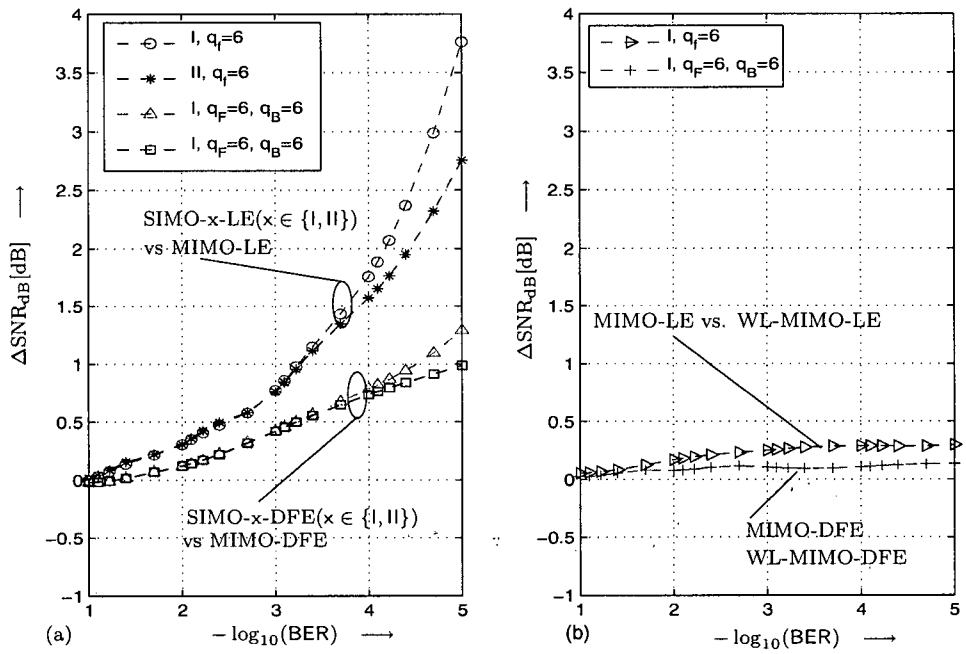

Figure 5.12: (a) Performance comparison for equalization with SIMO and MIMO filter optimization. CM4 and $N = 24$. LE: $\Delta\text{SNR}_{\text{dB}} = 10\log_{10}(\text{SNR}(\textit{SIMO-x-LE})) - 10\log_{10}(\text{SNR}(\textit{MIMO-LE}))$, $\text{x} \in \{\text{I},\text{II}\}$, *DFE:* $\Delta\text{SNR}_{\text{dB}} = 10\log_{10}(\text{SNR}(\textit{SIMO-x-DFE})) - 10\log_{10}(\text{SNR}(\textit{MIMO-DFE}))$, $\text{x} \in \{\text{I},\text{II}\}$. *(b) Performance comparison for equalization with MIMO and WL-MIMO filter optimization. CM4 and $N = 24$. LE:* $\Delta\text{SNR}_{\text{dB}} = 10\log_{10}(\text{SNR}(\textit{MIMO-LE})) - 10\log_{10}(\text{SNR}(\textit{WL-MIMO-LE}))$, *DFE:* $\Delta\text{SNR}_{\text{dB}} = 10\log_{10}(\text{SNR}(\textit{MIMO-DFE})) - 10\log_{10}(\text{SNR}(\textit{WL-MIMO-DFE}))$

and identical filter orders (q_f, q_F, q_B) is defined as

$$\Delta\text{SNR}_{\text{dB}} = 10\log_{10}(\text{SNR}(\text{MIMO-Y})) - 10\log_{10}(\text{SNR}(\text{WL-MIMO-Y})) \ , \quad \text{Y} \in \{\text{LE}, \text{DFE}\} \ . \tag{5.3}$$

For this low data rate scenario with $N = 24$, as can be seen from Fig. 5.12(b) that WLE and WDFE perform better than the corresponding "linear" schemes i.e., LE and DFE, with same filter lengths.

For the higher data rate scenario with $N = 6$, it can be seen that WL processing consistently improves performance of MIMO-LE (Fig. 5.13(a)) and MIMO-DFE (Fig. 5.13(b)).

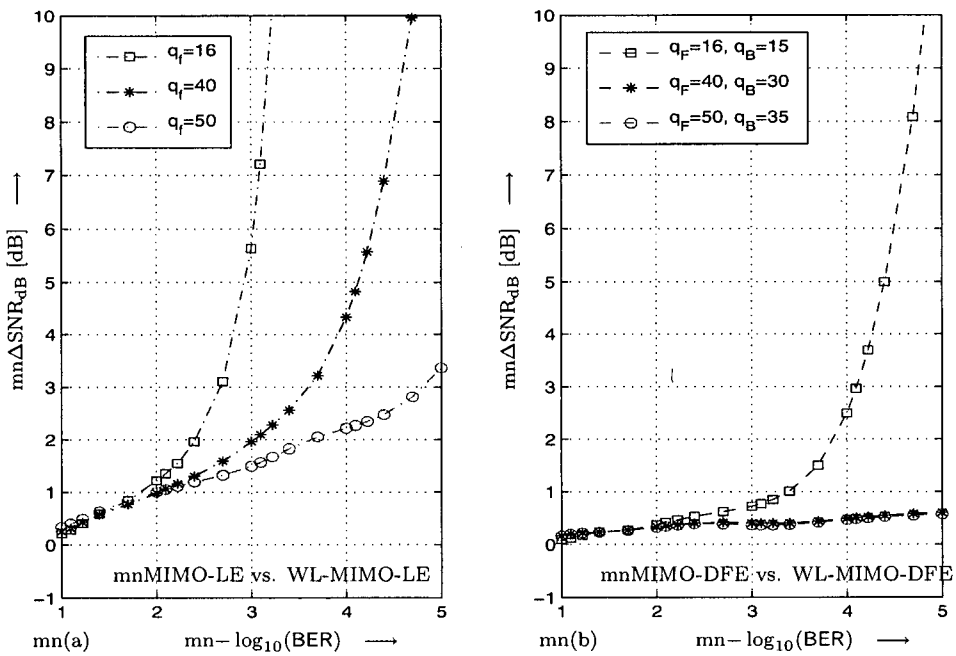

Figure 5.13: Performance comparison for equalization with MIMO and WL-MIMO filter optimization. CM4 and $N = 6$. (a) LE: $\Delta\mathrm{SNR}_{\mathrm{dB}} = 10\log_{10}(\mathrm{SNR}(\textit{MIMO-LE})) - 10\log_{10}(\mathrm{SNR}(\textit{WL-MIMO-LE}))$, *(b) DFE:* $\Delta\mathrm{SNR}_{\mathrm{dB}} = 10\log_{10}(\mathrm{SNR}(\textit{MIMO-DFE})) - 10\log_{10}(\mathrm{SNR}(\textit{WL-MIMO-DFE}))$. *Filter orders* $q_f = 16$, $q_f = 40$, *and* $q_f = 50$ *for LE and* $(q_F = 16,\ q_B = 15)$, $(q_F = 40,\ q_B = 30)$, *and* $(q_F = 50,\ q_B = 35)$ *for DFE.*

For relatively long filters with $q_f = 50$ and $(q_F = 50,\ q_B = 35)$ the gains in power efficiency are 0.6 dB and 3.4 dB at BER $= 10^{-5}$, respectively. WL processing becomes even more beneficial for shorter filter lengths ($q_f = 16$, and $q_F = 16$, $q_B = 15$), where $\Delta\mathrm{SNR}_{\mathrm{dB}}$ grows steeply with decreasing target BER, i.e., WL processing effectively lowers the error floor of MIMO-LE and MIMO-DFE. It should be emphasized that these gains come at no cost or even reduced computational complexity. In the following, we therefore concentrate on WL-MIMO equalization and present absolute performance results for 4BOK transmission.

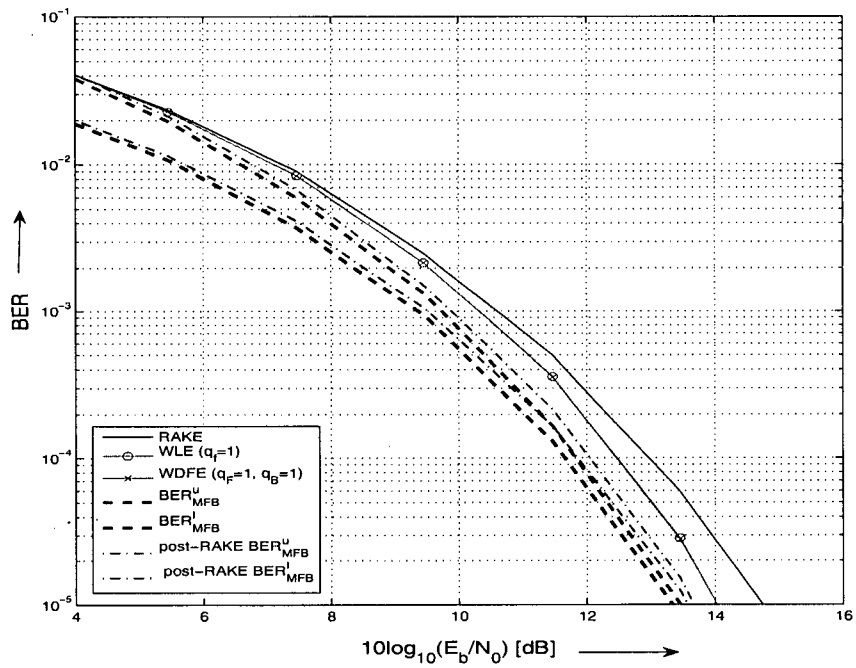

Figure 5.14: BER versus $10\log_{10}(E_b/N_0)$ *for CM1 and* $N = 24$*. RAKE combining without equalization, WLE, and WDFE (MIMO equalization). Also shown:* $\mathsf{BER}^{\mathsf{u}}_{\mathsf{MFB-I}}$, $\mathsf{BER}^{\mathsf{l}}_{\mathsf{MFB-I}}$ *according to MFB I and* $\mathsf{BER}^{\mathsf{u}}_{\mathsf{MFB-II}}$, $\mathsf{BER}^{\mathsf{l}}_{\mathsf{MFB-II}}$ *according to MFB II from Section 4.1.*

5.2.2.2 Equalization for 4BOK and MFBs

We show results for the three channel-rate pairs (CM1, $N = 24$), (CM4, $N = 24$), and (CM4, $N = 6$). For all three scenarios, we include the semi-analytical BER limits according to the MFBs from Section 4.1. Upper and lower BER bounds are denoted by $\mathsf{BER}^{\mathsf{u}}_{\mathsf{MFB-I}}$ and $\mathsf{BER}^{\mathsf{l}}_{\mathsf{MFB-I}}$ for MFB I and $\mathsf{BER}^{\mathsf{u}}_{\mathsf{MFB-II}}$ and $\mathsf{BER}^{\mathsf{l}}_{\mathsf{MFB-II}}$ for MFB II, respectively. For the sake of conciseness, we use WLE, WDFE, WDDFSE when referring to WL-MIMO-LE, WL-MIMO-DFE, and WL-MIMO-DDFSE, respectively.

CM1 and $N = 24$*:* Fig. 5.14 shows BER results for CM1 and $N = 24$ as functions of $10\log_{10}(E_b/N_0)$, where E_b is the average received energy per bit and N_0 is the one-sided noise power spectral density of the passband noise process. BER curves for the RAKE

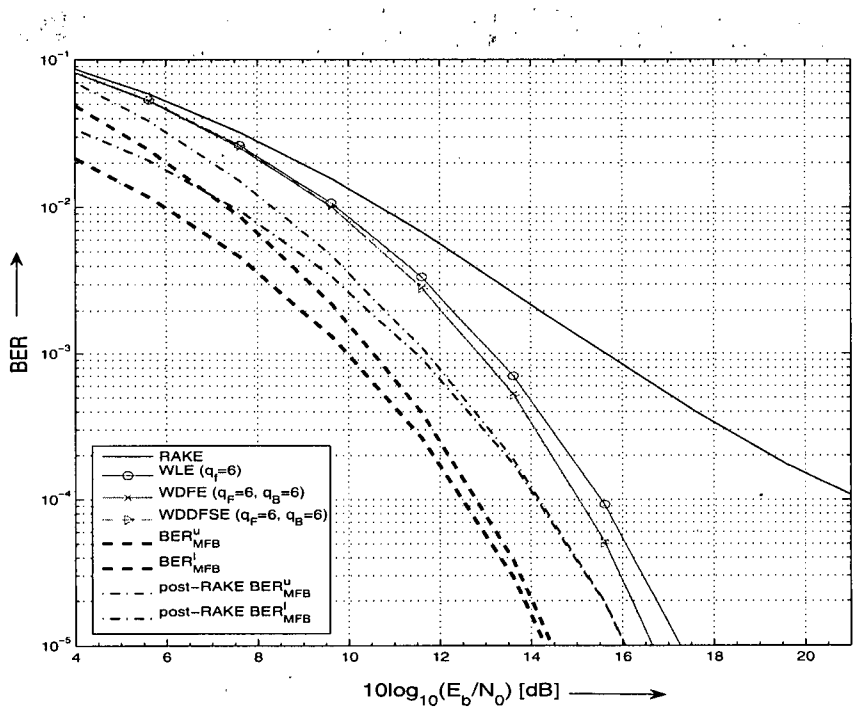

Figure 5.15: BER versus $10\log_{10}(E_b/N_0)$ *for CM4 and* $N = 24$*. RAKE combining without equalization, WLE, WDFE, and WDDFSE (MIMO equalization). Also shown:* $\mathsf{BER}^{\mathsf{u}}_{\mathsf{MFB-I}}$, $\mathsf{BER}^{\mathsf{l}}_{\mathsf{MFB-I}}$ *according to MFB I and* $\mathsf{BER}^{\mathsf{u}}_{\mathsf{MFB-II}}$, $\mathsf{BER}^{\mathsf{l}}_{\mathsf{MFB-II}}$ *according to MFB II from Section 4.1.*

receiver without equalization (labeled as "RAKE") and for WLE and WDFE are plotted. FFFs of order $q_f = q_F = 1$ and a single-tap FBF $\underline{\boldsymbol{F}}_B = \boldsymbol{F}_B[1]$ are employed.

It can be seen that for CM1 with a relatively short delay spread [P8002] and transmission with long spreading codes, i.e., relatively lower data rate, Wthe performance of LE and WDFE is almost identical. The BER bounds are closely approached by these schemes and more complex WDDFSE (not shown in Fig. 5.14) cannot further improve performance. Even the BER curve for RAKE combining without additional equalization is within 1 dB of the MFB for this transmission scenario. We also observe that upper and lower MFBs converge for $\mathsf{BER} \lesssim 10^{-3}$.

CM4 and $N = 24$*:* The results for the second scenario are shown in Fig. 5.15. FFFs

of order 6 are used for WLE, WDFE, and WDDFSE. As can be seen, the BER curves for RAKE combining without and with equalization diverge for error rates lower than 10^{-2}. This is due to the longer effective impulse responses $h_{\mu\nu}[k]$, $\mu, \nu \in \{1, 2\}$, for CM4, which require equalization.

We also note that the BER curves for RAKE combining with equalization run almost parallel to the BER bounds even for the short filter lengths adopted. WDFE provides a gain of 0.5 dB over WLE and achieves practically the same performance as WDDFSE. In particular, the gap of about 2 dB between $\mathsf{BER}^{\mathsf{I}}_{\mathsf{MFB-I}}$ and the BER for WDFE at low BERs cannot be reduced by using WDDFSE. Instead, comparing the curves for $\mathsf{BER}^{\mathsf{I}}_{\mathsf{MFB-I}}$ and $\mathsf{BER}^{\mathsf{I}}_{\mathsf{MFB-II}}$, it can be seen that RAKE combining with $F = 16$ does not sufficiently capture the received signal energy and that more fingers are required to close this gap.

CM4 and $N = 6$: Fig. 5.16 gives simulation results for spreading with $N = 6$ and CM4 channels. WL-MIMO equalizers with different filter lengths are chosen to illustrate the performance-complexity tradeoff. The curve for MIMO-DFE (not WL) with ($q_F = 50, q_B = 35$) is also included for comparison.

Clearly, RAKE combining without further equalization is not a viable solution in this case. We observe that WDFE outperforms WLE for the same filter orders $q_f = q_F$. WLE achieves a very similar performance as DFE for $q_f = q_F = 50$. Hence, for fixed power efficiency, WL processing achieves a similar gain over LE as decision-feedback processing, but it is less complex. Different from DFE, which may suffer from error bursts due to feedback errors, WLE can easily be combined with error-correcting decoders.

The application of more complex WDDFSE (only shown for $q_F = 50, q_B = 35$) is not beneficial as only marginal gains over WDFE are achieved. Again, the BER curves for WDFE run almost parallel to the lower theoretical MFB limit. More specifically, WDFE performs within 1 dB of the $\mathsf{BER}^{\mathsf{I}}_{\mathsf{MFB-II}}$ bound at $\mathsf{BER} = 10^{-5}$. As shown in Fig. 5.10 for

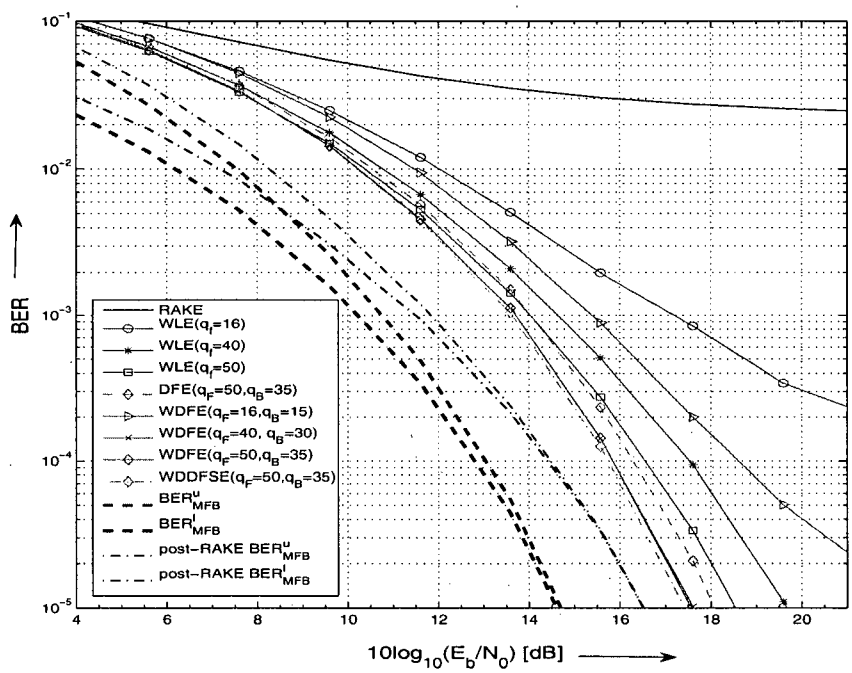

Figure 5.16: BER versus $10\log_{10}(E_b/N_0)$ *for CM4 and* $N = 6$. *RAKE combining without equalization, WLE and WDFE with different filter lengths, and WDDFSE and DFE for* $q_F = 50$, $q_B = 35$ *(MIMO equalization). Also shown:* $\mathsf{BER}^{\mathsf{u}}_{\mathsf{MFB-I}}$, $\mathsf{BER}^{\mathsf{l}}_{\mathsf{MFB-I}}$ *according to MFB I and* $\mathsf{BER}^{\mathsf{u}}_{\mathsf{MFB-II}}$, $\mathsf{BER}^{\mathsf{l}}_{\mathsf{MFB-II}}$ *according to MFB II from Section 4.1.*

BPSK DS-UWB that a relatively large number of $F \geq 30$ RAKE fingers would be required to close the gap of about 2-3 dB to $\mathsf{BER}^{\mathsf{l}}_{\mathsf{MFB-I}}$. Since BPSK and 4BOK apply the same set of spreading sequences, similar conclusions can be derived for the 4BOK case.

Chapter 6

Conclusions

In this work, equalization for DS-UWB systems using two different modulation schemes, BPSK and 4BOK, has been studied. The receiver for DS-UWB systems employs RAKE combining in order to capture the multipath energy. Due to the highly frequency selective nature of UWB channels, severe ISI occurs at the RAKE output. Furthermore, DS-UWB systems are designed for providing high data rates and so the chip-rates used are very high, about 1.3 GHz for lower band and 2.6 GHz for higher band. Therefore, implementation complexity is an important consideration in the receiver design of these systems. In this work, we focused on developing equalization techniques for DS-UWB systems that can be employed after RAKE. Post-RAKE equalization is peformed at symbol level, resulting in reduced implementation complexity.

In the first part of this work we have investigated equalization for DS-UWB systems with BPSK modulation as specified in the standard proposal [FKMW05]. To this end, we have (a) derived three versions of the MFB, which to a different extent take into account receiver suboptimalities, (b) considered the effective discrete-time impulse response at the RAKE combiner output and have analyzed the distribution of the zeros of the corresponding transfer function, and (c) studied several equalization strategies including the novel application of WL processing to DS-UWB. The results of our investigation can be

summarized as follows cf. [PLSL05a, PLSL05b]:

- From the MFB analysis, carried out for the IEEE 802.15.3a standard channel model, it can be concluded that suboptimum chip-matched filtering and chip-rate sampling do not incur a significant performance degradation, and that RAKE combining with a practical number of fingers results in performance losses of about 1-2 dB for channels with long delay spread.
- The analysis of the zeros of the channel transfer function suggests that LE is well suited for lower data-rate modes of DS-UWB, whereas non-linear equalization (DFE, DDFSE) is preferable for high data-rate modes. These findings have been confirmed by simulation results.
- The proposed WL processing was found to provide gains of up to 1 dB, which come at no cost, or even slightly reduce equalizer complexity. More specifically, simple WLE and WDFE schemes were shown to perform in close vicinity of the pertinent MFB, whereas the negligible gains with WDDFSE do not justify its higher complexity. WLE and WDFE are thus recommended for implementation.

In the second part of this work equalization for a 4BOK DS-UWB system is studied. To this end, we first have derived expressions for the BER according to the MFB, which serve as theoretical performance limits. Second, equalizer designs based on SIMO optimization methods have been considered. Further improving the design of these SIMO schemes, MIMO filter optimization based equalization schemes have been devised. In this context, an equivalent MIMO channel model for 4BOK DS-UWB, which facilitates the design of efficient equalizers using MIMO filter optimization, has been developed. Third, we have applied WL processing to these MIMO equalization schemes. The results of our investigations for the 4BOK case can be summarized as, cf.[PLSL05c, PLSL06]:

- RAKE combining without equalization is not a viable solution for 4BOK DS-UWB systems when aiming at higher data rates. Both SIMO and MIMO equalization improve the performance compared to RAKE combining without equalization.

- MIMO equalization with joint feedforward filtering of the two RAKE outputs for 4BOK DS-UWB is clearly advantageous over SIMO equalization with separate feedforward filtering. More specifically, even at lower data rates (such as 57 Mbps) MIMO equalization provides performance gains varying from 1 dB to 4 dB over SIMO equalization. At higher data rates SIMO based equalization techniques either cause error floors or provide high perfomance losses as compared to MIMO techniques, which perform close to the MFB limit.

- Low-complexity MIMO-LE and MIMO-DFE with WL processing provide performance gains over their "linear" counterparts and achieve power efficiencies close to the theoretical MFB limit. More specifically, MIMO-WLE outperforms MIMO-LE and achieves a very similar performance as MIMO-DFE. Hence, for fixed power efficiency, WL processing achieves a similar gain over LE as decision-feedback processing, but is less complex. The application of more complex WDDFSE is not beneficial as only marginal gains over WDFE are achieved. Therefore, MIMO based (W)DFE and WLE are recommended for implementation.

An interesting topic for further research would be to implement the MIMO-based equalization schemes developed for 4BOK DS-UWB systems in hardware and study the implementaion-specific issues. Moreover, throughout this work, perfect channel estimation was assumed. It would be interesting to investigate the performance of these equalization schemes with practical imperfect channel estimation.

Bibliography

[ADS00] N. Al-Dhahir and A.H. Sayed. Finite-Length Multi-Input Multi-Output MMSE-DFE. *IEEE Trans. Sig. Proc.*, 48(10):2921–2936, October 2000.

[Blu03] Bluetooth Special Interest Group. Specifications of the Bluetooth system, Version 1.2., November 2003.

[BP79] C.A. Belfiore and J.H. Park. Decision-Feedback Equalization. *Proc. IEEE*, 67(8):1143–1156, August 1979.

[BR78] C. L. Bennett and G. F. Ross. Time-domain Electromagnetics and its Applications. *Proc. IEEE*, 66(3):299–318, March 1978.

[CWVM02] D. Cassioli, M. Z. Win, F. Vatalaro, and A. F. Molisch. Performance of Low-complexity RAKE Reception in a Realistic UWB Channel. In *Proc. IEEE Int. Conf. Communications (ICC)*, volume 2, pages 763–767, May 2002.

[DH92] A. Duel-Hallen. Equalizers for Multiple Input Multiple Output Channels and PAM Systems With Cyclostationary Input Sequences. *IEEE J. Select. Areas Commun.*, 10(3):630–639, April 1992.

[DHH89] A. Duel-Hallen and C. Heegard. Delayed Decision-Feedback Sequence Estimation. *IEEE Trans. Commun.*, 37(5):428–436, May 1989.

[ED05] M. Eslami and X. Dong. Rake-MMSE-Equalizer Performance for UWB. *IEEE Commun. Lett.*, 9(6):502–504, June 2005.

[FCC02] FCC. Revision of part 15 of the commission's rules regarding ultra-wideband transmission systems: Report and Order, February 2002.

[FKMW05] R. Fisher, R. Kohno, M. McLaughlin, and M. Welbourn. DS-UWB Physical Layer Submission to IEEE 802.15 Task Group 3a (Doc. Number P802.15-04/0137r4), January 2005.

[Fon04] R. J. Fonatana. Recent System Applications of Short-Pulse Ultra-Wideband (UWB) Technology. *IEEE Trans. Microwave Theory Tech.*, 52(9):2087–2104, 2004.

[GH96] W. Gerstacker and J. Huber. Improved Equalization for GSM Mobile Communications. In *Proc. IEEE Int. Conf. Telecommunications (ICT)*, pages 128–131, April 1996.

[GSL03] W. Gerstacker, R. Schober, and A. Lampe. Receivers With Widely Linear Processing for Frequency-Selective Channels. *IEEE Trans. Commun.*, 51(9):1512–1523, September 2003.

[GT04] W. Gerstacker and D. Taylor. On Prefiltering for Reduced-State Equalization of MIMO Channels. In *Proc. 5. ITG Conf. on Source and Channel Coding*, pages 25–30, January 2004.

[IO04] Y. Ishiyama and T. Ohtsuki. Performance Evaluation of UWB-IR and DS-UWB with MMSE-Frequency Domain Equalization (FDE). In *Proc. IEEE Global Telecommunications Conf. (GLOBECOM)*, volume 5, pages 3093–3097, Nov.-Dec. 2004.

[Lin95] F. Ling. Matched Filter-Bound for the Time-Discrete Multipath Rayleigh Fading Channel. *IEEE Trans. Commun.*, 43(234):710–713, Feb.-April 1995.

[LS75] W. C. Lindsey and M. K. Simon. *Telecommunication Systems Engineering.* Prentice Hall, Englewood Cliffs, 1975.

[MFP03] A. F. Molisch, J. R. Foerster, and M. Pendergrass. Channel Models for Ultrawideband Personal Area Networks. *IEEE Wireless Commun. Mag.*, 10(6):14–21, December 2003.

[MPS05] D. Mattera, L. Paura, and F. Sterle. Widely Linear Decision-Feedback Equalizer for Time-Dispersive Linear MIMO Channels. *IEEE Trans. Sig. Proc.*, 53(7):2525–2536, July 2005.

[MWS03] B. Mielczarek, M. O. Wessman, and A. Svensson. Performance of Coherent UWB Rake Receivers with Channel Estimators. In *Proc. IEEE Vehicular Technology Conference (VTC)*, volume 3, pages 1880–1884, October 2003.

[NM93] F.D. Neeser and J.L. Massey. Proper Complex Random Processes With Applications to Information Theory. *IEEE Trans. Inform. Theory*, 39(4):1293–1302, July 1993.

[OSR+04] I. Oppermann, L. Stoica, A. Rabbachin, Z. Shelby, and J. Haapola. UWB Wireless Sensor Networks: UWEN – A Practical Example. *IEEE Commun. Mag.*, 42(12):27–32, December 2004.

[P8002] IEEE P802.15. Channel Modeling sub-committe report final, IEEE P802.15-02/368r5-SG3a, December 2002.

[P8004] IEEE P802.15. Multiband OFDM Physical Layer Proposal for IEEE 802.15 Task Group 3a (Doc. Number P802.15-03/268r3), March 2004.

[PB97] B. Picinbono and P. Bondon. Second-Order Statistics of Complex Signals. *IEEE Trans. Sig. Proc.*, 45(2):411–420, February 1997.

[PC95] B. Picinbono and P. Chevalier. Widely Linear Estimation with Complex Data. *IEEE Trans. Sig. Proc.*, 43(8):2030–2033, August 1995.

[PH03] D. Porcino and W. Hirt. Ultra-Wideband Radio Technology: Potential and Challenges Ahead. *IEEE Commun. Mag.*, 21(7):66–74, July 2003.

[PLSL05a] A. Parihar, L. Lampe, R. Schober, and C. Leung. Analysis of Equalization for DS-UWB systems. In *Proc. IEEE Int. Conf. on Ultra-Wideband (ICU)*, sept 2005.

[PLSL05b] A. Parihar, L. Lampe, R. Schober, and C. Leung. Equalization for DS-UWB Systems—Part I: BPSK DS-UWB. *submitted to IEEE Trans. Commun.*, October 2005.

[PLSL05c] A. Parihar, L. Lampe, R. Schober, and C. Leung. Equalization for DS-UWB Systems—Part II: MBOK DS-UWB. *submitted to IEEE Trans. Commun.*, October 2005.

[PLSL06] A. Parihar, L. Lampe, R. Schober, and C. Leung. Equalization for 4BOK DS-UWB systems. *submitted to IEEE Int. Conf. Communications (ICC)*, 2006.

[Pro01] J. G. Proakis. *Digital Communications.* McGraw-Hill, New York, fourth edition, 2001.

[Rap96] T. S. Rappaport. *Wireless Communications.* Prentice Hall, Englewood, NJ, fourth edition, 1996.

[RMMW03] P. Runkle, J. McCorkle, T. Miller, and M. Welborn. DS-CDMA: The Modulation Technology of Choice for UWB Communications. In *Proc. IEEE Confer-*

ence on Ultra Wideband Systems and Technologies (UWBST), pages 364–368, November 2003.

[RSF03] A. Rajeswaran, V. S. Somayazulu, and J. R. Forester. Rake Performance for a Pulse Based UWB System in a Realiztic UWB Indoor Channel. In *Proc. IEEE Int. Conf. Commun. (ICC)*, volume 4, pages 2879–2883, May 2003.

[RSZ+04] M. A. Rahman, S. Sasaki, J. Zhou, S. Muramatsu, and H. Kikuchi. Performance Evaluation of RAKE Reception of Ultra Wideband Signals over Multipath Channels from Energy Capture Perspective . In *Proc. Joint UWBST and IWUWBS*, pages 231–235, May 2004.

[SG01] R. Schober and W. H. Gerstacker. On the Distribution of Zeros of Mobile Channels with Application to GSM/EDGE. *IEEE J. Select. Areas Commun.*, 19(7):1289–1299, July 2001.

[SG02] R. Schober and W. H. Gerstacker. The Zeros of Random Polynomials: Further Results and Applications. *IEEE Trans. Commun.*, 50(6):892–896, June 2002.

[Sha48] C. E. Shannon. A Mathematical Theory of Communication. *Bell. Syst. Tech.*, 27:623–656, October 1948.

[Sur05] K. Surf. The Market For Ultra-Wideband Solutions, Park Associates White Paper at http://www.parksassociates.com, January 2005.

[SV87] A. Saleh and R. Valenzuela. A Statistical Model for Indoor Multipath Propagation. *IEEE J. Select. Areas Commun.*, 5(2):128–137, February 1987.

[TK04] K. Takizawa and R. Kohno. Low-Complexity Rake Reception and Equalization for MBOK DS-UWB Systems. In *Proc. IEEE Global Telecommunications Conf. (GLOBECOM)*, volume 2, pages 1249–1253, November 2004.

[VLC96] P.A. Voois, I. Lee, and J.M. Cioffi. The effect of decision delay in finite-length decision feedback equalization. *IEEE Trans. Inform. Theory*, 42(2):618–621, March 1996.

[WCS00] M. Z. Win, G. Chrisikos, and N. R. Sollenberger. Effect of chip rate on selective rake combining. *IEEE Commun. Lett.*, 4(7):233–235, July 2000.

[WMLM02] M. Welborn, T. Miller, J. Lynch, and J. McCorkle. Multi-User Perspectives in UWB. In *Proc. IEEE Conference on Ultra Wideband Systems and Technologies (UWBST)*, pages 271–275, May 2002.

[WPA] See: http://www.ieee802.org/15/pub/TG3a.html.

[YG04] L. Yang and G. B. Giannakis. Ultra-Wideband Communications: An Idea Whose Time Has Come. *IEEE Signal Processing Mag.*, 21(6):26–54, November 2004.

[YR94] J. Yang and S. Roy. Joint transmitter and receiver optimization for multiple-input multiple-output systems with decision feedback. *IEEE Trans. Inform. Theory*, 40(5):1334–1347, September 1994.

[Zig] See: http://www.zigbee.org.